DISSERTATION

ICARUS COSMIC RAY TAGGER EFFICIENCY

Submitted by

Tyler N. Boone

Department of Physics

In partial fulfillment of the requirements

For the Degree of Doctor of Philosophy

Colorado State University

Fort Collins, Colorado

Summer 2024

Doctoral Committee:

Advisor: Robert Wilson

William Fairbank
Michael Mooney
Alexander Brandl

Copyright by Tyler Boone 2024

All Rights Reserved

ABSTRACT

ICARUS COSMIC RAY TAGGER EFFICIENCY

The ICARUS Cosmic Ray Tagger (CRT) was constructed with the goal to tag cosmogenic muons passing through the ICARUS Time Projection Chamber (TPC). Construction and commissioning of the detector began in Fall 2019 with the Side CRT North wall and continued for several years through the installation of the Top CRT. In this thesis I will summarize my contributions to the CRT system and describe a measurement of the installed CRT detection efficiency using the TPC.

ACKNOWLEDGEMENTS

This work could not have been done without significant help and assistance from the many colleagues and friends that continue to work on the ICARUS experiment. The CRT and TPC groups have both been invaluable on this journey to try to tie the subsystems together with data. Many thanks to everyone in ICARUS and those working groups in particular for all of their support. I want to thank the DOE for many years of funding as this work was done, and to Fermilab for being a great place to work at with wonderful people. The Colorado State University will always be a second home to me, and I am grateful for having had the opportunity to be a student there.

In no particular order, thanks to: Chris Hilgenberg, Anna Heggestuen, Biswaranjan Behera, Antoni Aduszkiewicz, Donatella Torretta, Linda Bagby, David Warner, Jay Jablonski, Minerba Betancourt, Kelly Hardin, Claudio Montanari, Catherine James, Bruce Howard, Jacob Zettlemoyer, Tom Coan, Vito Benedetto, Justin Mueller, Gray Putnam, Jamie Dyer, Francesco Poppi, Valerio Pia, Laura Pasqualini, Laura Patrizii, and Geoff Savage. Without all of their efforts, none of this would have been possible, and I am honored to have been able to work with them over the years, whether on the CRT installation or on the later analysis.

Finally, thanks to my committee, for all of their feedback and guidance. I am so glad to have the opportunity to do this analysis in the hopes that it will serve the greater HEP community.

DEDICATION

To my family: Dad, Mom, Kelsey, and my grandparents. This accomplishment is yours as well, for I would not have completed it without your support. To my friends, too many to list here, I thank you for your continued friendship as I disappeared for a few years to make this happen. And to my cat GB: you will never read this, but you kept me sane, and are the best little buddy a guy could ask for.

TABLE OF CONTENTS

LIST OF TABLES

LIST OF FIGURES

Chapter 1

Introduction

The ICARUS (Imaging Cosmics and Rare Underground Signals) experiment is a Liquid Argon Time Projection Chamber (LArTPC) neutrino detector, originally designed for operation at the Laboratori Nazionali del Gran Sasso (LNGS) in Italy. The first demonstration of a large-scale LArTPC detector, it was the first ICARUS Time Projection Chamber (TPC) module (referred to as T300) and operated at Pavia in 2001 [4]. After a period of further development and the construction of a second TPC, the detector operated from 2010 to 2013 at Gran Sasso. At Gran Sasso, ICARUS operated underneath a mountain that reduced cosmic ray rates in the detector from the standard surface rate of 11 kHz [5] to approximately 35 mHz on average [6]; this is a factor of $\sim$300,000 reduction in rate. After several years at LNGS, ICARUS was moved to CERN for upgrades. In the summer of 2017 it was shipped to Fermilab to serve as the Far Detector in the Short Baseline Neutrino (SBN) Program. The major focus of the SBN proposal is the investigation of the possibility of a sterile neutrino in the $\Delta m^2 \sim 1eV^2$ range, motivated by anomalous measurements of neutrino flux in other previous beam experiments.

ICARUS has been operational for several years, collecting neutrino data since 2021. Software tools for data analysis remain under development, including for the Cosmic Ray Tagger (CRT) subsystem. Currently, analyzers are using the CRT as a simple event filter. This thesis presents the first measurement of the tagging efficiency of the installed CRT system using the TPC to provide well-reconstructed tracks to project back to the CRT and search for corresponding signals there. This will provide an estimate of the CRT's TPC correlation efficiency, which will be of use to future analyzers.

1.1 Short Baseline Neutrino Program

The Short Baseline Neutrino (SBN) program is a collection of three neutrino detectors located in Fermilab's Booster Neutrino Beamline. The near detector, the Short Baseline Near Detector

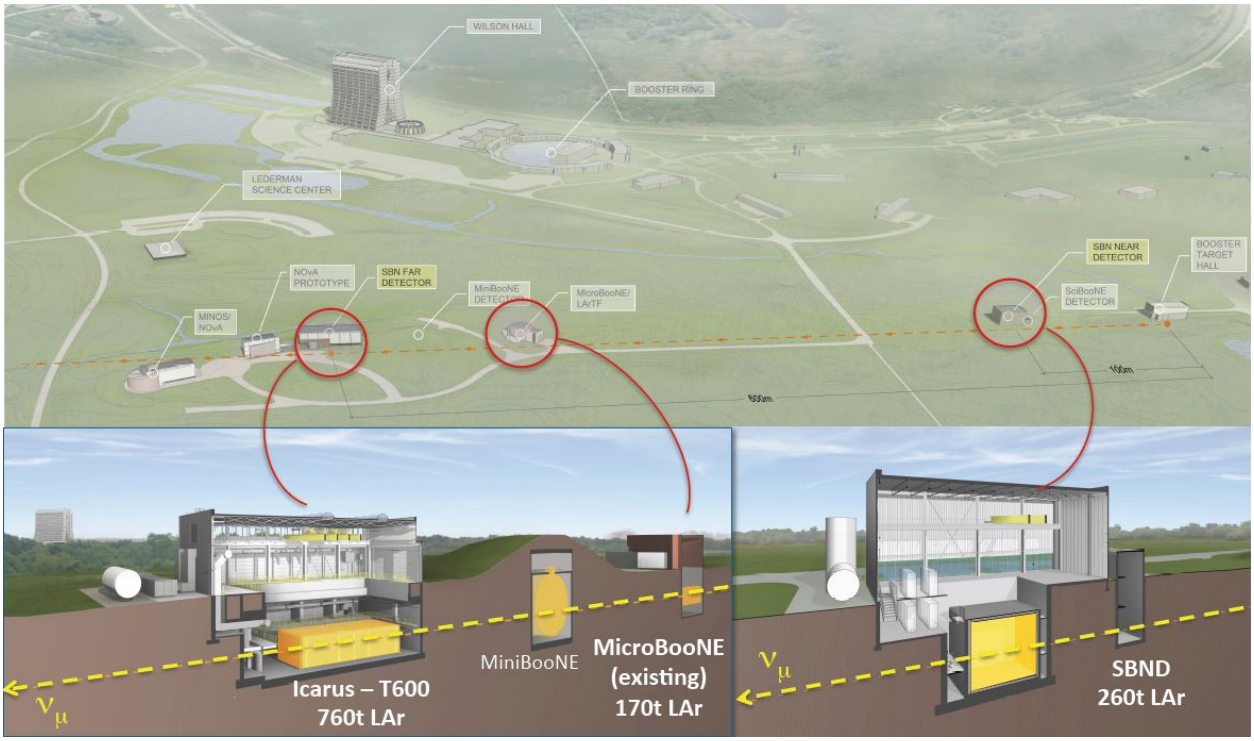

Figure 1.1: Bird's-eye view of the SBN program, including the Booster Beam source.

(SBND) [7], was built specifically for the SBN program at Fermilab; it is a LArTPC detector located 110 meters from the Booster target, having a total liquid argon mass of 270 tons and an active liquid argon mass of 110 tons. MicroBooNE was already being commisioned at 470 meters from the Booster target when the SBN program was formed, and will serve as a good check to measurements made by ICARUS and SBND. MicroBooNE is also a liquid argon experiment with 86.6 tons of active (170 tons total) liquid argon mass. ICARUS, whose active argon mass is 476 tons (760 tons total), was refurbished at CERN after its first data run at LNGS completed, and then shipped to where it sits now at 600 meters from the Booster target at Fermilab. Figure 1.1 shows the relative locations of the detectors in the beamline.

The Short Baseline Neutrino Program serves several physics and operational experience goals for high energy physics research [1]. A major physics goal is to address several different historical anomalous measurements using neutrino beams. The Liquid Scintillator Neturino Detector (LSND) experiment at Los Alamos also saw an excess of ν_e from its decay-at-rest pion beam source which could be explained by the presence of such a neutrino. Another motivating anomalous mea-

Figure 1.2: Checking some of the >53,000 TPC wire signals during commissioning.

surement is the MiniBooNE anomaly, which was an excess of observed ν_e by the MiniBooNE experiment; this could be explained by an irreducible background in the detector, or by the presence of another flavor of neutrino which has become known as the sterile neutrino. Investigating the sterile neutrino hypothesis is a key motivation for the SBN program.

Other physics goals for the SBN program include dark matter searches [8], studying neutrino interactions, and better understanding beam backgrounds for future experiments. SBN also serves as an operational training ground for running and maintaining Liquid Argon Time Projection Chambers in advance of the Deep Underground Neutrino Experiment (DUNE).

1.2 Bringing ICARUS to Fermilab

ICARUS was transported by boat across the Atlantic ocean in the summer of 2017. After arrival at Fermilab, the TPCs were kept in sealed containers outside the Far Detector building as the warm vessel (the name for the metal red container the TPCs are now sitting within) was prepped. Once the TPCs were placed in the warm vessel, a major campaign of checking TPC wire activity would commence, bringing in collaborators from all over the globe to participate.

Figure 1.3: The Far Detector building in which the ICARUS detector is housed. Photo credit: Anna Heggestuen.

1.3 Liquid Argon TPCs

ICARUS is currently the largest fully-commissioned Liquid Argon Time Projection Chamber (LArTPC) operating in a neutrino beamline. The initial concept for such a detector originated with Carlo Rubbia, head of the ICARUS collaboration, in 1977 [9]. The basic concept is that the liquid argon will be excited by high energy charged particles coming from the beam, creating scintillation light that can be read out by the PMTs for trigger and timing information; electrons ionized from the passing charged particles are drifted by a strong electric field to the wire planes, where induced and collected charge on those wires allow for reconstruction of the path of the charged particle through the argon. Combining the drifted electron signals in the TPC with the timing information coming from the PMTs allows for an image of the event to be reconstructed with spatial separation on the order of a few millimeters.

A challenge a LArTPC is the time it takes to drift ionized electrons to the wire planes, typically on the order of milliseconds depending on the strength of the electric field applied; for ICARUS, the drift time is 0.96 ms from an application of a field of 500 V/cm, created by a 147 kV potential from the central cathode in each TPC. During this time, if sufficient shielding is not in place, charged particles like cosmic muons can enter the detector and could mimic events from a beam interaction. The 0.96 ms drift time compared to the expected cosmic rate in the ICARUS TPCs of

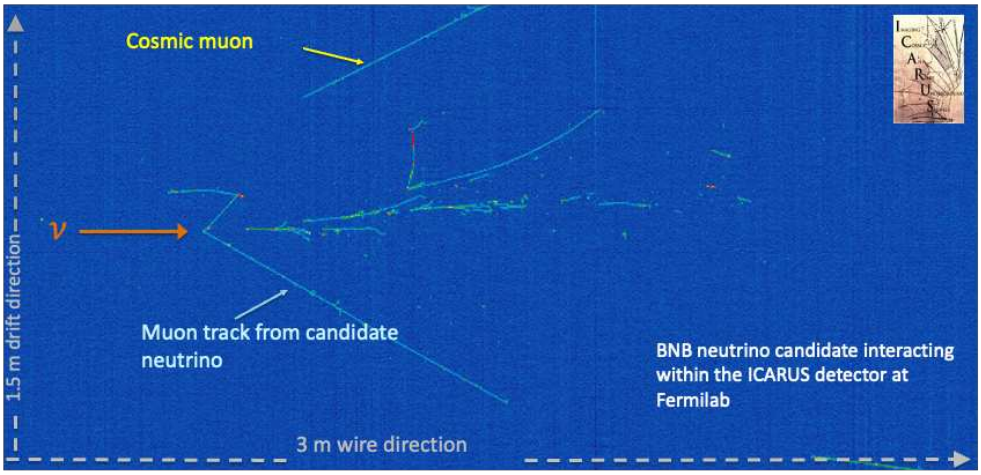

Figure 1.4: A BNB neutrino interaction and nearby a cosmic ray using the ICARUS TITUS Event Display. Created by Christian Farnese.

11 kHz means we should expect 11 cosmogenic muons to enter the TPC in a single drift. A more detailed description of the ICARUS TPC subsystem is given in section 4. Figure 1.4 shows an example of a neutrino interaction from the ICARUS TITUS Event Display, provided by Christian Farnese (INFN-Padova).

1.4 PMTs and the ICARUS Trigger

The trigger system is used to know when to start recording data for later analysis. For ICARUS, this can either be for beam activity, using timing information sent from the beam to know when it will arrive; or it can be based only on detector activity, specifically the light detectors. The core detectors used as the ICARUS trigger are the photomultiplier tubes (PMTs) located behind the wire planes of each TPC. Liquid argon is nearly transparent to its own scintillation light, so light generated from charged particles ionizing the liquid argon will illuminate the PMTs. This illumination will occur within a few tens of nanoseconds of the ionising particles entering the TPC.

There are 90 PMTs per TPC, arranged as shown in Figure 1.5; there are four TPCs in total in ICARUS, this will be discussed more in section 4. The total geometrical coverage of the PMTs is on the order of 5%. The TPC cathode is perforated such that it is 57% transparent to light collected

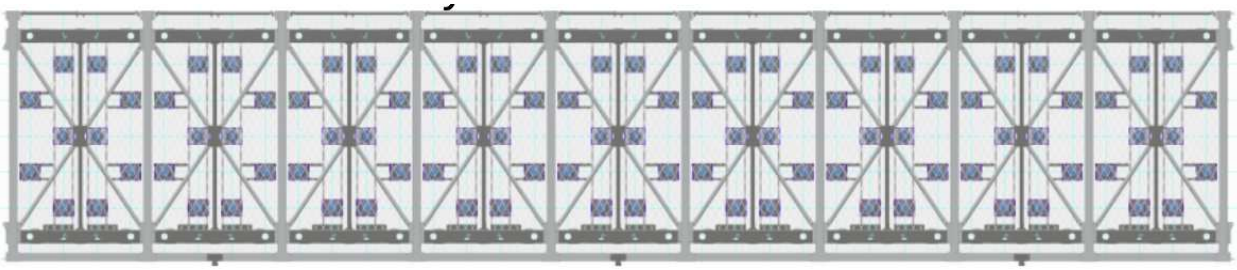

Figure 1.5: Layout of PMTs in the ICARUS TPCs; layout is the same for all TPCs, so this is an example of a single wall of them.

by the PMTs, meaning there will also be some light collected across the dual TPCs even for events whose TPC activity is fully contained in one volume.

To generate what is called a Global Trigger, five pairs of PMTs in a TPC must have experienced a coincident signal within a PMT window. Each PMT in these five pairs must report a waveform whose digitized signal waveform is above a programmed threshold, and each pair should have seen the signal within 160 ns of each other. Once a Global Trigger is generated, data is collected around this timestamp from the ICARUS subsystems and assembled into an event (see section 4.2 for more detail). It will then be the reference time for all data in that event.

1.5 Booster Neutrino Beam

The Booster Neutrino Beam nominally delivers 81 bunches of protons to a beryllium target over the course of a 1.6 μs spill [10]. This results in a production of many higher energy state particles which can be focused using the beam's focusing horn, which can apply a magnetic field to focus particles of either positive or negative charge in the direction of the beam. These particles travel down the decay pipe until encountering multiple absorbers which will catch any high-energy charged particles. See Figure 1.6 for a full diagram of the BNB target area. Each spill provides approximately $5\text{x}10^{12}$ protons on the target (POT). The protons have 8 GeV of kinetic energy, and the bunches are on average 19 ns apart and 1.15 ns wide. A diagram of the timing of a single spill from the BNB can be seen in Figure 1.7. The NuMI beam timing structure is shown in Figure 1.8.

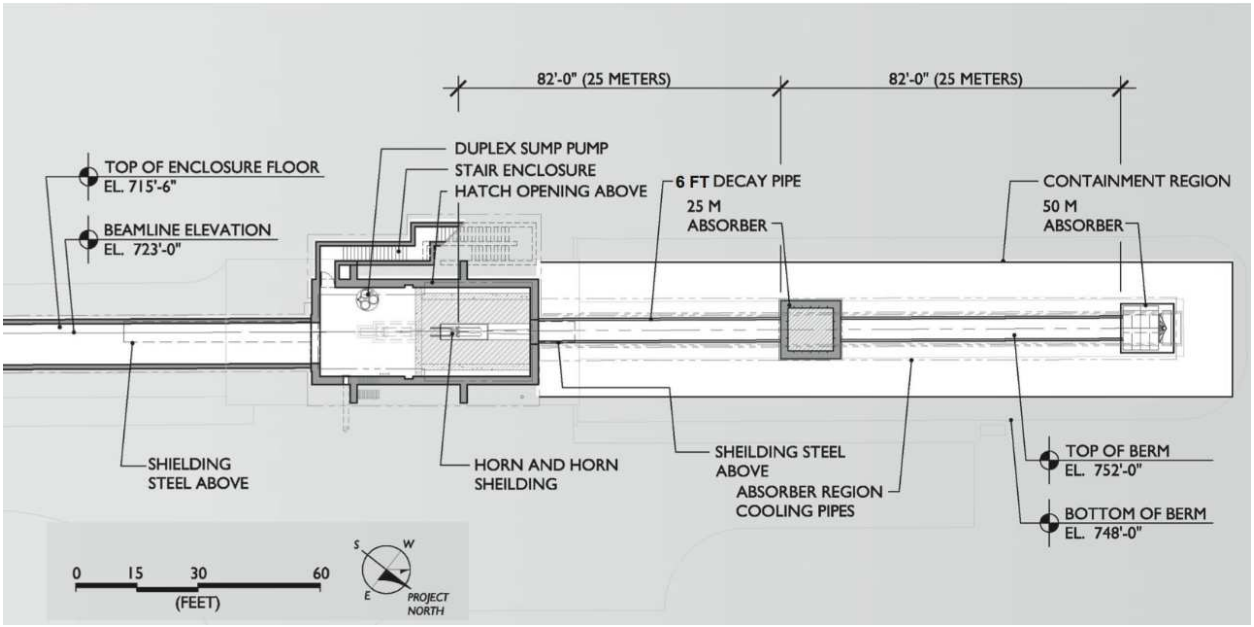

Figure 1.6: Diagram of the BNB target area, including the target, focusing horn, and decay tunnel with absorbers [1].

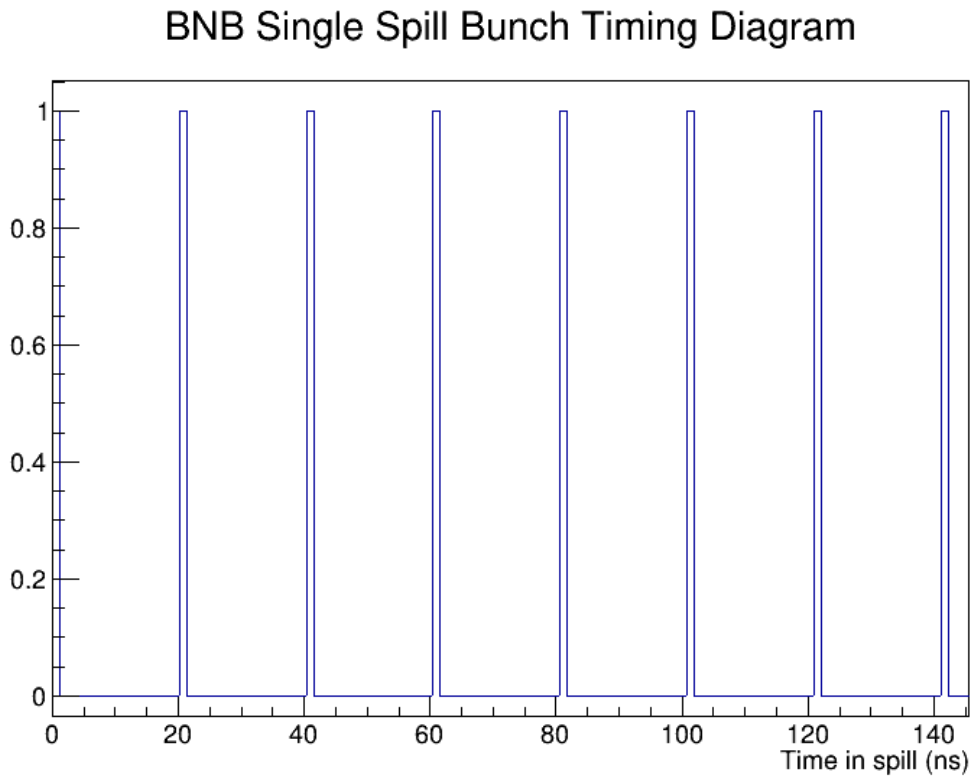

Figure 1.7: A section of the timing diagram of a segment of the BNB beam spill structure. Each bunch is 1.15 ns wide and 19 ns apart, with 81 bunches in each spill.

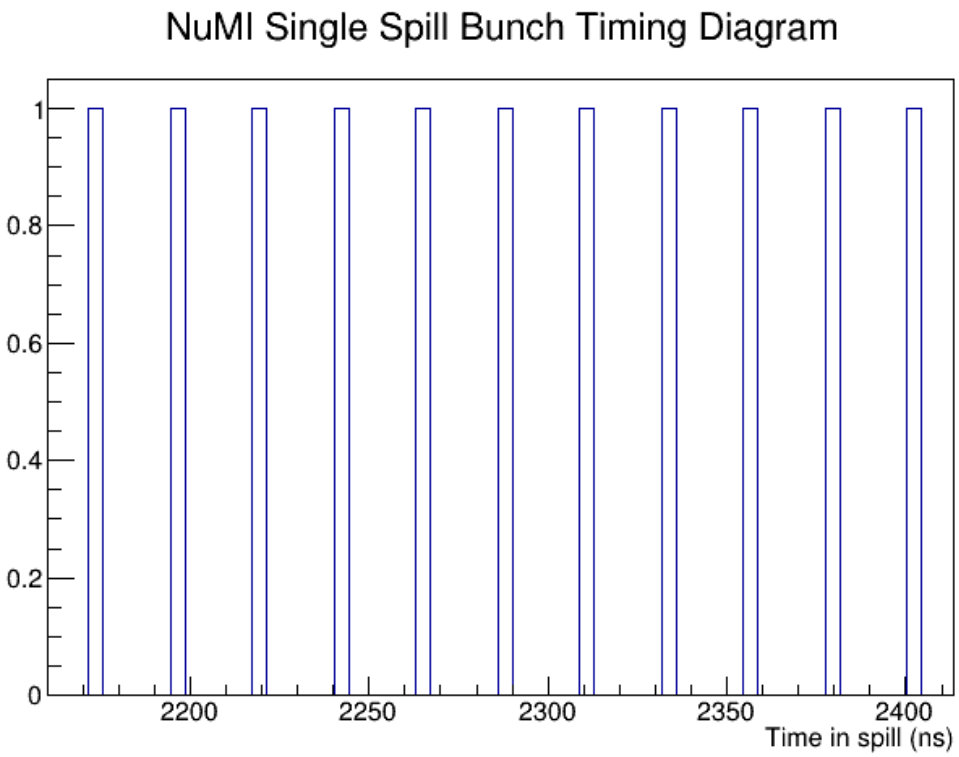

Figure 1.8: A section of the timing diagram of a segment of the NuMI beam spill structure. Each bunch is 4.04 ns wide and 18.8 ns apart, with 486 bunches in each spill.

1.6 Cosmic Rays as Neutrino Signal Background

The main signals being searched for in the SBN detectors are from neutrino interactions occurring in the Time Projection Chambers of the detectors. The primary signal of a neutrino is its paired lepton appearing in the TPC. This is because any neutrino interaction should produce the charged lepton, that will have its own signature in the detector and therefore be identifiable via the lepton. The kinetic energy of the protons delivered by the Booster Neutrino Beam is 8 GeV, so the only leptons with the energy to appear are the electron and the muon, making those two particles a key signal. Cosmic rays are then a continuous background bombarding ICARUS that must be contended with, as otherwise they can mimic the appearance of a muon neutrino.

Simulations by CSU postdoctoral researcher Biswaranjan Behera using the CORSIKA event generator [11] showed that the expected rate of cosmic muons in ICARUS even after the installation of a 3 meter concrete overburden above ICARUS would be about 13 per drift window (0.96

ms). This makes for a key background in need of removal, and can be reduced further by use of an external system to tag these incoming muons as coming from a non-beam source.

1.7 Overview of Thesis Contents

This thesis begins with a description of the preparation, testing, installation, and commissioning of the CRT, with an emphasis on my contributions. This is followed by a discussion of the CRT's functioning in the broader context of the experiment, with an emphasis on how CRT data products are created. Then, a short discussion of the TPC subsystem, due to its central role in the analysis to characterize CRT response. Following this, I present the studies performed that led to measurements of CRT detection efficiencies by region. Finally there is a discussion of how these measurements could impact future neutrino analyses, along with suggestions for future studies using the software tools developed for the efficiency measurements.

Chapter 2

Cosmic Ray Tagger

Prior to being moved to Fermilab, ICARUS was operated at the Laboratori Nazionali del Gran Sasso (LNGS) site in Italy [12], underneath a large amount of rock that acted as natural cosmogenic background suppression. The Cosmic Ray Tagger (CRT) was part of the original proposal for the Short Baseline Neutrino program as a way to adjust for the new operational environment. The CSU group, led by Bob Wilson, played a major role in the early development of the detector design, as documented in [13].

2.1 Overview

The ICARUS CRT consists of three subsystems: the Top, the Side, and the Bottom, each of which makes use of plastic scintillator as the core detection element. The Top and Side share a common readout Front End Board (FEB) and both use Silicon Photomultiplier (SiPM) to convert scintillated photons into recorable electrical signals. The Bottom system uses Photomultiplier Tubes (PMTs), the Bottom was in commissioning for most of the writing of this paper and was not used in the analysis. As such, there will be no further discussion of the Bottom CRT.

After a period of testing prototype designs at CSU, the collaboration decided to have collaborators at CERN and INFN construct the Top portion 'from scratch'. The Side walls use repurposed scintillator panels from the MINOS experiment [14], as will be discussed in subsection 2.1.4. Both subsystems share a general design principle of using strips of bulk scintillator with an embedded doped optical fiber to allow propagation of scintillated light to the light sensors. The specific geometry, arrangement of these strips of scintillator differs between subsystems as well as the types of scintillator and scintillator dopants being used.

2.1.1 Silicon Photomultipliers

The Top and Side CRT both use SiPMs to read out light from their respective modules. While the Top and Side modules differ in some ways, they are similar in concept: bars of scintillator coated in a highly reflective layer with one (for Side CRT) or two (for Top CRT) 1 mm diameter wavelength-shifting fibers running the length of the bar of scintillator. A charged particle passing through the bulk scintillator will deposit light into the scintillator. A portion of that light will then be absorbed by the wavelength-shifting fibers (which have high internal reflection) and be shifted from its original wavelength to 476 nm [15], at which the SiPMs have a high detection efficiency. The Hamamatsu S14160-3050HS Multi-Pixel Photon Counters (MPPCs) SiPMs used by the Side CRT have 50% photon detection efficiency at 450 nm [2], and the Hamamatsu s13360-3050HS MPPCs used by the Top CRT [16] have a 40% photon detection efficiency at the same wavelength. Each Top CRT SiPM contains 3,600 pixels which each can be held at a common voltage, while the Side CRT has 3,531.

When a SiPM is held at a voltage above its breakdown voltage, a single photon can initiate an avalanche of activity in the triggered pixel. The amount of current generated by the SiPM will be proportional to the number of pixels triggered in a 150 ns window when operated by our front-end electronics. This current is integrated and returned as an Analog to Digital Converter signal, or ADC. Hamamatsu, the manufacturer of the SiPMs used, recommends operating at 3 Volts above breakdown. Overvoltage also strongly effects the SiPM's photon detection efficiency, gain, and crosstalk. Crosstalk is the likelihood that one pixel triggering will cause an adjacent pixel to trigger.

Figure 2.1 shows the dependence of the key operational parameters of the Side CRT SiPMs with overvoltage from the SiPM datasheet [2]. The Side CRT SiPMs used for the Optical Readout Modules were from two different manufacturer batches: one batch had an average operating voltage (provided to us by Hamamatsu) of 41.5V, and the other had an average operating voltage of 40.7V, corresponding to the device breakdown voltages plus a 3V overvoltage. All ORMs were

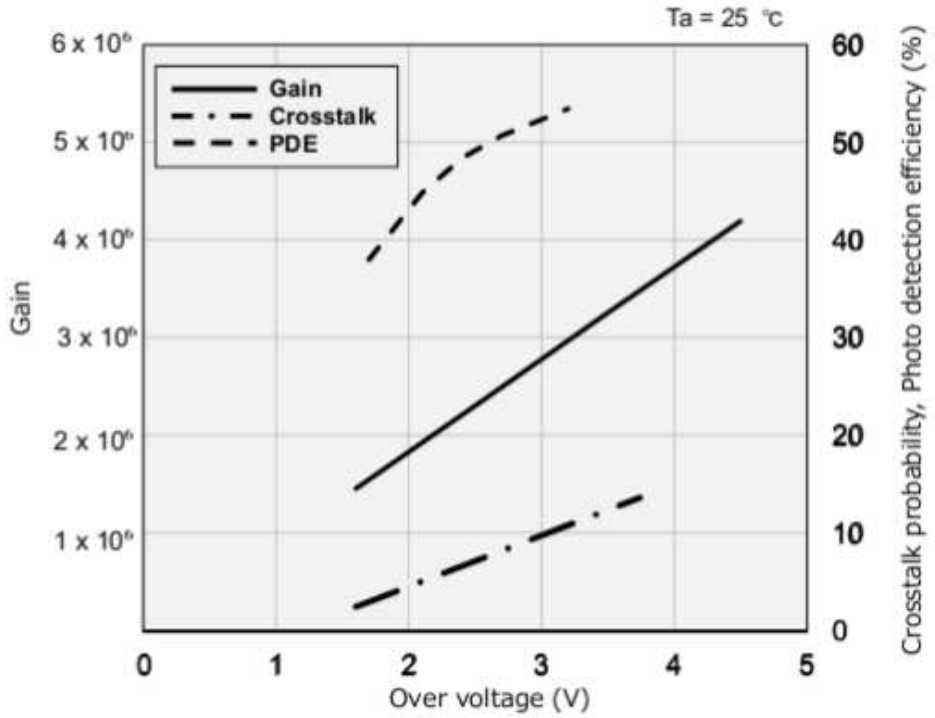

Figure 2.1: From the Hamamatsu S14160 series datasheet [2], the expected SiPM response as a function of overvoltage in terms of gain, crosstalk, and photon detection efficiency.

fabricated using SiPMs from a single one of these batches. These voltages are kept in the Side CRT hardware database maintained by the experiment.

SiPMs produce noise signals due to a thermal photon in the silicon, or due to trapped charge from a previous avalanche causing a second pulse. Thermal photons which originate inside the SiPM can cause an avalanche, leading to what is called the dark count rate [17]. Afterpulses come from trapped electrons in the silicon from a previous avalanche, and can cause a second pulse after the first has occurred [17]. Temperature is a key factor in the dark count rate, as higher temperature will mean more ambient thermal photons available to cause an avalanche.

2.1.2 Front-End Electronics

The Top and Side both use the CAEN DT5702 32 Channel SiPM Readout Board for Cosmic Rays Veto [3] as front-end electronics, and are often referred to simply as FEBs (short for Front-End Boards), pictured in Figure 2.2. Each channel on the board has a bias and signal pin on the

Figure 2.2: CAEN Model DT5702 Front-End Board used by the Top and Side CRT.

front of the readout. The bias pin allows for the SiPM attached to be held at the correct operational voltage, necessary to ensure that when a photon falls on the SiPM it causes the avalanche current that is read out by the signal pin. This current is measured, quenched after 87.5 ns [3] and an ADC counter converts the current into a number proportional to the amount of charge collected.

The A1702 requires a 5V input for power, using a keyed connector to ensure the board is not reverse-biased. There are two CAT6-compatible ports for data connection, and multiple boards can be daisy-chained together and connected to a single readout. There are two timing inputs, T0 and T1; T0 expects a Pulse Per Second (PPS) input to discipline the FEB's internal clock, allowing for nanosecond precision, while an input to T1 will force a trigger, useful for marking the approach of a beam trigger for our purposes. The FEBs also have a trigger input and trigger output; the trigger input alone does not cause the FEB to trigger, rather an onboard trigger of a given FEB must happen within 150 ns of a trigger input pulse in order for the FEB to trigger an output. The FEB does not necessarily require a trigger input, and will ignore this requirement if there is nothing connected to the port. If a triggering event occurs and is valid to be recorded, a 22 μs deadtime is induced on the FEB while the data is recorded to the internal buffer.

The triggering logic of the Front End Board is summarized in a block diagram shown in Figure 2.4. There are two modes that the FEB can be set to for onboard trigger logic: even-odd adjacent AND mode, or single channel 'OR32' mode. The even-odd adjacent AND trigger mode requires at least one adjacent pair of channels out of the 32 on the board (if channels are numbered 0-31,

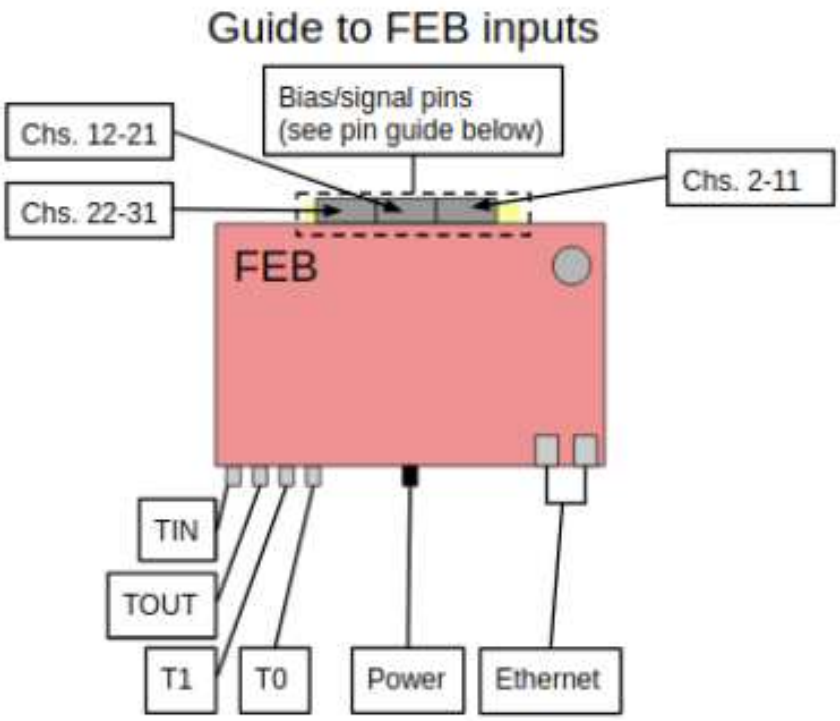

Figure 2.3: A diagram of the Front-End Board (FEB) inputs.

then an adjacent pair is 0+1, 2+3, 4+5....) to see a signal above background within 30 ns of each other. If one of these pairs sees this, the FEB will read out the ADC of each of the 32 channels to the DAQ. An example of the timing used for this triggering can be seen in Figure 2.5; the 'track and hold' signal referenced is the 150 ns window for any board with a TIN to see a signal from that TIN as described in the previous paragraph. The single channel OR32 mode simply requires any of the 32 channels to be above threshold to read out all 32 channels to the DAQ.

The FEBs have a trimmer resistor used to set the onboard bias voltage. This voltage can range from 20 to 90 V, and can be further adjusted via software settings to adjust between a +0.5 and +4.5 V offset using the bias setting in the FEB configuration file. This 0.5-4.5V adjustment can be done individually for each channel, allowing for fine-tuning of individual channel biases. This was done for the Top CRT during commissioning of the modules. The Side CRT has two possible bias settings for the ORMs, depending on which batch the SiPMs on the ORM are from; the bias setting is set based on the average voltage of SiPMs in the batch, so there will still be some spread

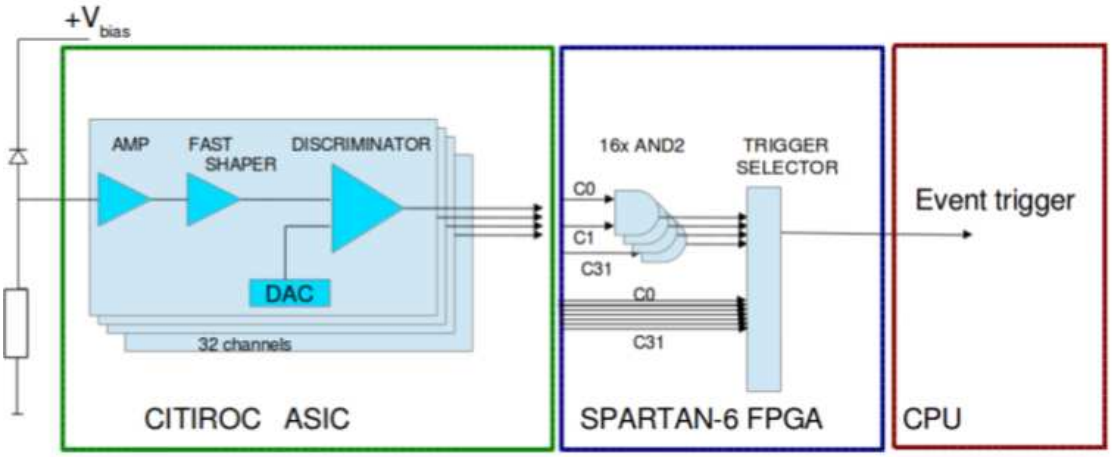

Figure 2.4: Block diagram from the CAEN FEB manual of the FEB trigger logic [3].

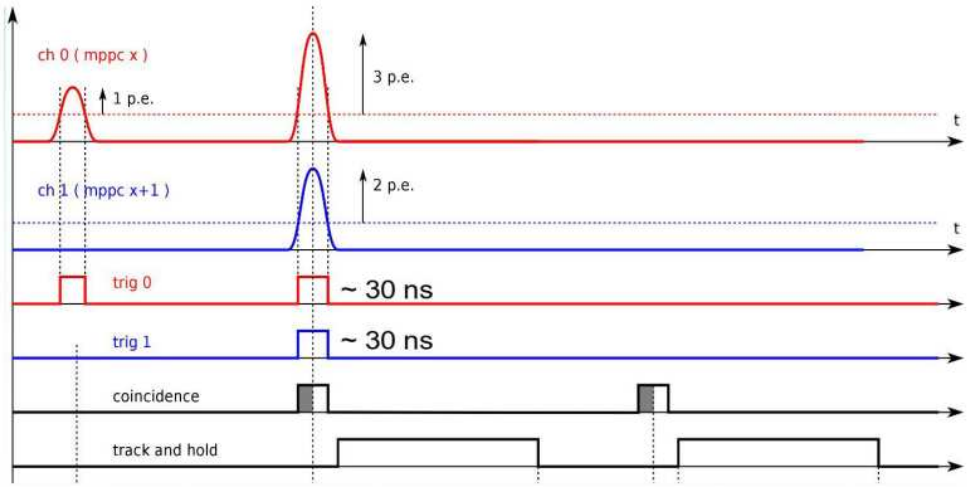

Figure 2.5: Timing diagram from the CAEN FEB manual of the timing logic used to determine if channels will create a trigger [3].

Table 2.1: Map of CRT servers to FEB chains.

CRT Region FEB chain	CRT Server name
Side CRT North Inner	icarus-crt01
Side CRT North Outer	icarus-crt01
Side CRT West-Center Inner	icarus-crt03
Side CRT West-Center Outer	icarus-crt03
Side CRT East-Center Inner	icarus-crt04
Side CRT East-Center Outer	icarus-crt04
Side CRT West-North Inner	icarus-crt05
Side CRT West-North Outer	icarus-crt05
Side CRT East-South Inner	icarus-crt06
Side CRT East-South Outer	icarus-crt06
Side CRT West-South Inner	icarus-crt07
Side CRT West-South Outer	icarus-crt07
Side CRT East-North Inner	icarus-crt08
Side CRT East-North Outer	icarus-crt08
Side CRT South Inner	icarus-crt09
Side CRT South Outer	icarus-crt09

in gains due to some uneven application of overvoltage to each individual SiPM, but will still be within no more than 0.10 V of the recommended operating voltage.

FEBs can be daisy-chained in groups of up to 256, having a series of 8 switches on the front of each device that can be used to set the address of the FEB in binary. This address applies to the last hex bit in the device's MAC address, allowing for each FEB to have a unique identification number on the server they are connected to. In practice on both CRT walls, the daisy chains are much smaller than 256. There are 93 FEBs that service the Side CRT, and 123 that service the Top CRT [18]. There are also 9 Bottom CRT FEBs, with one FEB per Bottom CRT module. The CRT data servers are located on the West Mezzanine of the Far Detector building and serve as the point of connection between the FEBs and the larger ICARUS DAQ system. Table 2.1 shows the correlation between FEB chains in each subsystem and their corresponding server.

The Top and Side FEBs each use their own range of mac5s on the hardware level, but for practical purposes in data analysis we have a shared system of identifiers for all FEBs in the combined Top+Side+Bottom system. The range of the collective software identifiers used for each subsystem during reconstruction of data products is outlined in Table 2.2. Later on in section 2.1.4, the

Table 2.2: Software Mac5/ID ranges of the CRT subsystems used during reconstruction.

CRT Subsystem	Software Mac5/ID Range
Side CRT	1-93
Bottom CRT	94-107
Top CRT	108-231

specifics of the correlation between the hardware and software IDs for the Side CRT FEBs will be provided in a series of figures detailing the arrangement of the FEB layout.

The FEB timing connections are the T0 and T1 inputs. When a highly stable pulse-per-second (PPS) signal is fed to this input, the FEB will use the period between pulses to further discipline its 20 MHz temperature-compensated voltage-controlled crystal oscillator, allowing for the calculation of correction frequencies to further improve the FEB's Allan variance to $1.9\text{x}10^{-9}$ over a 1 second observation period [19]. All Top and Side CRT FEBs get a PPS signal distributed from the trigger rack GPS source, distributed to the timing distribution boxes used by both subsystems.

2.1.3 Top CRT

The Top CRT (including the Top Roof and Top Rims) is entirely made of square panels, each of which contains two layers of scintillator (see Figure 2.6). The bars in both layers run in perpendicular directions to create what is called X-Y coincidence; by looking for signals in both layers, and isolating the triggered channels, reconstruction can find the crossing point of the triggered scintillator strips and save it as the CRT Hit location. Each strip is 23 cm wide and has two fibers running the length of it, with each fiber 6 cm from each long edge of the strip. This means modules have 64 23x23 cm squares which act as potential CRT Hit locations when signals are reconstructed from data, and any hits found in a square are reconstructed at its center. The bulk scintillator also differs from the Side, using different dopants in the bulk polystyrene: 2% pTP and, depending on the layer, 0.05% or 0.03% POPOP [13].

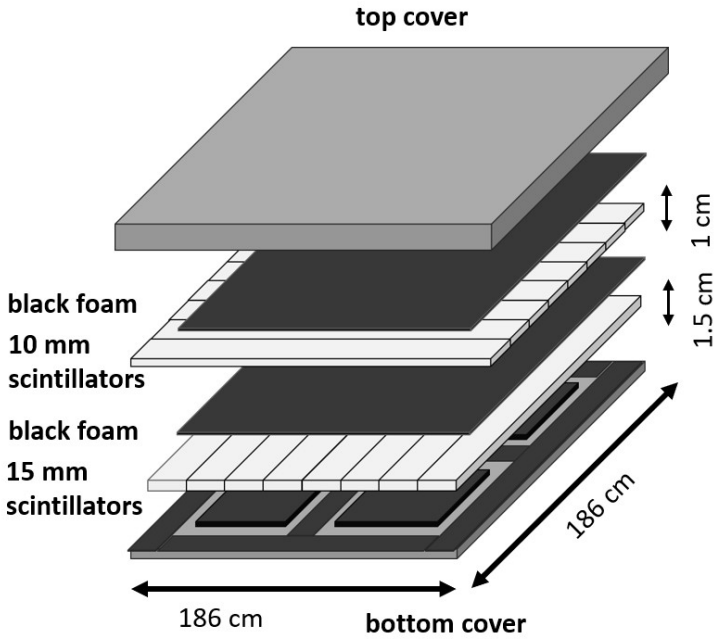

Figure 2.6: An exploded view of the Top CRT modules.

2.1.4 Side CRT

The Side CRT uses repurposed scintillator modules taken from the decommissioned MINOS [14] experiment. The modules are 8 meters long, 80 centimeters wide and a centimeter in thickness. There are 20 individual scintillator strips running the length of each module, each strip being 4 cm wide and 1 cm thick. Each strip has a single optical fiber running along its length; optical fibers are then gathered in the module snout for readout by light sensors as shown in Figure 2.8. The Side CRT also uses Silicon Photomultipliers as light readout, allowing it to also use the same front-end electronics. Like the Top CRT, the Side CRT also makes use of doped polystyrene scintillator. According to technical descriptions of the MINOS scintillator, polystyrene was mixed with 1% by weight of 2,5-Diphenyloxazole (PPO) and 0.03% by weight of 1,4-bis(5-phenyloxazol-2-yl) benzene (POPOP) [14]. These are the organic fluours which produce scintillation light as a charged particle passes through, and differ in overall composition from the Top panels. The strips were co-extruded with titanium oxide on the outside to prevent other light sources from entering into the strips, unlike the Top scintillator strips which were painted with a reflective layer. The MINOS scintillator has aged since its construction in 2001/2002, with estimates from the group

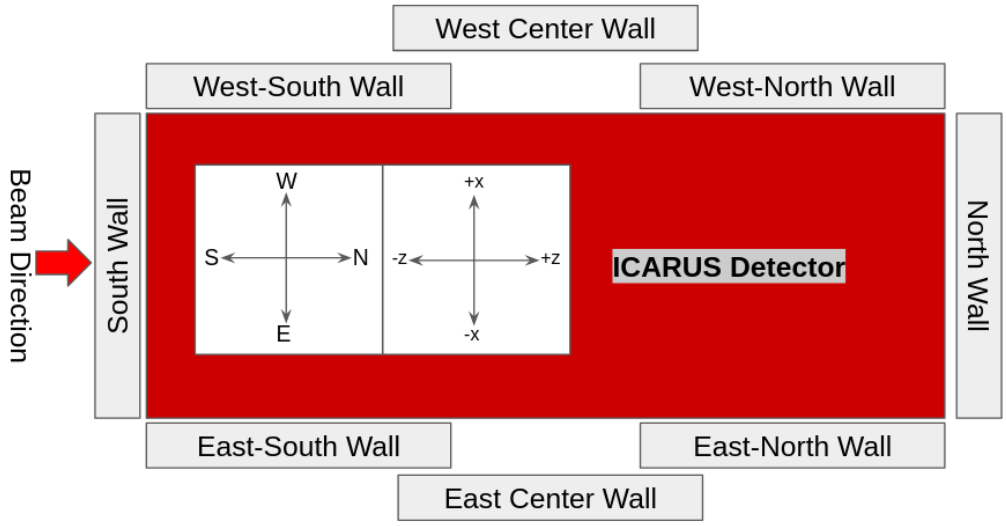

Figure 2.7: A top-down view of the Side CRT walls and their relative positions.

at the time that the light yield loss was expected to be 1.2% per year [14]. The detector at the time used Hamamatsu R5900-00-M16 PMTs for readout and observed that minimum ionizing particles (MIPs) which passed through the center of the modules to be roughly 6 photoelectrons summed over both ends. Projecting this forward to 2024, a similar PMT should measure roughly 4.6 photoelectrons. This was done using PMTs, which have less average light yield compared to the SiPMs being used now.

Figure 2.7 shows an overview of where all eight Side CRT walls are located with respect to the detector and the detector geometry.

Optical Readout Module design

The Side CRT group was tasked with finding a way to read out the MINOS module snouts; in their previous life at MINOS, the panels were read out by PMTs. In order to reduce the amount of high voltage necessary to run the CRT, as well as from previous experience using the devices in other R&D projects at CSU, Silicon Photomultipliers were the obvious choice. CSU Engineers Dave Warner and Jay Jablonski worked with Professor Robert Wilson and graduate student Chris Hilgenberg to develop what became known as the Optical Readout Module (ORM) which would cover all of the optical fibers on the MINOS snout, pictured in Figure 2.9. Each SiPM in an ORM

reads out two of the fibers coming out of the snout as shown in Figure 2.10. Several prototype modules were produced before the final design was settled on, which I will discuss here.

The ORM is made of 3 separate layers sandwiched and secured together mechanically via two screw, washer, and nut assemblies. The outermost layer of the ORM is a black plastic casing which houses everything, providing mechanical support an optical isolation for the SiPMs once installed. An important feature is the onboard alignment pin for securing to the MINOS snout, along with the small hole for a metal alignment pin which is fitted snugly into the MINOS snout. Alignment is crucial for the ORMs, as each SiPM had to be within 0.15 millimeters of their optimum placement in order to still fully cover two fibers at once based on a study performed early on in development. The middle layer is an alignment plate for the SiPMs, used to hold them in place during soldering and kept on to get proper spacing between the MINOS module fiber ends on the snout and the faces of the SiPMs. The innermost layer is the PCB which the SiPMs are soldered on; each ORM has 10 3x3 mm Hamamatsu S14160-3050HS [13] SiPMs soldered on this PCB in an arrangement that allows each SiPM to read out two optical fibers from the MINOS snout.

ORMs have a handedness due to the need for the active SiPMs to be in different positions with respect to the onboard alignment pin (see Figure 2.11). The handedness was eventually called normal or inverted, with the position meaning the closeness of the SiPMs to the onboard alignment pin. This is necessary to fit onto the two kinds of snout on each MINOS module due to the relative placement of differently-sized alignment pins and which fiber ends are active on the snout.

Optical Readout Module Production at CSU

Production of the Optical Readout Modules was done at the CSU High Energy Physics lab. Engineers Dave Warner and Jay Jablonski oversaw undergraduate engineering students Krista Grossman, Will Mingus, Jameson Richard, and Will Sheridan in their efforts to make use of a solder stencil and soldering oven to properly install the SiPMs and 20-pin connector on the printed circuit board, then install the board inside the ORM housing. Once fully assembled, the ORMs were placed first into zip-up anti-static bags, then into a holding box which signaled the ORMs were ready for Quality Control (QC) testing.

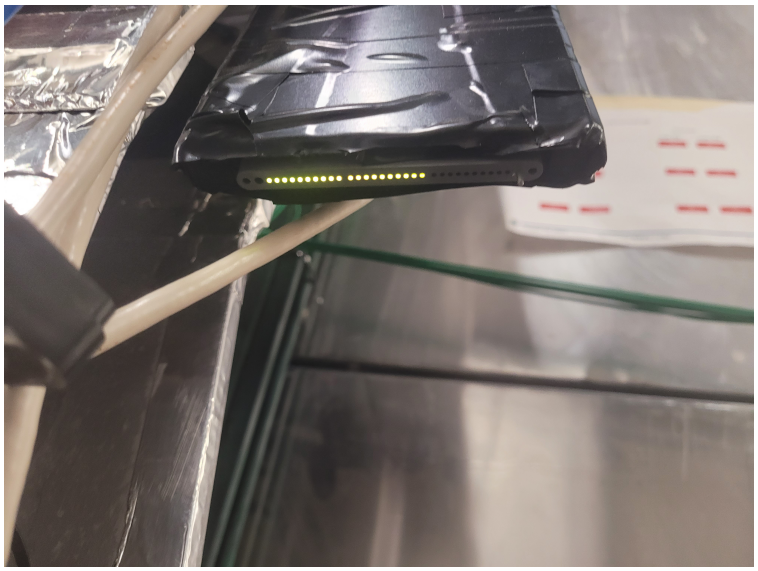

Figure 2.8: A MINOS snout with light illuminating the other end to make the active channels identifiable.

Figure 2.9: Optical Readout Module.

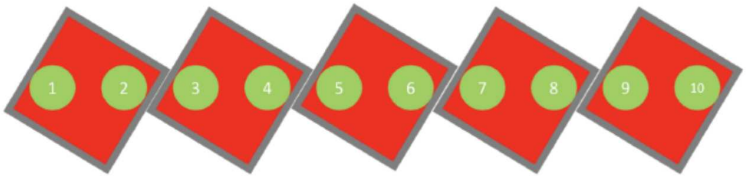

Figure 2.10: Alignment needed to have an ORM read out MINOS module snout fibers.

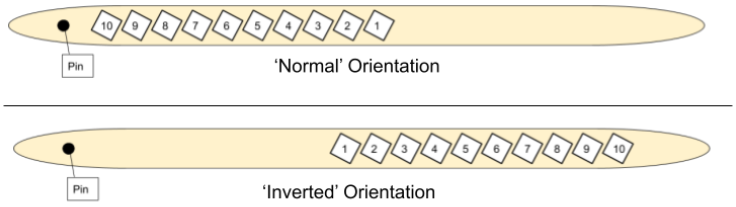

Figure 2.11: Cartoon of ORM orientation with respect to the onboard alignment pin. SiPMs are numbered in order of channel number; the orientation does not change the order in which SiPMs will be read out by a 20-pin connector.

Optical Readout Module Quality Control Tests at CSU

Quality control on the Optical Readout Modules (ORMs) consisted of two major checks: one for Silicon Photomultiplier (SiPM) alignment with its onboard alignment pin, and another for correct response by the SiPMs to a pulsed LED signal. Alignment checks were always done first to ensure that production was not having difficulty keeping the SiPM alignment in tolerance, which was necessary to achieve to within 0.15 mm for each SiPM, as well as check for rotation to ensure it was always 28° with an allowed error of 1°.

Checking alignment required use of a Coordinate Measuring Machine (CMM). The CMM consists of a camera held above a glass stage that can be moved along two horizontal axes; the focus on the camera lens was used to determine distance between the camera and the object. As the stage was moved, a display with coordinate information would change while the view through the camera would change on a nearby computer screen. By setting up a custom axis to be along the middle of the ORM by use of the onboard alignment pin and the hole for the other alignment pin, the relative positions of the individual SiPMs could be measured with respect to the alignment pin.

Engineer David Warner provided the positions of where the centers of each SiPM should ideally sit. A foot pedal input was installed for the CMM which allowed for the operator of the CMM to simultaneously hold the CMM on a precise location with the control knobs and have the coordinate information output to a spreadsheet. All four corners of a given ORM would be measured, using the corner where the packaging and silicon cells met as a reference. By averaging the positions of all four corners, a center location could be extracted for that SiPM as well as that SiPM's rotation. Quickly a set of functions that could be copied and pasted into each spreadsheet was developed that did all of the calculating of each SiPM position and angle with respect to the ideal, and any with even a single SiPM out of place was set aside and marked as bad.

If a module passed its CMM check, it would be moved to be tested for light response. This was a simple check done with a rig created by engineer Jay Jablonski which allowed for up to 3 ORMs to be easily slotted in, facing a light emitting diode (LED) with a light guide between them

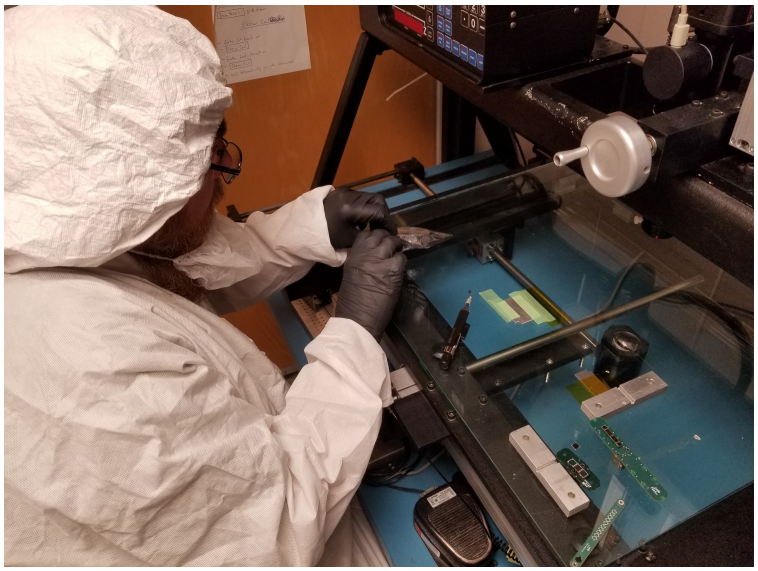

Figure 2.12: The CMM being used by CSU technical staff Jay Jablonski.

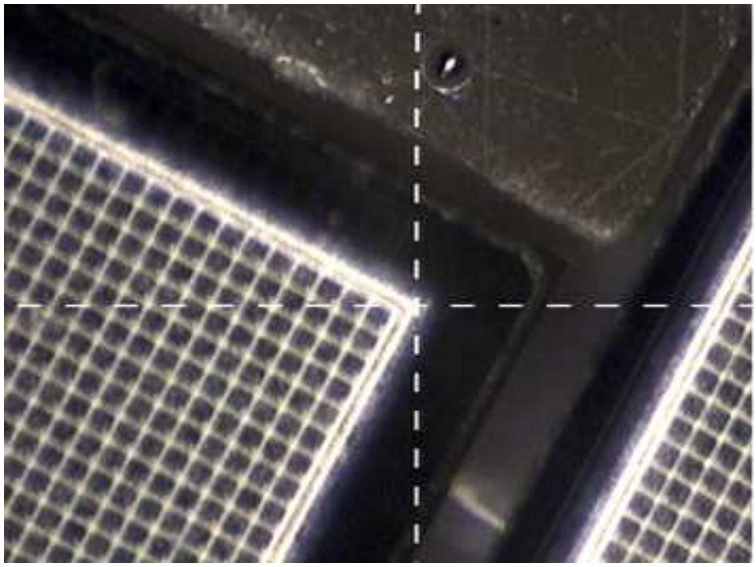

Figure 2.13: Close-up view of a SiPM through the CMM camera.

to maximize exposure. The LED was pulsed with an external pulser, and the ORMs could be read out by a prototype FEB that was on loan to the CSU group by Igor Kreslo from the University of Bern. An example of this setup can be found in figure Figure 2.15, which shows the ORM rig facing the LED down the light guide.

The Front End Board was operated with a prototype standalone DAQ that allowed for histograms of observed data recorded by each channel on the FEB. This includes a page that allows observation of all 32 channels, allowing for quick surveying of all channel responses. It also allows for the user to set an acquisition time in seconds to control how much data would be collected in a given run of the DAQ.

There were a total of three tests run on each set of ORMs to complete the test battery. The LED would be held at a constant voltage throughout all three, however an initial informal test of varying the voltage was always done to check that no channels had 'stuck' ADC. This was very occasionally observed, a SiPM's response would appear to not change with different applied bias voltages, and any sign of this would cause the ORM to be set aside as bad. The first test had the FEB threshold set to setting 290, roughly a 6 PE threshold from our experimentation with the Bern FEB being used at the time. The LED was then pulsed and data taken for 60 seconds. The mean light yield would then be surveyed on the view that allowed all ADC histograms on the FEB to be seen, and allowed for quick identification of any problem channels. The threshold would then be dropped to 4.5 PEs and run for 60 seconds again to see how much of a shift could be observed in the signal. The final test included plugging in an input to the FEB's TIN from the LED pulser to force the FEB to only read out at the same time the LED was being pulsed, with the goal being to obtain a high-quality signal and running for an additional 60 seconds. The mean light yield from each of these tests would then be calculated and saved for each SiPM on each ORM. Each data set also allowed for a gain measurement, so the gain from those measurements is also saved to the permanent CRT hardware database.

Once 3 ORMs were ready to be tested, they were be placed in the dark box in the ORM holding rig, with their positions for this test noted in a log. Data would be taken with the LED at different

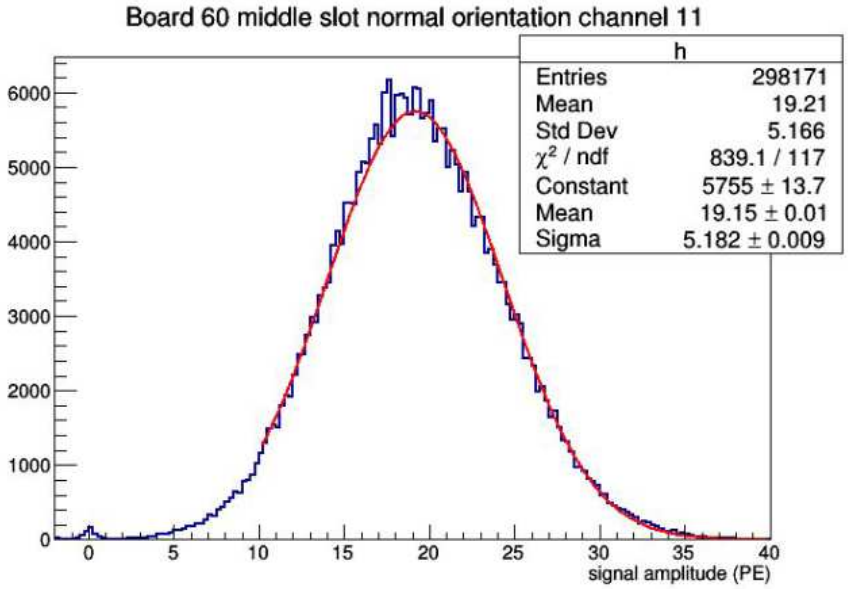

Figure 2.14: Example light yield measurement of a SiPM at the CSU test stand.

voltages to accomplish different goals. Low light was used to create spectra that could be fit by the calibration algorithm to check that the pedestals and gains of each channel were not out of line with the other ORMs. More light would be used to see if there was an obvious change in the signal recorded by each channel; this done by direct observation of the signals coming from the standalone DAQ. The QC tester would increase the applied voltage to the LED, and watch for a corresponding increase in signal size from all of the connected channels on the standalone DAQ screen. If any channel appeared to be acting unusually from either test, it would be set aside and marked as bad.

If everything appeared to be in order with the ORM, it would be repackaged in its anti-static bag and placed in a holding area until a request came for shipment. Once there were enough to begin shipping, each anti-static bag would be further wrapped in anti-static foam before being loaded into either a resealable plastic bag with other ORMs, or in a cardboard box which was used for the last ORMs made at CSU. ORMs of the normal and inverted types were always stored together for organizational purposes. Three ORMs were sent to the University of Houston for their DAQ test stand and remain there. The rest were either shipped via mail, or taken by myself when I moved

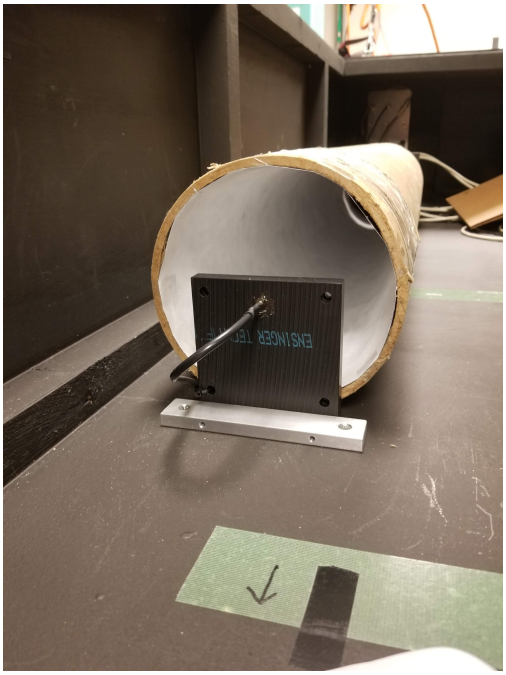

Figure 2.15: Dark box used at CSU for initial light response checks of ORMs.

from Colorado to Fermilab in the summer of 2019, ready to be further tested at the Wideband test stand.

Additional Quality Control Checks at Fermilab

Much of the work at Fermilab with the ORMs has been documented in Chris Hilgenberg's doctoral thesis [13]. ORMs were brought to Fermilab and tested on a setup which used three MINOS modules stacked on top of each other (with small foam spacers between). The top and bottom of the three modules were referred to as the reference modules, while the middle was the test module. ORMs undergoing the QC test would be placed on the test module, which had one end for both the normal and inverted type modules. There were also four hodoscopes on top of the modules, two at each end to cover all of the strips inside the modules. See Figure 2.17 for a diagram of this setup, and Figures 2.18 and 2.19 for reference to what the setup looked like during testing.

As documented in [13], there were early signs of the CAEN FEB's noise sensitivity at Wideband. Several weeks were spent getting the FEBs to behave in a reliable way; initially, any prox-

Figure 2.16: ORMs in anti-static bags and anti-static foam awaiting shipment to Fermilab.

imity of anything even mildly conductive or minor shift in cable positionings would cause large shifts in observed trigger rates. After careful re-cabling of the power inputs to keep them separated from the signal cables, grounding the FEBs directly through a chassis screw, and isolating the CAEN-provided power supplies electrically on anti-static foam pads, a workable test environment was achieved.

Once a stable configuration was found, testing began in earnest. Francesco Tortorici and Catia Petta from the University of Catania, Antoni Aduszkiewicz from the University of Houston, Chris Hilgenberg from CSU, Britny Delp who was a summer research student at Fermilab, and myself all took part in doing the ORM testing in shifts. The testing regimen began with installing a normal and an inverted ORM on the test MINOS module. Once installed, the ORMs would be connected to the test FEBs, which were on a daisy chain with the other FEBs running the reference modules. A light leak check was conducted, and if all was well testing could commence. A standard check of event rates was done across all 6 ORMs (the two test and four reference) to ensure that the test ORMs did not have too many or too few compared to previous ORMs, with the reference modules serving as a way to check that any excess/lack of events was not due to any external factors. Then a data run would be taken in which the trigger outputs of each of the test FEBs was counted and

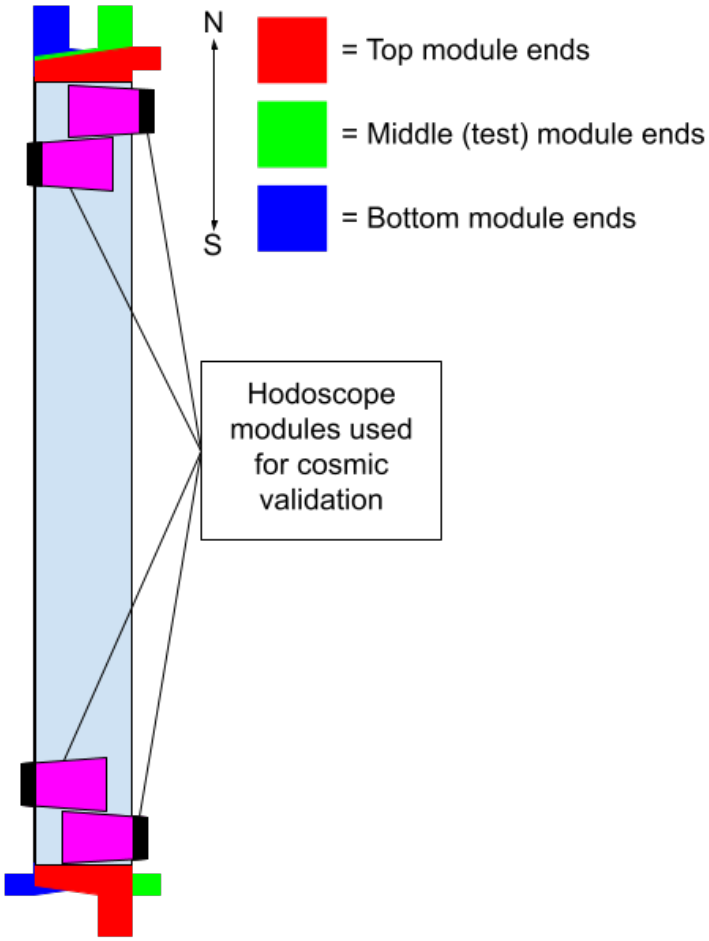

Figure 2.17: Overhead-view of the test setup at Wideband. The three stacked module ends are differentiated by color, as pointed out in the legend in the image. The hodoscopes are pink to differentiate them from the other objects, with their 'dead' area which housed the electronics running the PMTs in black.

Figure 2.18: University of Houston postdoctoral researcher Antoni Aduszkiewicz and (at the time) CSU graduate student Chris Hilgenberg align the hodoscopes on the MINOS modules at the Wideband test stand. Photo credit: Robert Wilson.

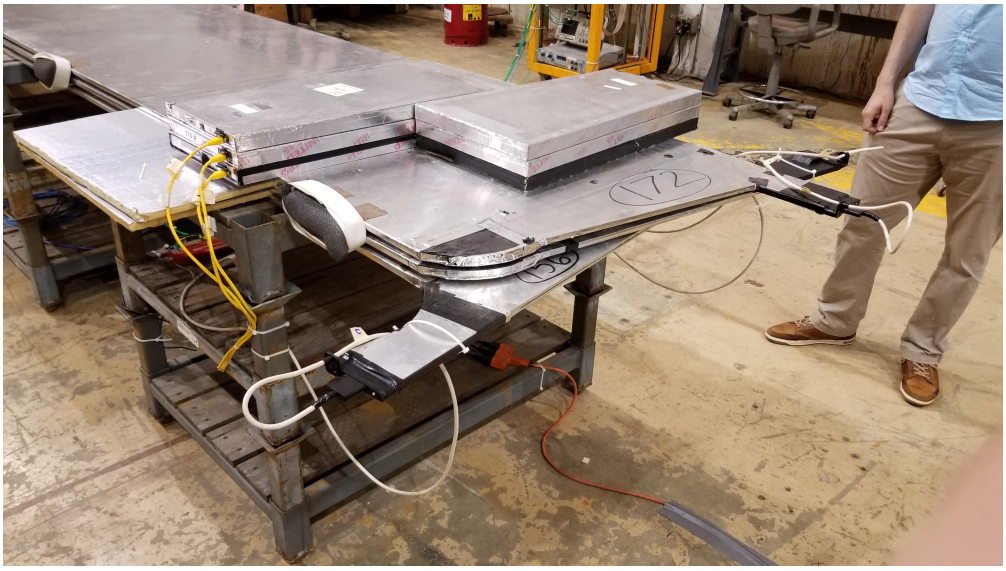

Figure 2.19: A closer look at the south end of the Wideband test stand to better show the module ends and placement of hodoscopes. Photo credit: Robert Wilson.

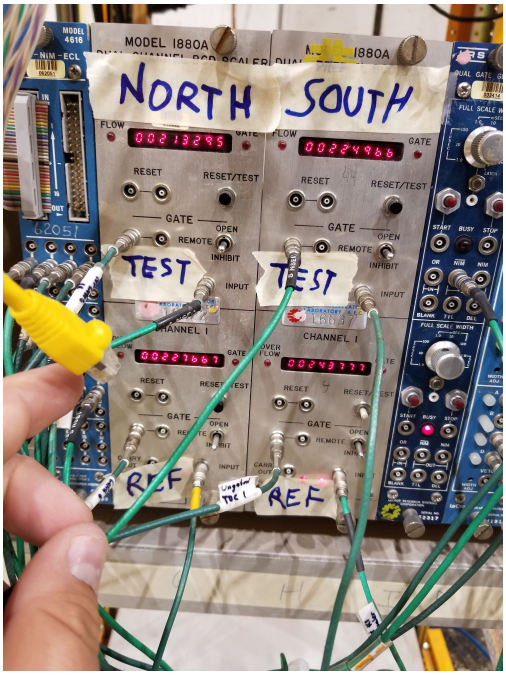

Figure 2.20: The counters used at Wideband to count signals seen by the hodoscopes compared to those seen by the test modules.

compared to the number of trigger outputs in the reference modules, allowing for a simplistic efficiency measurement to be conducted on each ORM. The data was kept and archived, and the tests were tracked on a spreadsheet including the efficiency to build an understanding of typical ORM behavior.

To do an efficiency test, the hodoscopes had their outputs connected in parallel to a single line that carried all hodoscope triggers. These signals were then sent to the trigger inputs of all test FEBs as well as two counters on the test utility rack. The counters would count the number of triggers from the hodoscopes, as well as the number of triggers that came from the FEB TOUTs. This allowed for an easy calculation of the number of triggers from cosmics in the hodoscopes versus the number of triggers from the FEBs that were coincident with the hodoscope signals, allowing for an easy calculation of the efficiency of each test ORM. See Figure 2.18 for a picture of the overall setup. Figure 2.20 shows the counters used for both of the test modules; North and South were used to denote the inverted and normal test snout respectively.

The average efficiency of the test module with a normal type ORM was found to be 91.3%, while the average efficiency with an inverted type was found to be 93.0%. The difference between the average end efficiency is likely due to a few factors. First, the amount of light coming out of a strip at one end can differ from that at the other, even if the light is produced directly in the center of the strip due to uneven response to scintillation light in the fibers, potentially causing more light loss on one end than the other. Also, the cosmic hodoscopes used along the module may themselves have different detection efficiencies, leading to fewer being validated on one end versus another.

Any ORM with an efficiency more than 1% below the average was marked as bad; these were set aside to be used for test stands and as backups if all other ORMs failed. Roughly 10 of these ORMs are stored in the Side CRT cabinet in the ICARUS detector pit in a cardboard box, with a few being stationed in the dark box setup on floor 6 of Wilson Hall at Fermilab.

Data was taken from throughout the runs to measure the response of each SiPM from the data obtained while the ORMs were attached to the test MINOS module. The average light yield for each SiPM was measured along with the gain measured for the same channel and saved to the CRT Hardware database for each SiPM. For normal ORMs, the average SiPM light yield was 19.3 PEs with a standard deviation in the averages of 1.7 PEs (see Figure 2.21 for the distribution); for inverted ORMs, the average SiPM light yield was 16.9 PEs with a standard deviation in the averages of 1.7 PEs (see Figure 2.22 for the distribution). This sets a scale of expected signals for throughgoing muons at roughly normal incidence for the Side CRT modules, though the individual MINOS modules themselves have some variation in light yield from the scintillator.

271 ORMs were needed for the full Side CRT installation. A total of 351 ORMs were produced at CSU. Out of these, 302 would be put through the full testing battery at Fermilab. Three ORMs that didn't pass the testing were sent to collaborators at the University of Houston for use in a test stand prior to the Fermilab test stand being constructed. The remaining ORMs were rejected either due to bad SiPM alignment, or with if one or more SiPMs were not responding as expected in the initial checks done for light response at CSU.

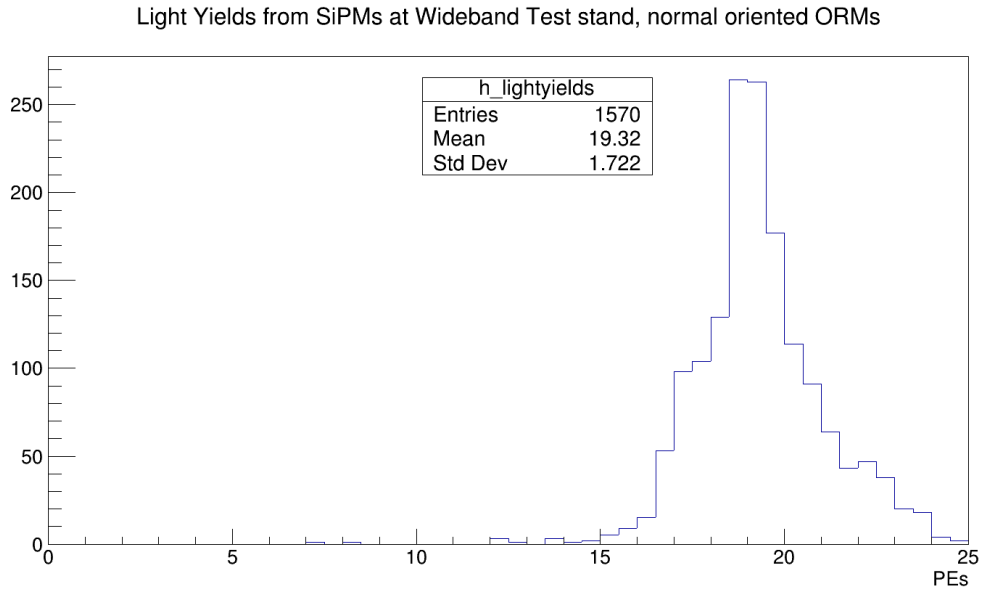

Figure 2.21: SiPM light yield from the Wideband test stand for normally oriented ORMs.

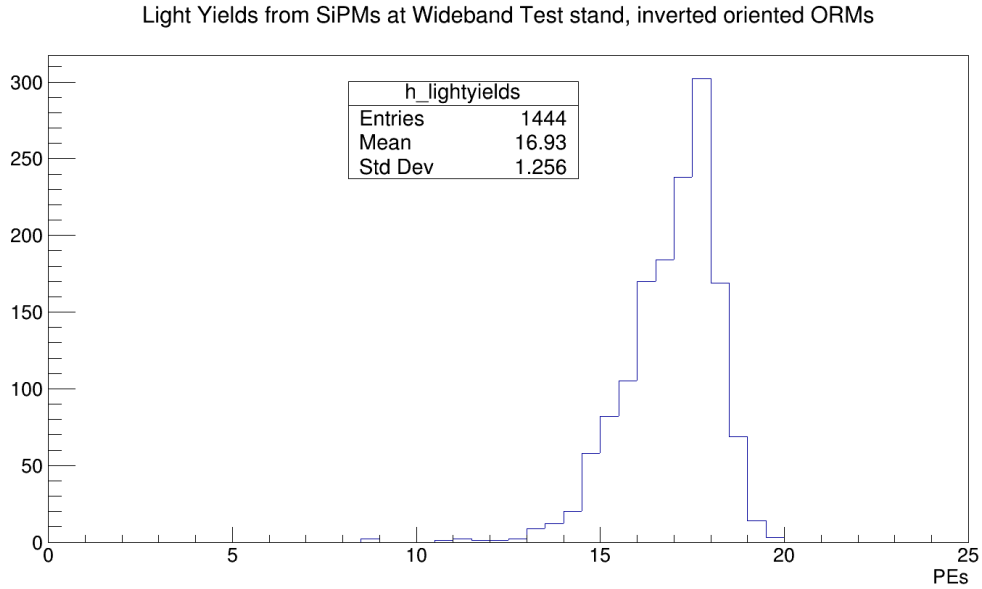

Figure 2.22: SiPM light yield from the Wideband test stand for inverted oriented ORMs.

MINOS module arrangement

The Side CRT consists of eight walls: North, South, West-North, West-Center (Rolling), West-South, East-North, East-Center (Rolling), and East-South. The North and South walls have their own module layouts, requiring MINOS modules that had been cut along their length in order to fit into the space, the procedure for which will be discussed in Section 2.2.1. All walls are double-layered, with all but the South wall in what is referred to as XX coincidence, meaning that strips in the modules run horizontally parallel to each other. The South Wall has XY coincidence, as the outer layer has modules in a vertical orientation.

The East and West Side CRT regions are separated into East/West-North, East/West-Center, and East/West-South; the first direction states whether the wall is on the detector east or west side, then the second direction gives the relative position of that wall along the north/south axis. The Center walls are both on rolling platforms and sit slightly in front of the other sections on a given side. The rolling platforms allow access to the readout electronics and module ends which would otherwise sit behind the center wall. Due to overhanging cable trays which run from off-detector equipment to the top of the detector, the Center walls are 8 modules tall (which due to the double layered nature gives a total of 16 modules for each Center wall), while the other walls on the East/West side are 9 modules tall.

On all walls with XX coincidence, a 1 inch vertical offset was made between layers to avoid having gaps in the modules line up with each other. This was done by ensuring that the starting modules of each wall were put at a slight offset, then requiring a new vertical layer of modules be installed as close to flush with the module below it as possible.

The South Wall is where the BNB neutrinos enter the detctor, while the East walls are where NuMI neutrinos will enter [20]. These Side CRT regions could be used in searches for muons that are induced by neutrino interactions just upstream of the detectors, for what are often called ‘rock’ or ‘dirt’ muons.

FEB Arrangement

A key factor in reconstructing particle interaction positions in the Side CRT is how the FEBs are arranged. Analyzers need to know each FEB's connected ORMs/MINOS module ends so that reconstruction can be performed. As discussed in section 2.1.2, FEBs have both a software ID used in reconstruction, as well as a hardware identifier that is referred to as a 'mac5' because the set of switches on the face of the FEB allow for the setting of the last bit of the device's mac5 address. These identifiers are referred to as the software mac5 and the hardware mac5. Table 2.3 contains all of the associations between the hardware and software IDs for the Side CRT FEBs. Figures 2.23 through 2.32 show the relative placement of FEBs with their software IDs and hardware IDs.

All walls save for the South Wall follow the general principle of how inner/outer MINOS modules correlate to inner/outer FEBs as shown in Figure 2.23. All Side walls save the South have four columns of FEBs; two columns are located near each edge of the wall. Any FEB which does not have another FEB between it and the MINOS module ends is called an outer FEB, and thus is connected to the outer Side CRT layer. Similarly, any FEB that has a FEB between it and a module end is called an inner FEB, and thus is connected to the inner Side CRT layer. For an example of this, Figure 2.23 has labels for the inner and outer layers, as well as guides as to which FEBs correspond to the inner and outer layers. The remainder of the figures are missing these guides but show the overall geometry for completeness.

Each FEB has 32 active channels, while the ORMs have 10 channels, so the maximum allowable modules per FEB is three. Thus, the FEBs are typically vertically positioned in front of the module which occupies its middle channel range to allow for cables from all three ORMs on the MINOS snouts to reach the pins. For the Side Center walls which only have eight modules, the FEBs with only two modules attached are on the pit level, occupying channels 2-21.

Trigger, timing and timestamp distribution

CRT FEBs have two timing inputs as well as a trigger input and a trigger output. The two timing inputs are called T0 and T1; if a pulse per second input is provided to T0, it will discipline the onboard clock, while T1 can be used to generate a trigger event which is useful for passing

Table 2.3: Side CRT Hardware ID to Software ID map.

Hardware ID	Software ID	Hardware ID	Software ID	Hardware ID	Software ID
1	92	36	54	67	29
3	88	37	71	68	27
4	90	38	69	69	25
5	86	39	67	70	26
6	93	40	68	71	28
7	89	41	70	72	30
8	91	42	72	73	11
9	87	43	65	74	9
10	23	44	63	75	7
11	21	45	61	76	8
13	19	46	62	77	10
14	20	47	64	78	12
15	22	48	66	79	5
16	24	49	47	80	3
17	17	50	45	81	1
19	15	51	43	82	2
21	13	52	44	83	4
22	14	53	46	84	6
23	16	54	48	85	73
24	18	55	41	86	74
25	59	56	39	87	75
26	57	57	37	88	76
27	55	58	38	89	79
28	56	59	40	90	78
29	58	60	42	91	77
30	60	61	35	92	81
31	53	62	33	93	80
32	51	63	31	94	83
33	49	64	32	95	84
34	50	65	34	96	85
35	52	66	36	97	82

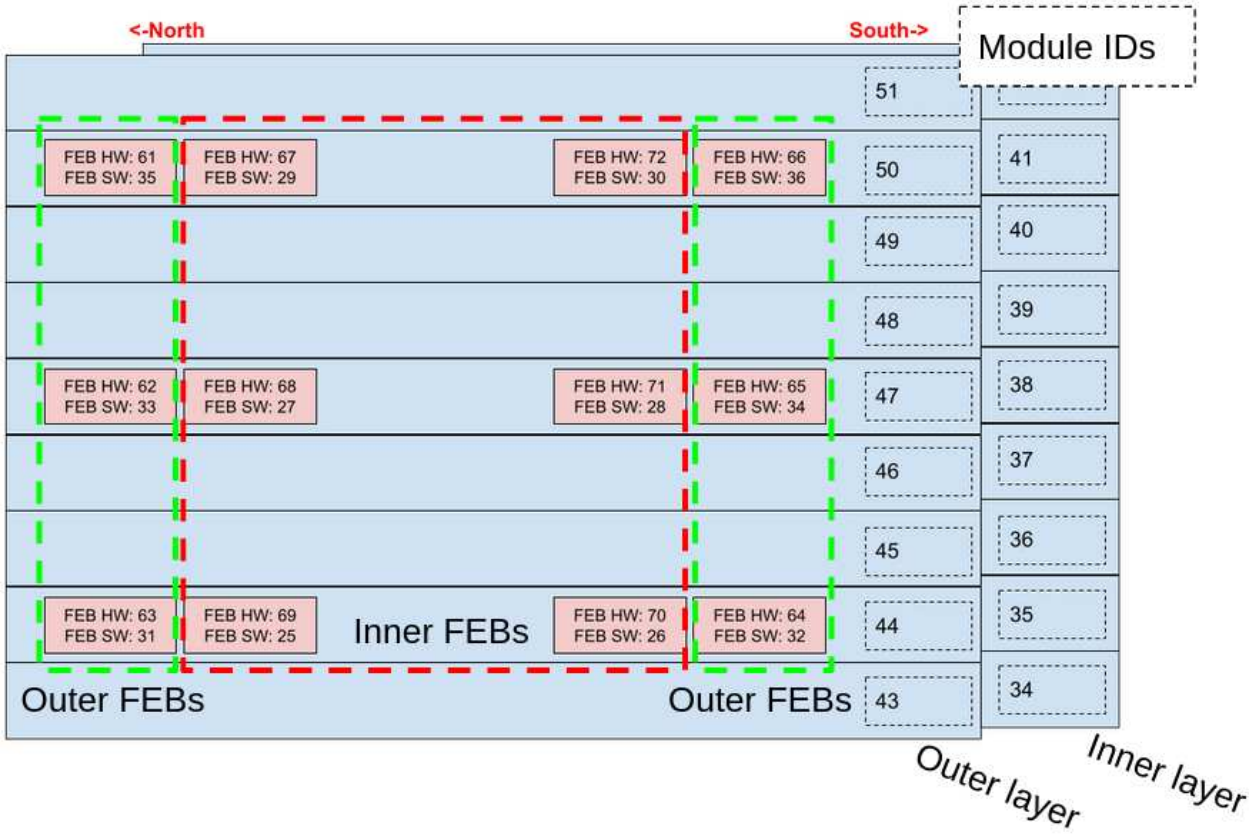

Figure 2.23: Diagram of the West-North Wall FEBs, MINOS modules and how FEBs correspond to MINOS modules; following figures follow the same convention of inner vs. outer FEBs corresponding to MINOS modules, though with different FEB and MINOS module ID numbers.

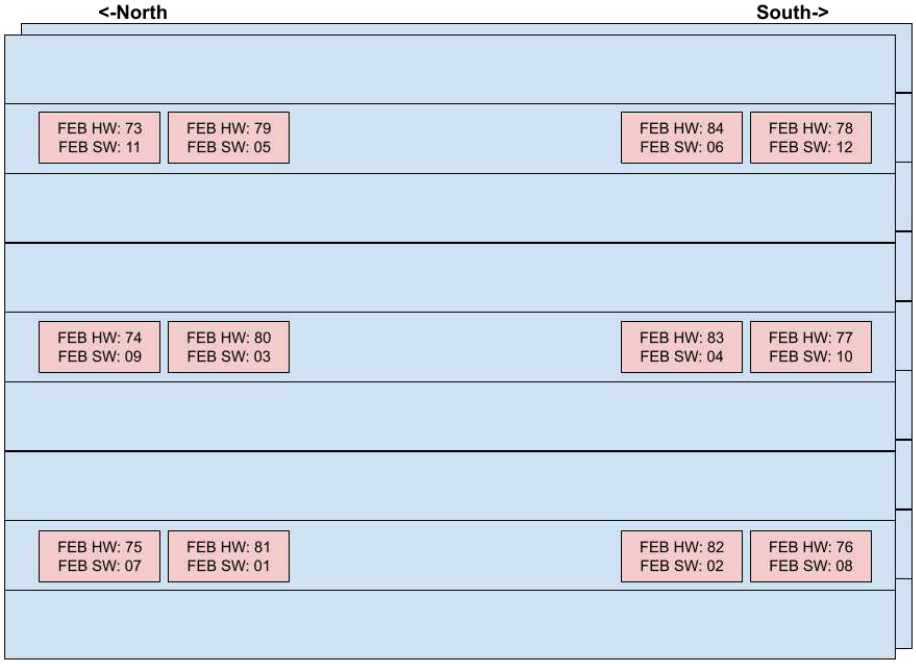

Figure 2.24: West-South wall diagram.

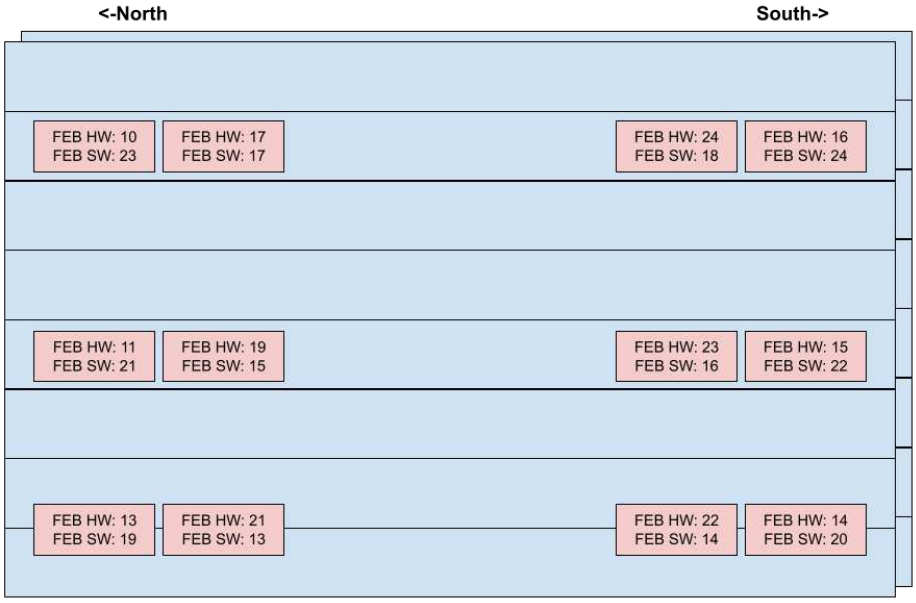

Figure 2.25: West-Center wall diagram.

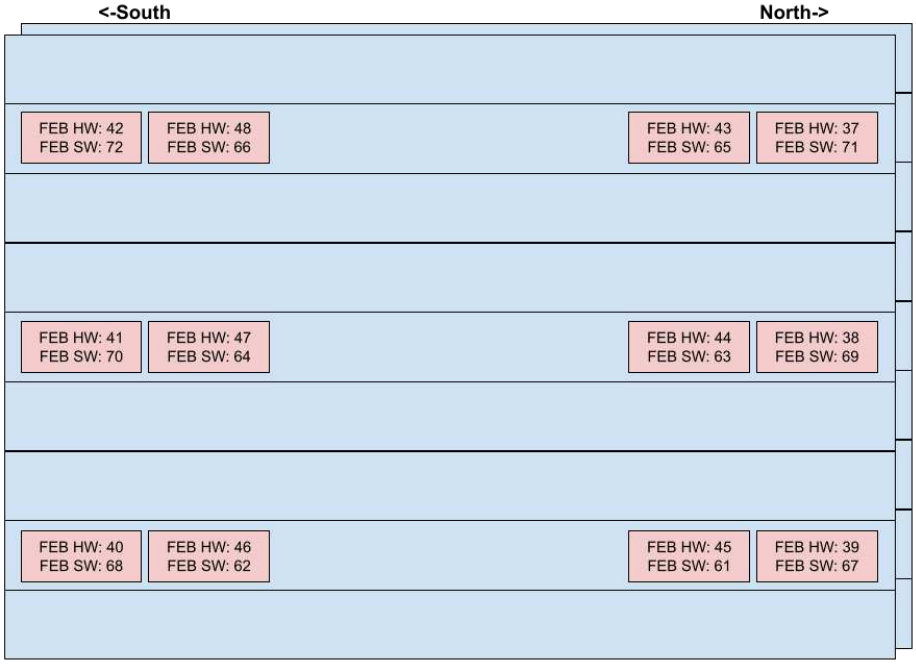

Figure 2.26: East-North wall diagram.

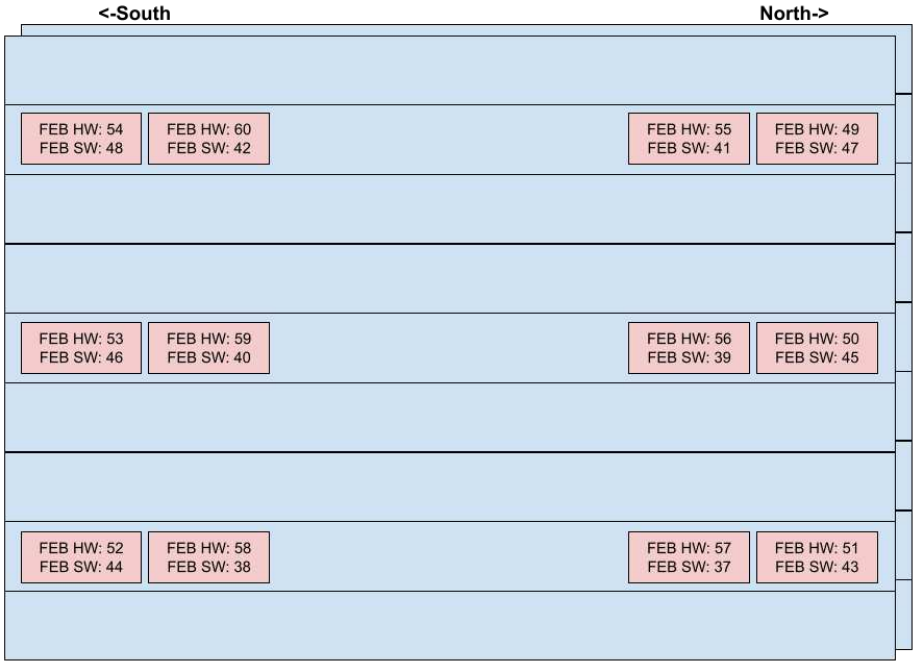

Figure 2.27: East-South wall diagram.

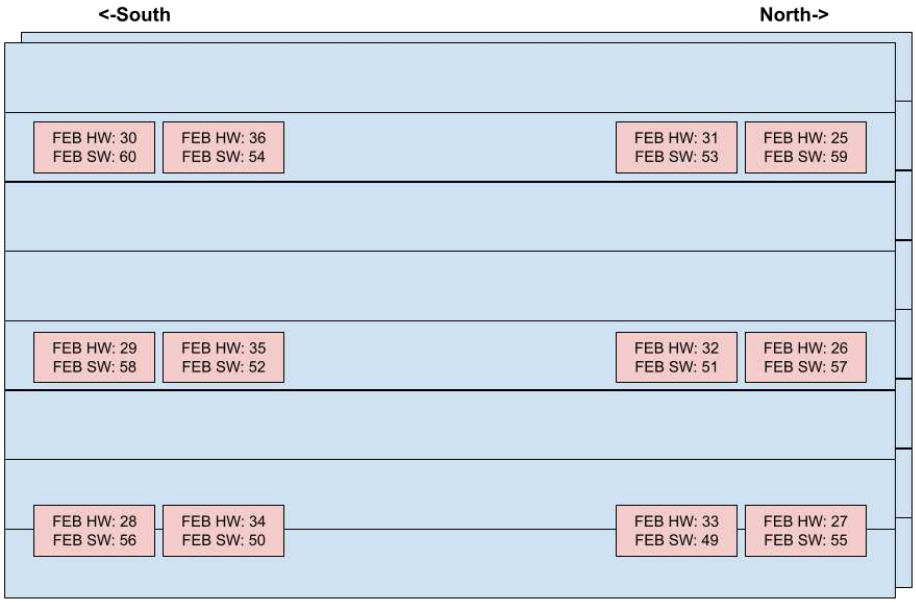

Figure 2.28: East-Center wall diagram.

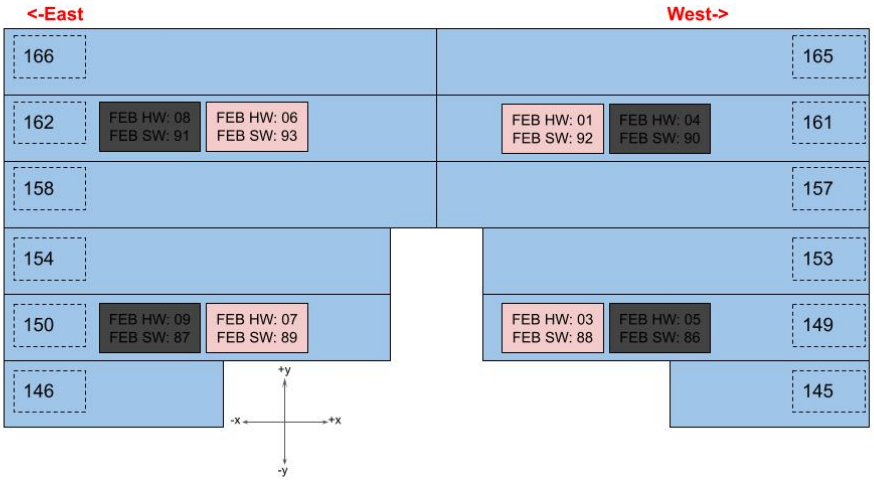

Figure 2.29: Inner North wall diagram. FEBs serving this layer are in light red, those serving the outer layer are darkened.

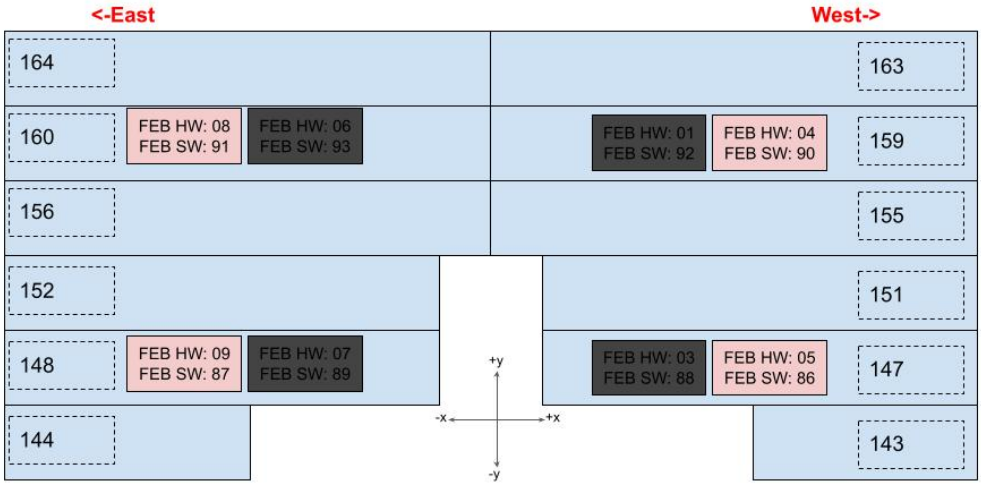

Figure 2.30: Outer North wall diagram. FEBs serving this layer are in light red, those serving the inner layer are darkened.

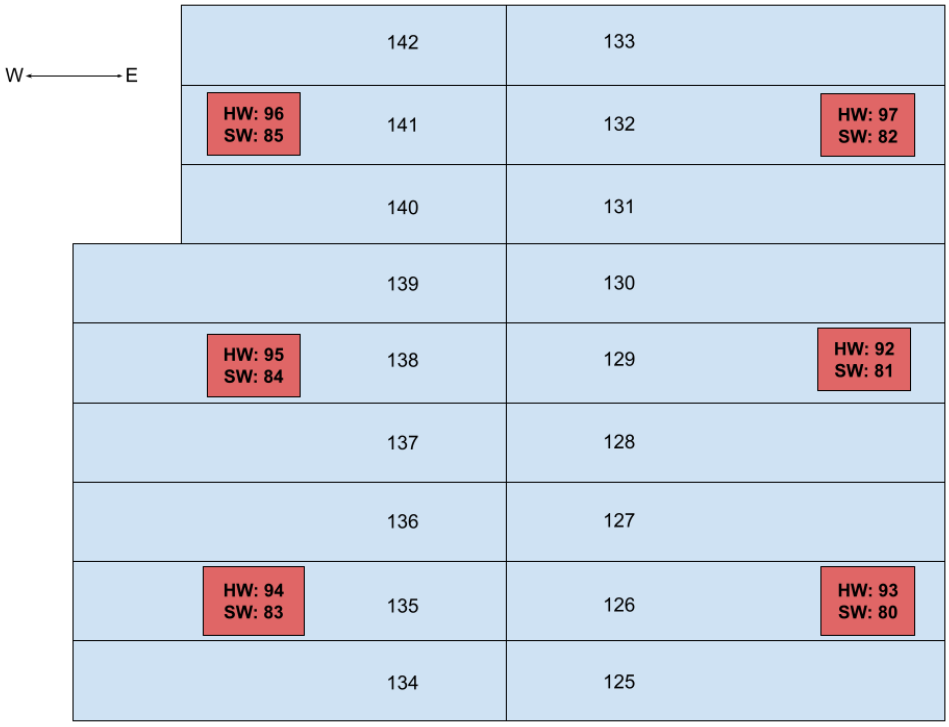

Figure 2.31: Inner South wall diagram.

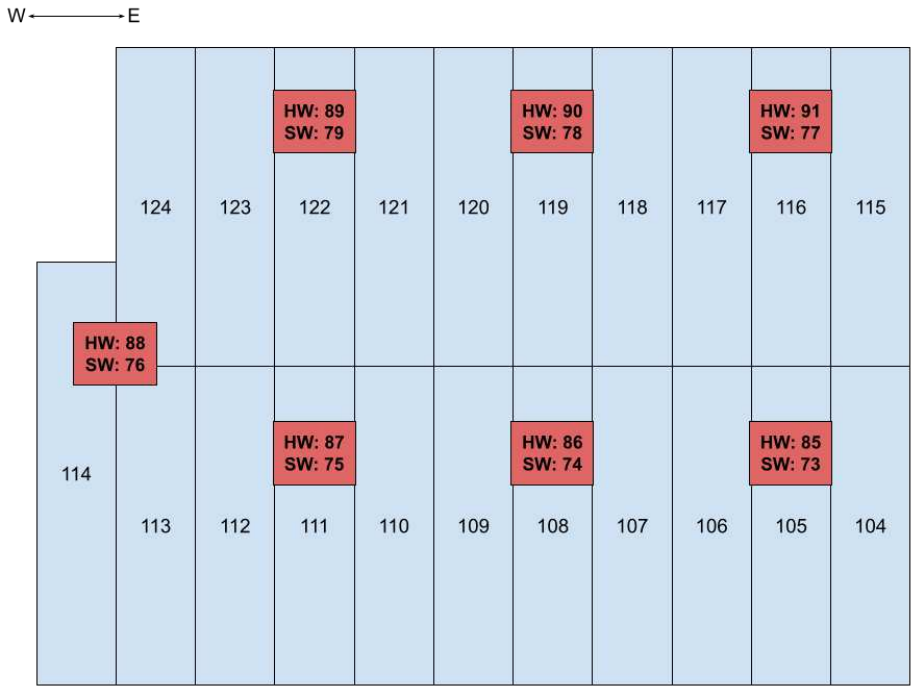

Figure 2.32: Outer South wall diagram.

beam triggers to the FEB. The Side CRT uses a pulse per second generated by the White Rabbit system [21] run by the ICARUS trigger to discipline the FEBs as discussed in section 2.1.2, and a trigger signal also used by the PMT system is provided for the T1. These cables travel from the ICARUS trigger rack on the East Mezzanine to the timing distribution units in both of the Side CRT Utility Racks. The Side CRT West Utility rack is on the other side of the building from the trigger rack, so the cables are run through the mezzanine floor and routed along bridal rings mounted to the bottom of the ICARUS walkway; the Side CRT East Utility rack is directly below the trigger rack, so the routing goes through the floor directly to the rack.

The Side CRT's FEBs are held in coincidence loops within each wall by having the trigger output of the FEBs running ORMs on the inner layer connected to the trigger input of FEBs running the ORMs on the outer layer, as well as the reverse (trigger input of inner layer is connected to trigger output of outer layer). This then requires a signal above threshold be observed in both layers within 150 ns for data to even be sent to the DAQ from the Side CRT. This assists with

noise suppression and any near-vertical cosmics that may only go through one of the two layers of a given wall.

ORM Cables

The final piece of hardware needed to enable system commissioning was the cables that go from the ORMs to the FEBs; the basic design is a 20-pair twisted pair cable with two 2x10 connectors on each end. One wire goes to the signal pin, the other to the bias pin on the FEB to provide the correct overvoltage to the SiPMs. These cables were produced by KSM Electronics, a company located near Fermilab. Several prototype cables were tested at the Wideband test stand by myself and Chris Hilgenberg. One potential problem we noticed in first prototypes was that the outer channels on the 2x10 connectors appeared to have a lot of excess strain on the wires, while the inner channels had too much excess wire length. We requested that the individual channel wires be cut in a V shape to ensure all channels had equivalent resting strain.

2.1.5 Modules Position Survey

The geometry of the Top CRT was measured by experts working with a survey team from Fermilab. The geometry of the Side CRT was measured by Biswaranjan Behera using a tape measure and some known points inside the detector hall. The values in the sections below are what I used to define the sensitive areas of the CRT geometries in my CRT-TPC analysis. These values come straight from the geometry used in the current ICARUS reconstruction, using data files with the positions of the centers of the modules in each subsystem to extrapolate the total range of each CRT region.

Top CRT Geometry

The Top CRT consists primarily of the Roof region, with four small Rims surrounding it. Each of these regions can be abstracted as a rectangular volume with set minimum/maximum X, Y, and Z values. Table 2.4 gives a full account of the geometry used for later analysis to represent the sensitive area of the CRT modules in each region.

Table 2.4: Top CRT geometry.

Region Name	xmin	ymin	zmin	xmax	ymax	zmax
Top Roof	-562	617.4	-1142	562	617.4	1442
Top Rim East	-555	403	-1142	-555	589	1442
Top Rim West	555	403	-1142	555	589	1442
Top Rim North	-553	433	1533	554	617	1533
Top Rim South	-552	403	-1143	369	589	-1143

Table 2.5: Side CRT geometry.

Region Name	Inner or Outer wall	x (cm)	ymin (cm)	ymax (cm)	zmin (cm)	zmax (cm)
West-North	Inner	526.22	-336.788	408.152	359.34	1159.34
West-North	Outer	534.49	-336.788	408.152	359.34	1159.34
West-Center	Inner	556.055	-326.508	335.562	-407	393
West-Center	Outer	564.325	-326.508	335.562	-407	393
West-South	Inner	526.22	-336.788	408.152	-1173.34	-373.34
West-South	Outer	534.49	-336.788	408.152	-1173.34	-373.34
East-North	Inner	-526.22	-336.788	408.152	359.34	1159.34
East-North	Outer	-534.49	-336.788	408.152	359.34	1159.34
East-Center	Inner	-556.055	-326.508	335.562	-407	393
East-Center	Outer	-564.325	-326.508	335.562	-407	393
East-South (bottom)	Inner	-526.22	-336.788	325.282	-1173.34	-373.34
East-South (bottom)	Outer	-534.49	-336.788	325.282	-1173.34	-373.34
East-South (top)	Inner	-526.22	326.172	408.152	-1109.34	-309.34
East-South (top)	Outer	-534.49	326.172	408.152	-1109.34	-309.34

Side CRT Geometry

The North and South Side CRT walls have a non-rectangular shape, and thus their geometry will be represented by figure 2.35 for the North and figures 2.34 and 2.33 for the South wall. All others can be abstracted as rectangular volumes of active area, similar to the Top CRT. These rectangular volumes are detailed in table 2.5, and like the Top CRT geometry are directly pulled from the current ICARUS reconstruction files.

2.2 Side CRT

The Side CRT is meant to cover as much of the side walls of the ICARUS warm vessel as possible using scintillator panels from the decommissioned MINOS experiment. The modules

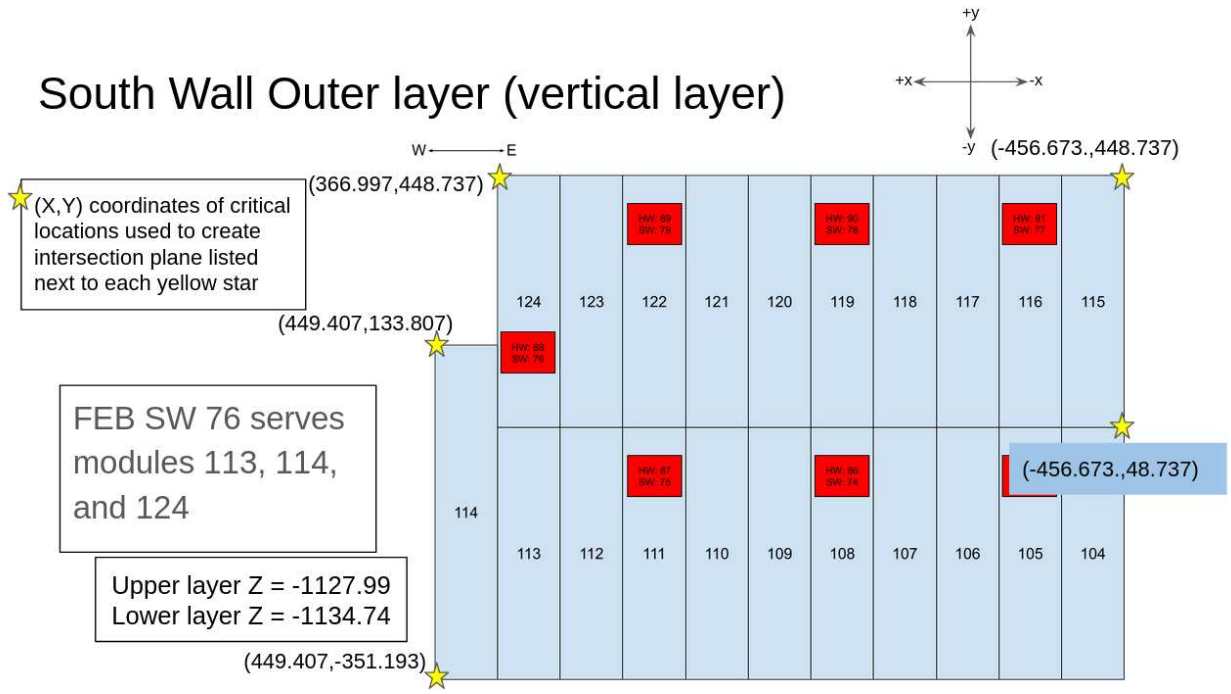

Figure 2.33: Outer South wall geometry.

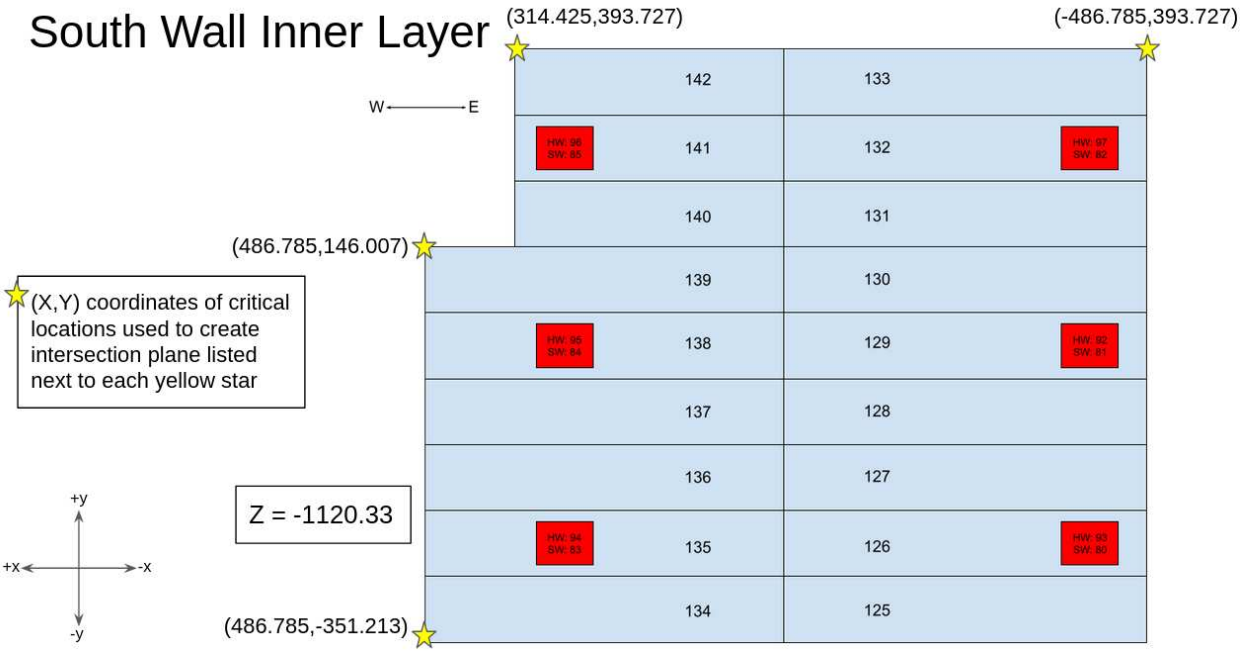

Figure 2.34: Inner South wall geometry.

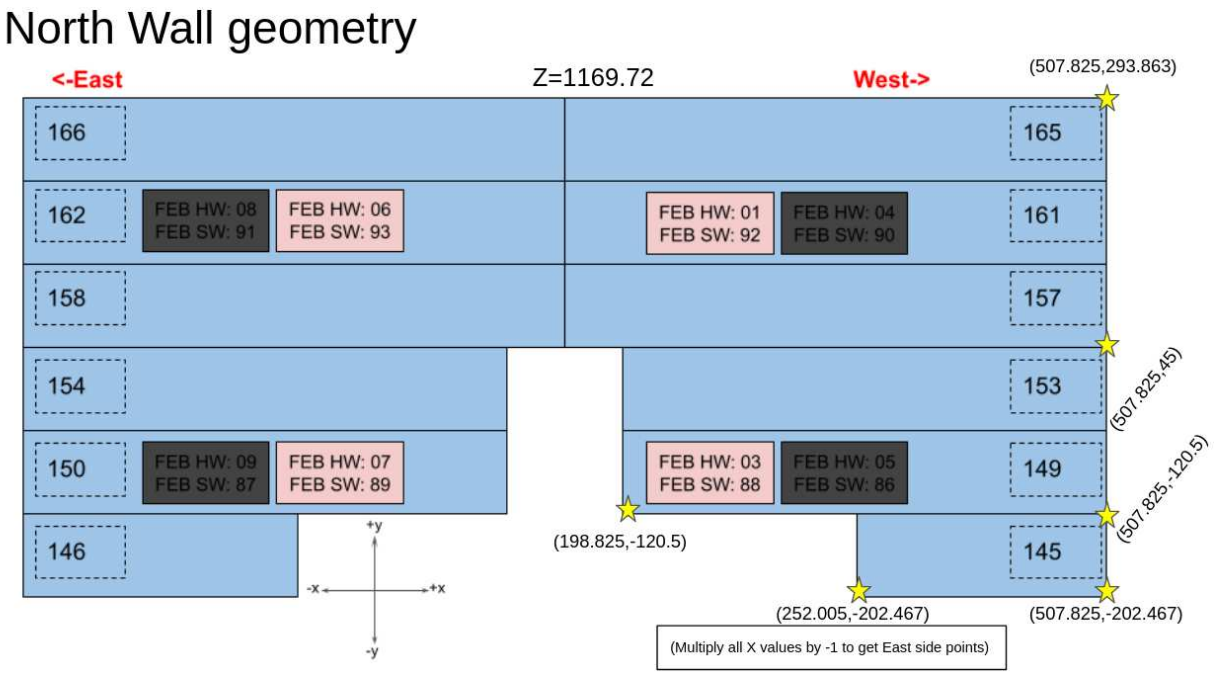

Figure 2.35: North wall geometry.

have dimensions 8 x 0.84 x 0.01 meters. In some spaces, that length would run into critical support systems for processing the liquid argon, so some modules were cut along the 8 m dimension to fit on the North and South walls.

2.2.1 Cutting CRT Modules

Cutting modules occurred at the Wideband test stand, and required a technician to operate a circular saw to cut through the metal, scintillator as well as the embedded optical fibers. The place of the cut would depend on the position that the module was going to be placed, and would be drawn on the module with black marker for the technician to cut along. Once the cutting was done, a CRT expert would then commence with the process of polishing the ends of the scintillator using increasing grit count sandpaper, finishing off with a blow torch to try to make the end as smooth as possible. This was in preparation for a strip of Mylar that would then be applied to the polished scintillator, which would then be held in place by a strip of hard plastic G10 material. The Mylar/plastic would then be attached with black electrical tape (Scotch Super-33), then finally the end of the module would be sealed with black electrical tape.

Figure 2.36: Chris Hilgenberg uses a blowtorch in the final stage of preparing the cut modules to be mirrored with Mylar and then sealed with electrical tape.

Once a module was cut, a test would be made using the Wideband test stand, which included a computer running the CAEN-supplied standalone DAQ. An ORM would be installed on the cut module snout, and connected to a FEB that was in turn connected to the computer. A light leak check would then be performed, which involves running the ORM with minimal threshold applied on the FEB while shining a bright flashlight at different angles of the cut and taped module end. The CAEN standalone DAQ has a mode for monitoring rate, and if the rate jumped while a bright light was being shined at a particular area of the module, it would be taped further to seal the light leak. Once modules passed their light leak tests, they would be loaded into boxes to be transported over to the Far Detector Building for installation.

2.2.2 Installation at the Far Detector Building

Final installation of the Side CRT began with the North Wall in late 2019. Technicians from Fermilab carried MINOS modules down to the detector from surface level via the main stairwell. The modules had all been cut to fit with the cryogenic tanks and pumps which cluster around the north side of the detector. The support posts for holding the MINOS modules in place had

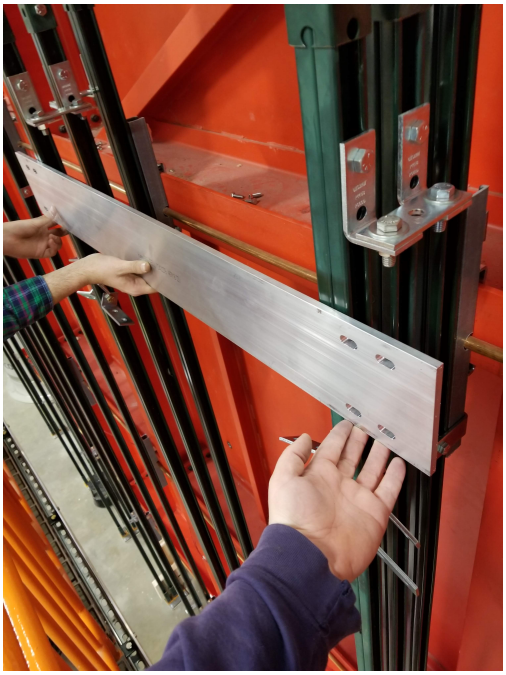

Figure 2.37: Example of the guard panels for the rolling walls while fitting for installation on the stationary wall supports. This one was too long and needed to be re-machined to fit between the support posts.

also been installed by Fermilab technicians for the North and West Central walls; in future wall installations, this was sometimes done with a mixture of technicians and myself. Installation of the ORMs, FEBs, West Side CRT Utility Rack, and cables were done by Chris Hilgenberg and myself in late 2019 and early 2020.

The East-Center and West-Center walls, being on rolling platforms, needed preparation before installation to minimize possibility of hard collisions with the mezzanine walkway as well as the stationary walls on a given side. To this end, Chris Hilgenberg and I did the installation of panels on the outside of the mezzanine walkway and the front support posts on the stationary walls. This required a few pre-cut metal pieces to need to be adjusted so that the alignment with the support posts was correct. It also required installation of rolling balls in a socket to be mounted on metal struts and connected to the center wall supports. This means any minor collision while moving a center wall should be mitigated by the rolling ball in a socket hitting the metal panels, rather than a shear collision of two large planes of metal.

There are eight Side CRT walls in total; the first two installed were the North and West Center wall, prior to FD access being closed to most everyone due at first to the filling of the detector with liquid argon in late February 2020. In mid-March 2020 access was lost due to the COVID-19 pandemic restrictions. Chris and I were able to get the two installed walls cabled up in time before we were unable to access the building, allowing us to do early work on learning how to collect data with them through use of the early ICARUS DAQ system.

The remaining walls were installed throughout the course of 2020 and early 2021. Wall installation has several phases, and at times multiple walls were in different phases of this installation procedure. The South Wall was the last to be installed due to its difference in design from the other Side Walls and the need for the installation of a jib crane which could lower the MINOS modules into place where the overhead crane in the Far Detector building could not.

MINOS module installation

The first step was the installation of support structures: the Unistrut support posts first needed to have their bases installed in the concrete floor of the ICARUS pit level, all of which was done by Fermilab technical staff. Then those support posts were pounded into place with a rubber mallet, requiring multiple people to hold the post in place and align it with the receptacle in the base. Once the posts were in place, the Unistrut [**?**] posts directly next to the warm vessel had to be secured to the vessel using pieces of machined fiberglass with 3/4 inch bolts and spring sockets which could be embedded in both the fiberglass pieces as well as the Unistrut.

Once the support posts were in place, the bottom shelves on which the MINOS modules rest were installed, with an offset of 1 inch between the two layers to prevent lateral gaps between layers. The shelves also used spring sockets in the Unistrut secured with 3/4 inch bolts. Once the shelves were in place, the first modules for that wall could be installed.

For the West Rolling wall, each individual MINOS module was loaded onto the building crane with support straps in the loading dock of the Far Detector building. The modules would then be carefully moved over the top of the ICARUS detector and rotated by the crane, with others holding on to ropes tied to each end to help prevent collisions and keep the module from spinning. The

Figure 2.38: Installation of the fiberglass pieces that would hold the Unistrut support posts to the warm vessel.

module would then be lowered all the way down to its final position, and have the support straps removed by wedging wooden blocks underneath the module to give clearance for removing the straps. Once a module was in position, the next set of shelves needed to be installed to be ready for the module that would go above the previous, usually done by two people while a crew of 3-4 would head upstairs to load another module. This took several days of work, so during the COVID lockdown in March-June of 2020 Fermilab technician Kelly Hardin who had been overseeing the installation came up with a new strategy. He had a rig made that could hold several modules and could also fit on top of the ICARUS detector between the TPC flanges and utility racks so that multiple modules could be first brought down to the top of the detector, then individually loaded from there into the final position, making the process faster.

ORM Installation

Installation of ORMs is a multi-step process. First, the MINOS module snout that needs an ORM needs to be cleaned and inspected for active fibers; by shining a flashlight on the snout, the active fibers are clear from the non-active ones, and the installer must note where the larger

Figure 2.39: The Far Detector Building loading dock where the modules would be brought in from a truck.

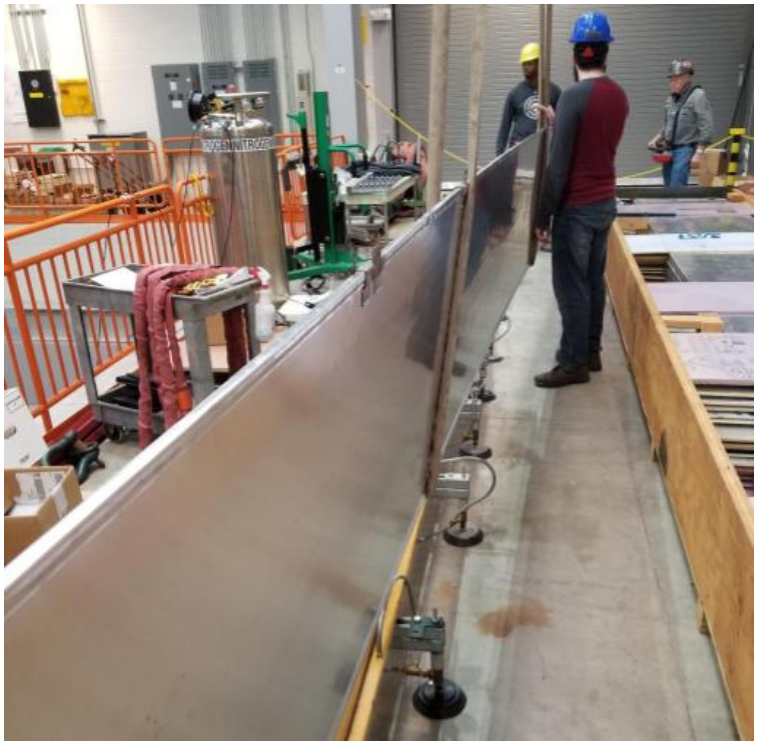

Figure 2.40: During the West Center/Rolling Wall installation, modules were initially loaded one at a time at the loading dock.

Figure 2.41: Fermilab technician Kelly Hardin had a rig created to be able to transfer multiple MINOS modules from the loading dock to the top of the ICARUS detector.

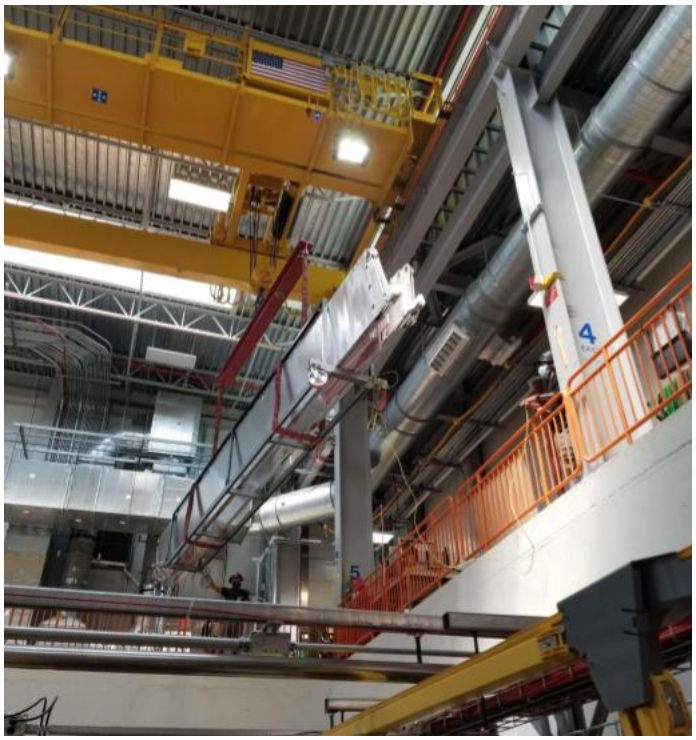

Figure 2.42: Multiple MINOS modules being transferred from the loading dock to the top of the detector via the building crane.

alignment pin hole is with respect to the active fibers. The positions of the active fibers and the larger alignment pin hole inform what type of ORM is necessary, either the normal or inverted type as discussed in Section 2.1.4. Once the correct type of ORM is identified, one is selected from the box of ORMs which passed QC tests at both CSU and Fermilab test stands. A metal alignment pin must also be inserted into the MINOS snout prior to ORM installation, following use of a Kimwipe and isopropyl alcohol to clean the snout end of any dust that may have accumulated. First the metal alignment pin must be installed, followed by the ORM. Due to the possibility of the metal pin to scratch the SiPMs for ORMs of the inverted type, one must take special care to ensure the pins are aligned before sliding the ORM into place. Once on the snout, the installer then takes two long hex screws and puts them through alignment holes on the ORM, then using a torqued hex driver to drive the screws in place without over-tightening, which could cause the SiPMs on the ORM to crash into the snout.

Following this, the twisted-pair ORM cable is installed on the ORM. The convention used for the majority of the installation was to use the key on the ORM cable (a small triangular symbol on the 20-pin connector on each end which allows for easy understanding of the continuity of channels on each end of the cable) to be facing up with respect to the serial number on the back of each ORM; this way, all of the other sides of the cables would then need to be placed the same way on the FEBs, with the key facing away from the installer as they face the FEB front.

Once the ORM cable was confirmed to be on without missing any pins on the connector, a plastic shroud was slid down the cable and brought into alignment with the back of the ORM. The shroud had two screw-holes which fit into the back of the hex screws which held the ORM to the MINOS module, and also needed a torqued screwdriver to ensure that over-tightening did not occur, as over-tightening could bow the ORM housing and introduce a gap (and thus a light leak) between the ORM housing and shroud. It became custom procedure to test that none of this bowing occurred by feeling along the ridge where the ORM housing and shroud met, allowing for the tightness of the final stage screws to be adjusted to make sure the meeting of the two pieces was flush.

The final step of ORM installation involved doing a light leak check similar to those done on cut modules described in Section 2.2.1, which required that the FEBs and related cables were already installed and active. The key difference with that light leak check was the area being tested for leaks; not only was the snout checked for leaks, particularly around the seam between the ORM and snout, but also the outer modules themselves were tested to check for any leaks that could have been introduced in the modules during their trip from ground level to the final location.

FEB installation

FEB installation required use of metal support fingers (as referred to by Dr. Thomas Coan, who assisted in the creation and first installation of fingers on the North Wall) which allowed for two FEBs to be attached to a metal piece that then attached to a small piece of Unistrut, which itself could be attached to the support posts for the MINOS modules. Fingers would first be assembled as a unit; the FEBs would be attached to C shaped pieces of metal with holes drilled in them for mounting, as well as holes for attaching to a bar of Unistrut. These C shaped metal pieces would then be installed onto the Unistrut. Once the FEB-finger assembly was ready, the assembly could then be attached to the support posts for the MINOS modules.

FEBs were installed with the length of the ORM cable in mind, and sometimes would need to be adjusted to ensure that the 84-inch long ORM cables could reach the FEB pins without any significant strain being placed on the cable. For all walls save the South Wall, FEBs were installed in columns on the support posts closest to the module snouts. Each FEB has 32 channels, and each ORM has 10, so up to 3 ORMs can be installed on one FEB. For the East-North, East-South, West-North, and West-South walls, this meant that each layer of the given wall had 3 FEBs on each side, for a total of 12 FEBs with 30 channels used for each. The East-Center and West-Center walls had a similar number of FEBs, however given those walls were only 8 modules tall, the bottom FEBs only had 20 filled channels out of 32.

Figure 2.43: Front-End Boards mounted on a finger which extends from the main support post.

Cabling

Once FEBs were installed, the final step in the initial installation of a wall was to install all necessary cables. Cable types included: CAT6 data, RG174-LEMO timing, twisted pair ORM, and power which required multiple stages; I will refer to these as data, timing, ORM, and power cables generically in this section. Each type of cable also had its own origin; timing and power both begin at a given Side CRT wall's utility rack (see Section 2.2.2 for further details), ORM cables stay within the wall, and data cables need to be run from the Side CRT servers on the West Mezzanine level of the Far Detector Building.

Typically, the first cables to be installed would be the ORM cables, in order to make sure that all module snouts were within range of the FEB. The convention was to have the ORMs which were physically lower than the others would be assigned to lower channels on the FEB starting with channels 2-11, then 12-21, and finally 22-31. In the analysis code, this range will be shifted to have the apparent active channels be 0-29 in order to make managing the rest of the analysis code easier, which may explain any confusion by those familiar with this layout versus the output of the reconstruction. ORM cables have a key which allows for the cable orientation to be surmised from either end. Since installed ORMs do not have a visible key due to light tightening, a convention was made to have the key on the ORM side always facing up if one is looking at the ORM in such a way that the serial number of the ORM is readable/not upside down. This then allows for

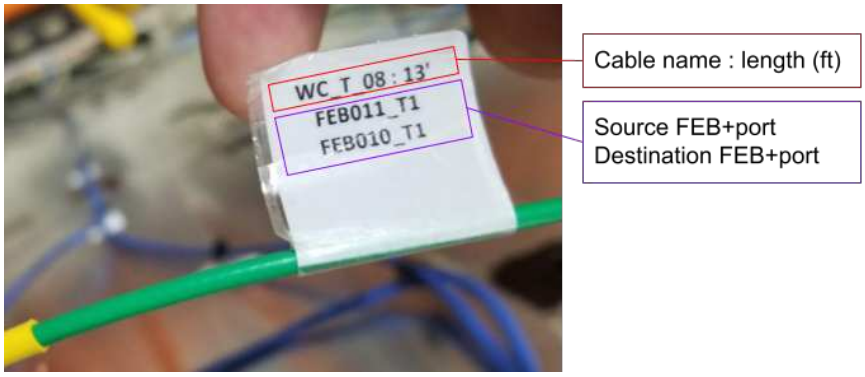

Figure 2.44: Example of a cable label for all data, timing, and coincidence cables.

confidence in getting the correct orientation on the FEB side across all module snouts, with the key facing away from the user as they face the FEBs as they sit on the given wall.

To keep cables organized, a labeling system was developed; for an example, see figure 2.44. Each cable on all walls save the North and West Center (which had an on-the-fly system of labels made that are less easy to read) uses this system, which allows for any cable to be identified on either end and clearly mark where the other side should be. There are three lines of text on each label. The top line first has the cable name with three terms separated by underscores. The first term is the wall the cable belongs to: NN for North, SS for South, EN for East North, EC for East Center, ES for East South, WN for West North, WC for West Center, and WS for West South. The second term is either a C for coincidence, T for timing, or D for data. The final term is a number purely used for identification purposes. The first line then has a colon and a number which represents the length of the cable in feet. The final two lines show the source and destination of the cable, first with the FEB number (going by the hardware mac5 addresses) and then the port on that FEB that the cable is attached to. Each cable also has a plastic cover to prevent the ink from fading due to skin contact from anyone investigating the Side CRT.

Side CRT Utility Racks

The Side CRT has two Utility Racks, East and West, which are identical with respect to the components they house and their function in the subsystem. Figure 2.46 shows the West Utility Rack with all of the essential pieces present, though prior to having spacers and an access door

Figure 2.45: Example of FEBs once all cables were installed.

added for full safety compliance. The RPS stands for Rack Protection System, connected to a smoke alarm which had to be tested for functionality. If the RPS smoke detector goes off, it shuts down the rest of the rack, the power distribution of which was directed through the RPS. The network switch allows for operators to access the power distribution remotely and to allow monitoring of the same.

The timing distribution unit was built at the University of Pittsburgh and was based on a MicroBooNE timing distribution system. Figure 2.47 shows the interior of one of these units. Optical inputs from the trigger rack are fed into the T0/T1 inputs; the T0 is split and sent directly to the 24-channel fanout, while the T1 is first routed through a delay generator which applies a 2 μs delay to the signal, preventing the trigger timestamp from causing a deadtime over any actual triggers that could occur during the beam exposure, before then being routed to the 24-channel fanout.

Wiener PL512 power supplies are used to provide power to the FEBs. The units allow for the voltage to be monitored at the distribution boxes on the walls, ensuring constant 5V can be provided to each FEB and be adjusted to ensure any power loss from propagating over the long cables that go from the supply to the distribution boxes can be adjusted for. It has since been discovered that a very high ramp-up voltage needs to be applied when turning on the FEBs as they can enter a 'stuck' state in which they appear on, but do not respond to queries from the DAQ if the voltage is too slowly increased from 0V to 5V. Thus the current voltage ramp up is set to 1000

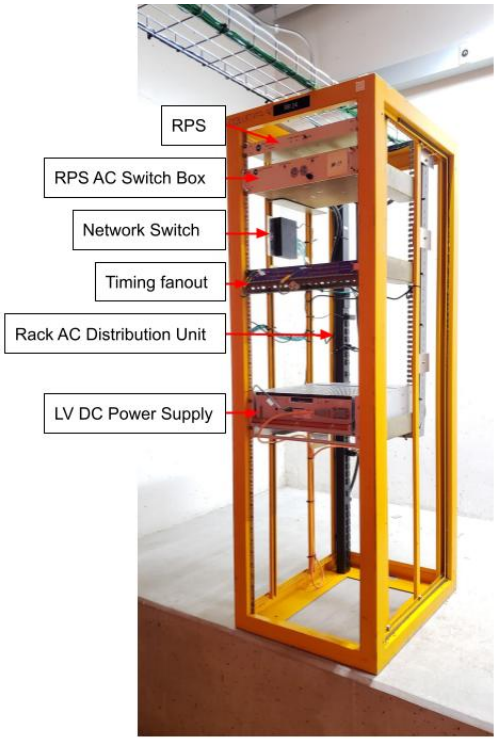

Figure 2.46: Diagram of the West Utility Rack from commissioning.

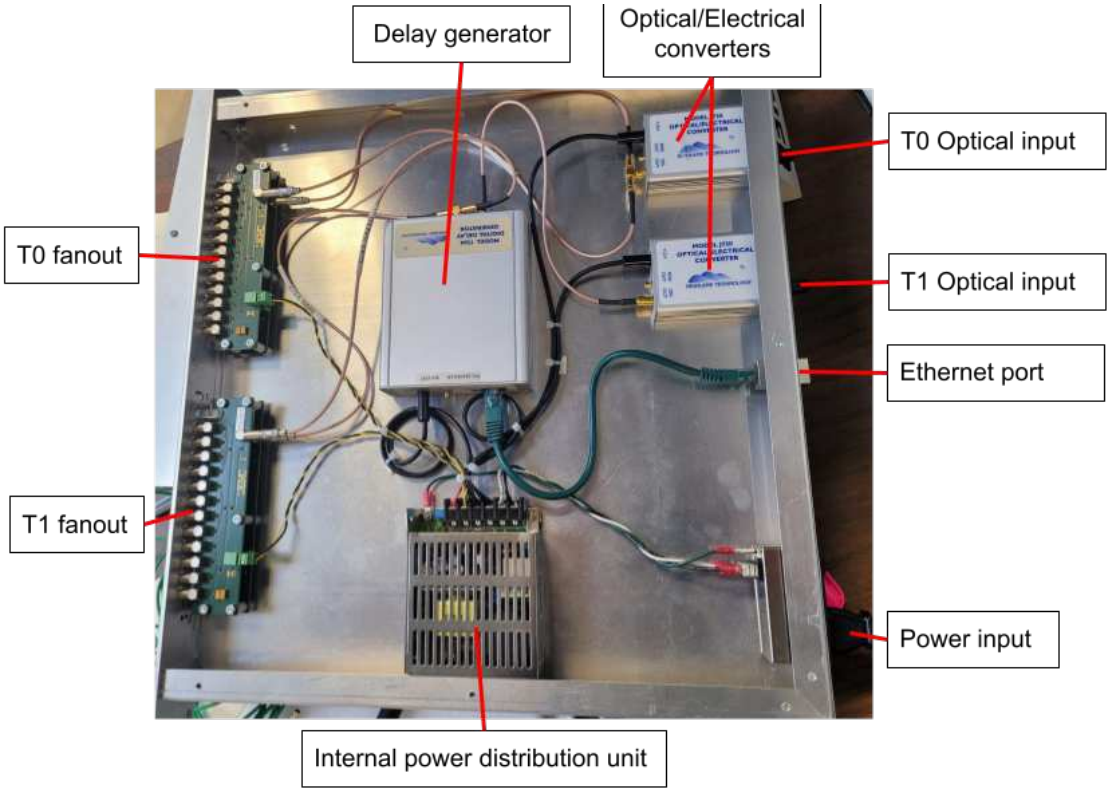

Figure 2.47: Inside of the CRT Timing Distribution Units.

V/s, which has prevented FEBs from being stuck as they were early in commissioning. The power supply is also connected to the network so that ICARUS shifters have the ability to monitor the voltage as well as remotely turn channels on or off for debugging any problems that could arise from disconnected or stuck FEBs.

Chapter 3

ICARUS Cosmic Ray Tagger: Operation and Output

After the initial commissioning of the Side CRT was complete, there was still a lot needed to get it fully running within the ICARUS system and to check for functionality. As an example, it was observed during the commissioning that there was a high amount of electrical noise in the detector hall, especially in FEBs on the north end of the hall near the cryogenic pumps. Electrical noise was also observed during the time testing ORMs at the Wideband test stand, even when the power supplies provided by the FEB manufacturer were replaced with a higher quality model. It was discovered that any metal part of the FEBs (such as the metal on the ethernet ports) is sometimes connected to the board's ground, depending on the FEB. This leads to the board ground for those FEBs being influenced by anything it is touching. Since the FEBs rely on the ground as a reference for the voltage difference across SiPMs and the signal readout, any noise on the ground will directly influence the SiPM signal. Identifying the source of and mitigating electrical noise became a priority after the initial Side CRT installation was complete.

3.1 Side CRT Noise Mitigation

For several months after the South Wall installation, there were efforts to find ways of mitigating the high amount of noise observed by the Side CRT Front-End Boards. At first, it was not understood what could be causing the noise beyond some general theories. With direct input and assistance from Fermilab electrical engineer Linda Bagby, I began doing tests on the power distribution for the Side CRT. One of the first tests was done in November of 2020, looking at the voltage output of our third-stage power cables on an oscilloscope, thus checking what was being directly plugged in to the FEBs. I found on at least two FEBs a ripple of 80-100 mV with an average period of 34 ns.

Another early test I performed was to have a dark box set up in the bottom area of the Far Detector hall, next to the Side and Bottom CRT Utility racks (near the center of the Side West

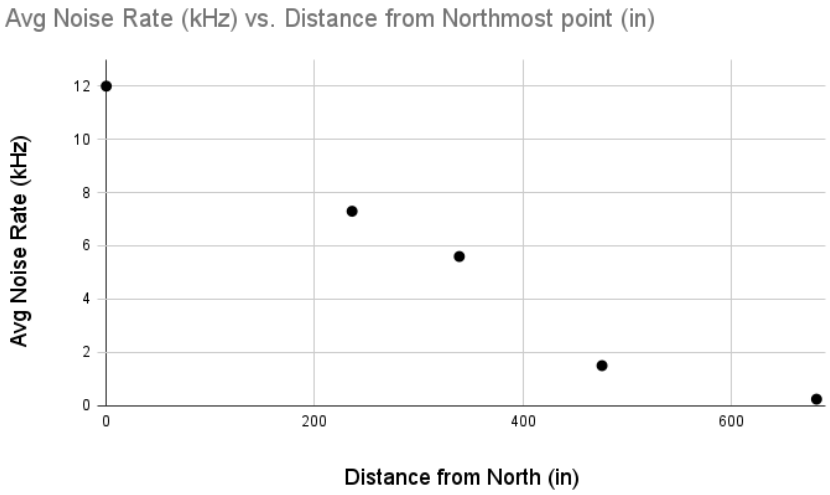

Figure 3.1: The average noise rate of a FEB with no active SiPMs as the bulk of its power cord was positioned at different points along the West Side CRT Walls.

walls). The dark box had a single ORM inside it with no light source, as the goal was to only look for what the rate would be for an ORM with no expected signal. The programmable threshold of all SiPMs was set to 215, which had been established as the 0 PE threshold setting for the FEBs; anything under that had been observed in the lab to cause near constant triggering not on the order of the expected dark rate. This high rate persisted even when the SiPM voltage was set to zero.

The final piece of the setup was a spare CRT Power Distribution Box (PDB) which was connected to the FEB, while its 155' cable was kept in a bundle that could be moved along the West Side walls. I then used the FEB's standalone DAQ program to sample the average rate when putting the power cable at various positions along the wall. The results of this study are shown in Figure 3.1. This indicated that there was a noise source being picked up by the CRT power distribution on the more northern PDBs.

Another investigation involved using a spectrum analyzer connected to an induction sensor to identify any directly observable noise on the MINOS modules and understand their frequencies. After finding evidence of noise directly on the MINOS module casings, a ground strap was connected all of the support posts which hold up the MINOS modules. This grounding strap runs

Figure 3.2: Fermilab Engineer Linda Bagby demonstrates use of a spectrum analyzer to look for which frequencies may be more pronounced on an input FEB power cable on the Side CRT.

along the concrete floor of the building, daisy chainging between support posts to ensure all posts are kept on the same ground.

The strongest noise signals were found to be coming from the cryogenic pumps in the north area of the Far Detector Building. ICARUS technicians attempted to contain the noise coming from the cryogenic pumps during a downtime in August of 2021, though unfortunately no significant effects were observed before and after the intervention on the Side CRT noise rates. These noise signatures have been observed to be stronger in proximity to the pumps. As a result, some FEBs on the North and West-North wall are operated with a 6.5 PE threshold instead of the standard 4.5, as their data rate would overwhelm the DAQ as well as possibly overwrite the internal FEB buffer between polls from the DAQ, potentially losing real muon data due to noise.

3.2 CRT Calibration Procedure

To translate the Analog-to-Digital-Converter (ADC) raw data coming from the SiPMs into energy readings, they must be calibrated to obtain a conversion between the ADC units and scintil-

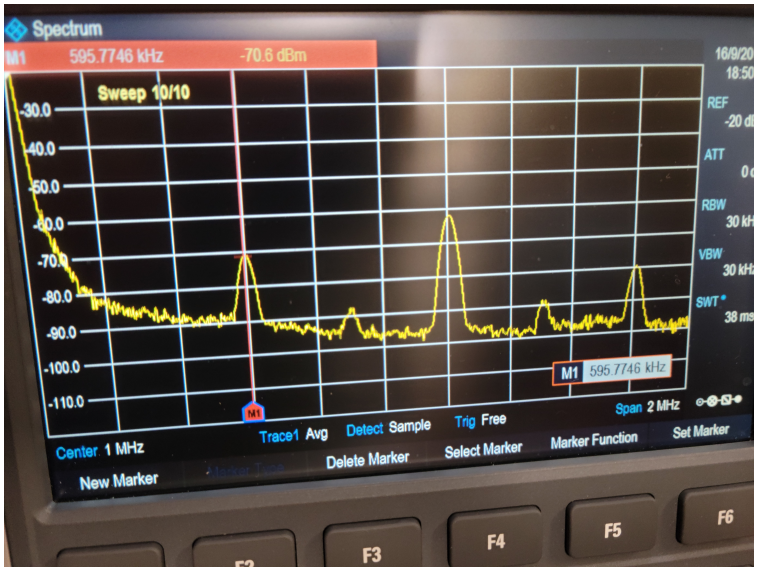

Figure 3.3: Suspected noise signals monitored on both the input FEB inputs as well as the chassis to the cryogenic pumps.

lation signal. To do this we look for how many ADC appear to correspond to a single photoelectron signal by observing the low-PE signal peaks from a SiPM. The spacing between these peaks will translate to the number of ADC that corresponds to one photoelectron. This allows for a calculation of the number of photoelectrons observed by each SiPM, which is proportional to the energy deposited in the scintillator.

The calibration procedure involves calculation of two main parameters: the pedestal, which is the equivalent of a null reading from the SiPMs, and the ADC conversion factor, which we call the gain. A SiPM will record a pedestal ADC value when it has not been impinged with light or had a dark noise trigger. The FEBs report the ADC of all SiPMs when even one of the 20-30 (Side) or 32 (Top) channels on a given FEB is triggered, therefore we can make use of non-triggered channel ADCs to obtain this number.

Gain in this context refers to the conversion between ADC and photon energies. To measure this, triggered data for each channel must be collected over a period to get the ADC distribution of that channel. In ideal circumstances, this distribution has clear photopeaks due to the Poisson statistics of how the device operates. These peak positions can be recorded, and the average separation between successive peaks should give the conversion between gain and ADC. Doing this

with the Side CRT at the Far Detector building is a challenge due to a combination of low statistics over time and high noise that requires a higher threshold than ideal blocking out the lower-PE peaks that would be larger and easier to fit.

The Side CRT calibration code was initially developed by Chris Hilgenberg in the early days of the CRT commissioning. It was used to determine if the values seen on the commissioned ORMs was consistent between channels. My work in furthering the effort involved taking his code and getting it to work within the ICARUS full detector software framework. The goal was to find an optimal way to run over large data samples to get the necessary statistics for resolving the PE peaks. Due to the Side CRT's thresholds for noise mitigation and the other trigger conditions placed on the Side CRT FEBs, this can take a long time to collect, typically on the scale of a day of running on the ICARUS DAQ. The current iteration of the calibration code works in multiple steps by first extracting the CRT DAQ information from raw data, then iterating through the DAQ information to sort ADCs reported to the DAQ into individual by-channel histograms. These histograms are then fed to the calibration analysis, which looks at each channel's ADC spectrum and tries to extract pedestal and gain.

3.2.1 Pedestal and Gain Calculation

The process of obtaining a per-channel pedestal and gain calculation involves taking first the raw ICARUS data and pulling out the CRT's DAQ stream information, obtaining the raw ADC values for each channel. The calibration analysis module loops through the DAQ stream and extracts ADC information into one histogram per FEB channel. Once enough statistics for each channel has been collected to the point that the PE peaks can be resolved, the data product that has the by-channel histograms can then be submitted to a second stage analysis which looks for a pedestal in the lower ADC region. It then applies a ROOT TSpectrum to do peak finding. The peaks are collected and analyzed by an algorithm which first sorts the peak positions, then tries to determine the peak number (i.e. first PE peak, second PE peak, etc.) from the placement of the pedestal and the expected gain of the devices of each of the supplied peaks. The algorithm also

filters what it classifies as bad peak IDs from TSpectrum, which can sometimes fit what is actually a fluctuation in the ADC between obvious peaks.

Once the gain fit algorithm has a list of 'good' peak numbers and their ADC positions, a plot is made of the ADC versus peak number. The plot is then given a linear fit, whose slope gives the conversion between ADC and PEs. This can sometimes go wrong when the wrong peak number is assigned relative to the channel's pedestal, causing the gain measurement to either be lower or higher than expected, and re-running on the same data produces the same bad measurement.

To mitigate bad measurements of the gain in the Side CRT, multiple data sets from which these measurements are made can be sourced, averaging over gain measurements from the past X measurements and throwing out any that are large outliers in order to account for this problem. In one study, I found that after 5 ICARUS runs, 63 out of all 2,710 Side CRT Channels were left with unacceptable gain measurements. I took the accumulated good gain and pedestal measurements for each channel across the 5 data runs, then averaged them to create a master calibration for the Side CRT. By creating a list of channels by FEB ID and local channel, then listing the averaged pedestal and gain in a comma-separated values file, I could then provide that file to graduate student Jaesung Kim who was maintaining the ICARUS online databases. He in turn uploaded the file to the database, and provided a HTTP link that could be used in the ICARUS analysis code to call the gain and pedestal for a given channel with a simple function. This then allowed the reconstruction to have access to the calibration values, and continues to be the main calibration used for the Side CRT.

3.3 CRT Hit Reconstruction

CRT hit reconstruction involves taking raw data from the front-end electronics and interpreting those data as instances of cosmogenic activity in the detectors at spatial locations and with an accompanying timestamp. The Top CRT and the Side CRT have very different designs, and as such need different approaches to interpreting the data coming from their respective FEBs. Given

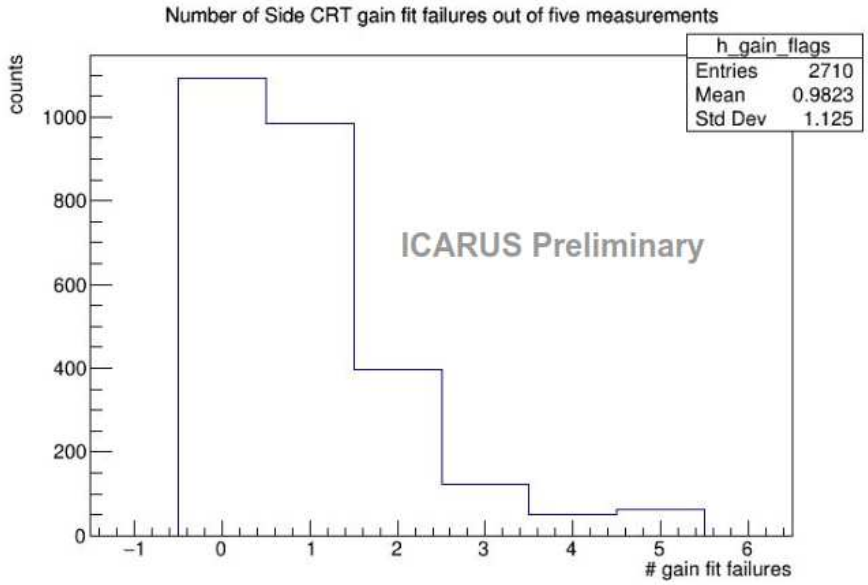

Figure 3.4: Number of times each channel failed a gain calibration measurement out of five separate measurements.

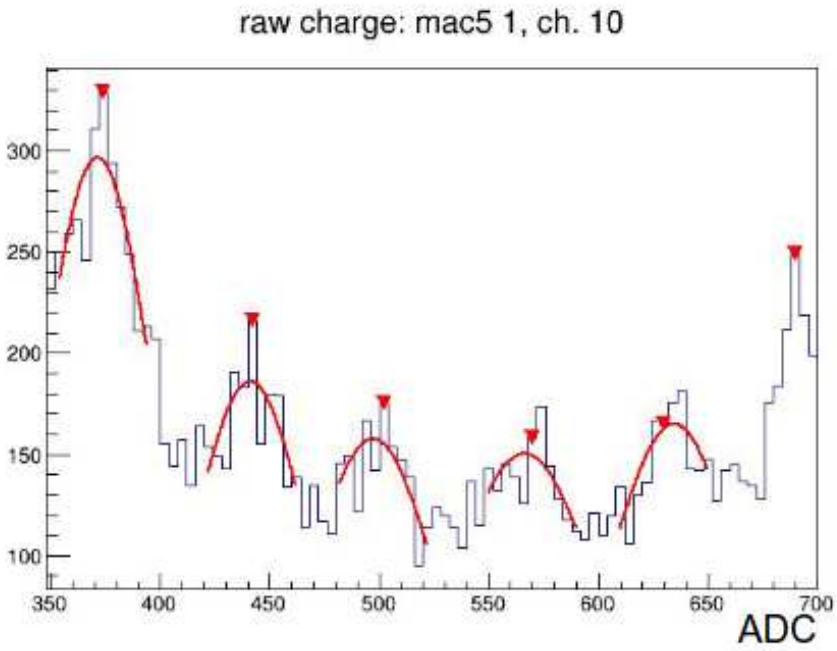

Figure 3.5: Visible PE peaks being fitted by TSpectrum in the calibration processing.

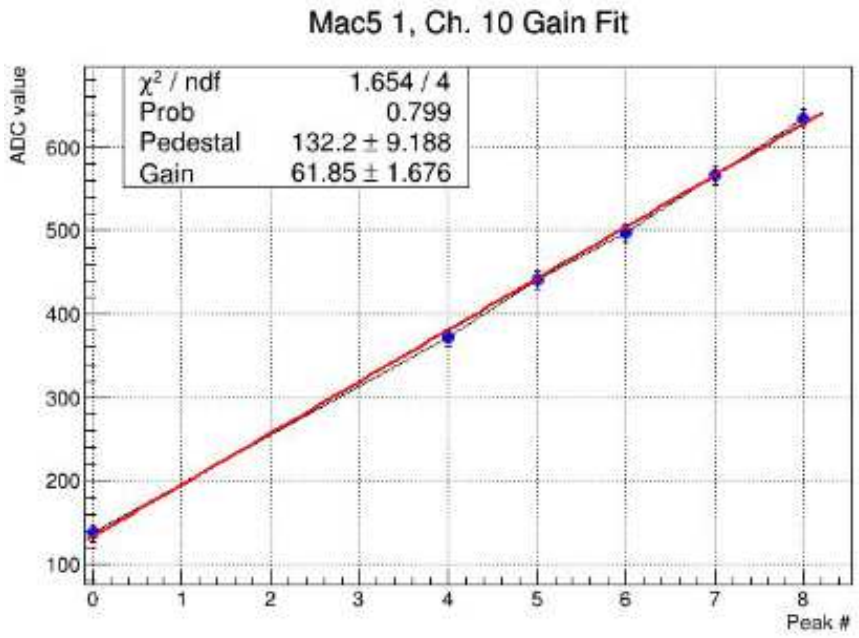

Figure 3.6: PE peak ADC versus asserted ADC peak number to obtain the ADC-PE conversion factor, or gain for this channel.

this, the hit reconstruction for Top and Side is handled separately, though both create the same reconstruction data product which is called a CRT Hit.

Ideally, CRT Hits represent what is believed to be true cosmogenic activity in the detector. They contain a reconstructed location of where the cosmic is calculated to have been based on the FEB signals, timing information about when the hit occurred, and information about which channels on which FEBs saw how many PEs. Creating a CRT Hit out of FEB signals thus requires an understanding of the hardware configuration of each CRT subsystem; the Top CRT has all uniform modules, so reconstruction within the modules is standardized and then geometry tools are used to translate the local module coordinates into detector coordinates, while the Side CRT has different protocols based on which wall the signals come from.

3.3.1 CRT Hit Reconstruction

CRT Hit reconstruction begins with a preselection stage, searching through raw data and only taking CRT Hits which occur within 3 milliseconds of the event trigger timestamp. Side CRT FEB data that have no channel with a signal above 7.5 PEs are also excluded. This data is collected

into possible coincidences between FEBs on each wall, and then those coincidences are further examined. Timestamps of the FEB readouts allow for a time difference to be calculated between two FEBs that trigger in coincidence, allowing for an estimate of the hit position along the detector strip. If such coincidences can be found within a few nanoseconds in each layer of the particular CRT region (inner vs outer), they are collected into a CRT Hit.

Anna Heggestuen has been working on making quality flags for the Side CRT Hits. These flags help to tag some potentially concerning signals observed during the Side CRT Hit reconstruction; for example, sometimes the timing of two FEBs on either end of a strip was such that the reconstructed position was outside of the physical bounds of the strip. These flags can be used in the future for more detailed Side CRT analysis.

Side CRT

The Side CRT reconstruction requires checking for signals between different FEBs, since the Side CRT scintillator strips are double-ended and the readouts at opposite ends are attached to different FEBs. The first thing that the function MakeSideHit in the CRT Hit reconstruction code does is to search for coincident signals between FEBs whose channels are paired for all walls with double-ended readout (all but North and South).

Coincident signals on the same wall are collected in a vector for further analysis. That vector is then iterated over, checking groups of FEB signals from a given Side CRT region within a 150 ns coincidence window. If channels that measure opposite ends of a given strip are found to be above the 7.5 PE software threshold, the relative position along the axis of the strip is calculated using the timestamps of the two FEB triggers, and the propagation velocity of light in the wavelength shifting fibers. If only one end of a strip is read out, the hit position is set at the exact middle of the strip while adding a flag to the hit for quality control monitoring. For further reference, Figure 3.7 gives an example of how signals from channels on either side of a strip are used to determine where along the strip the signal came from using timestamps from each FEB.

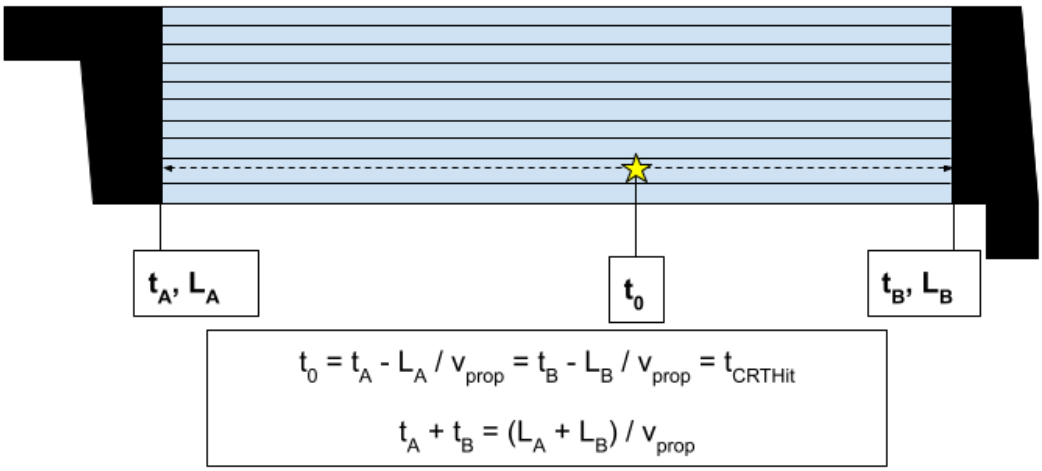

Figure 3.7: Guide for how coincident signals from two ends of a module strip are converted into a single time and position along the strip.

Once all strip coincidences have been evaluated, the individual strip positions calculated from signals above threshold on all FEBs are averaged to calculate a final position for the CRT Hit; the first timestamp amongst all the signals is saved as the time for that CRT Hit.

The North Side wall is a simpler process as only one side of the module ends are instrumented; the hit reconstruction algorithm therefore looks for which strips are triggered, averages the center positions of those strips and uses that as the CRT Hit position. The South Side wall uses XY coincidence, with a layer of horizontally oriented strips serving as the inner wall, and two sets of vertically oriented modules serving as the outer wall. The CRT Hit reconstruction looks for FEBs with large PE signals within 150 ns of each other in each layer (inner+outer), assigning the hit position to the overlap position of the strips that were triggered in the region. These differences will matter later when evaluating performance, as they set these regions apart from the other Side walls.

Top CRT

The Top CRT reconstruction process is relatively straightforward compared to the Side's. Each module uses a single FEB and has XY coincidence between its layers. When a Top CRT FEB

records a signal above threshold, it sends the signal to the DAQ for decoding. The Top CRT uses a function called MakeTopHit which takes in the FEB data and searches the channels in each layer for which has the highest PE signal. It associates the X position with the highest signal in the bottom layer, and the Z position with the highest signal in the top layer, creating a grid of 64 possible hit reconstruction positions due to the geometry of having 2 layers of 8 crossed bars. The position is first calculated in local coordinates of the module, then a geometry service re-orients the coordinates for that specific module to the full detector.

Chapter 4

Reconstruction Data Objects

4.1 TPC Data Products

The ICARUS detector has four physical TPC regions between the two T300 modules. Each T300 has a dual-sided TPC which shares a common cathode. Electrons from ionized argon are pulled towards the collection and induction wire planes under the influence of the electric field across the drift region, which is 500 V/cm. Waveforms from the wire planes created by the induced or collected charge from the drifted electrons are processed through the software decoder to create TPC Hits, which in turn are clustered by Pandora [22] reconstruction algorithms to create TPC Tracks. TPC Tracks can be thought of as representing a group of associated hits in the TPC, along with parameters produced by the Pandora reconstruction such as a start and end point of the track, or whether the track has been identified 'clear cosmic'. Clusters of TPC Hits are further analyzed to create TPC Trajectory Points that smooth out the clusters of hits into a series of points along the calculated track trajectory.

The Pandora clear 'cosmic tag' has three possible settings, listed here from most generic to most specific in their cuts on track parameters: Cautious, Nominal, and Aggressive. Cautious looks only for whether the track falls within certain parameters of being within the beam gate, as well as fiducial cuts on the endpoints of the track to see if the track was contained in the detector's fiducial volume during the time of the beam spill. The Nominal and Aggressive settings add a requirement on the track angle with the vertical axis, as well as the curvature of the track [22].

Before TPC waveforms are processed by reconstruction algorithms into hits, they undergo a process called 'coherent noise removal'. If similar changes in waveforms are found across multiple wires in the TPC, it is identified in the pre-reconstruction processing stage as coherent noise, and the waveform is adjusted to remove that noise. This can lead to TPC tracks which have a near-

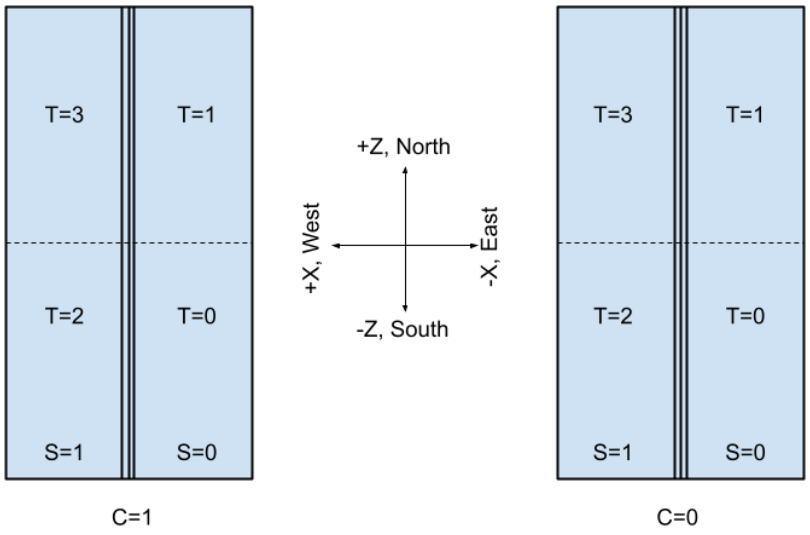

Figure 4.1: Figure showing which areas of the T600 correspond to which C and T values in geometry. Use in conjunction with table 4.1 to better understand the TPC geometry; the S is used sometimes for inner-TPC checks and is kept here for completeness

vertical angle to have sparse hits available, as the coherent noise removal will have detected similar waveforms in time.

The geometry used for the detector simulation and reconstruction separates each T300 into four "logical" TPCs; the two physical ones, and another cut in the middle along Z. Table 4.1 summarizes the geometry of each TPC, using the logical layout described in Figure 4.1.

Table 4.1: Simulated TPC coordinates used in reconstruction. Figure 4.1 provides a guide to how C and T values correspond to TPC volumes in the detector hall.

C	T	xmin (cm)	ymin (cm)	zmin (cm)	xmax (cm)	ymax (cm)	zmax (cm)
0	0	-358.49	-181.86	-894.951	-210.29	134.96	0
0	1	-358.49	-181.86	0	-210.29	134.96	894.951
0	2	-210.14	-181.86	-894.951	-61.94	134.96	0
0	3	-210.14	-181.86	0	-61.94	134.96	894.951
1	0	61.94	-181.86	-894.951	210.14	134.96	0
1	1	61.94	-181.86	0	210.14	134.96	894.951
1	2	210.29	-181.86	-894.951	358.49	134.96	0
1	3	210.29	-181.86	0	358.49	134.96	894.951

A track is identified as a 'cathode-crosser' if it crosses the sensitive area of any two TPCs that share a common cathode. This allows for precise timing reconstruction of the track, as the two segments across detectors can be correlated to provide a T0 for the track. Cathode-crossers are valuable for studying PMT-TPC matching, calibrating the difference in timestamps between the subsystems. Tracks that are not cathode-crossers but are instead reconstructed in a single TPC are referred to as 'contained', due to its hits being contained in a single TPC volume.

The ICARUS TPC has a maximum drift time of 0.96 ms. The estimated cosmic rate in the TPC was simulated for the SBN Program Proposal [1] and a followup study was performed by Biswaranjan Behera in 2021 [5], finding that there should typically 11 muons per TPC during the maximum drift time.

Important for later discussions of analysis are the differences in active vs. fiducial volume; analyzers make use of this distinction to mark tracks as likely contained versus coming from an external source. The active volume is defined as the volume that the TPC can read out; the fiducial volume defines the acceptance region for analyses within the active volume. In the SBN proposal, this was assumed to be 25 cm from the lateral, top and bottom faces, 35 cm from the upstream (southern) faces and 50 cm from the downstream (northern) faces of each TPC. For current analyzers, the cut used to determine if a track is likely a cosmic or similar charged particle generated outside the detector is 10 cm from the faces. This will be used later in section 5.3 when discussing how tracks were selected that have a high likelihood of being from a cosmic source.

4.2 Data Terminology

ICARUS packages data with labels to help analyzers know when the data was taken. The top-level label is the run number, which is set when the data acquisition system is launched. The data is time-ordered, which allows downstream analysis to break it down into further categories. This includes the event number, which represents a unique 6 ms of data acquisition during the run, centered on a PMT trigger condition which can change depending on the preset trigger configuration for the run. Each ICARUS subsystem saves different amounts of data around this trigger;

the PMT saves +/- 1 ms while the CRT saves +/- 3 ms of data around the trigger timestamp. The TPC is more complicated, as it saves 4,096 'ticks' of TPC time around the timestamp, which can represent tracks from varying start/end times depending on their original distance from the wire planes. These ticks range from 0 to 4,096, with tick 846 representing the time at which a track created at trigger time 0 ns will cross the cathode, and tick 3216 being roughly (not accounting for differences in drift velocity) when that same track should cross the anode planes. These ticks can then be converted into X positions within the detector.

Each event contains unique data compared to all other events in the run, meaning event A will not contain cosmics present at a different time in event B of the same run. Events can be broken down even further into *slices* which vary in time width, focusing on periods where a defined track vertex is found. My analysis ignores slices, as they are mainly for neutrino analysis, and instead works on a track-by-track basis, using the run and event number to ensure that TPC tracks are being compared to CRT Hits collected in the same time frame.

4.3 Data Selection and Processing

ICARUS uses a system of file organization developed at Fermilab named Serial Access to Metadata (SAM). The online service of SAM named SAMWeb allows for files to be referenced via their metadata. This is particularly useful for the analysis performed here, allowing for raw files associated with triggers from outside the beam arrival to be easily collected and analyzed in a by-run basis. ICARUS organizes its raw data first by run, then by the different beam-on/beam-off tags.

To select data for this analysis, the main goal was to have data with purely cosmogenic signals with enough statistics to measure the efficiency of each CRT region. By using the SAMWeb client along with the run log used by the ICARUS experiment to track run numbers and other critical information about each run, I was able to select long runs where the neutrino beams were not running and the detector was operating in a calibration mode. This meant that nearly all data for

these runs should be cosmogenic activity only, and selecting long runs meant each input dataset to the analysis would yield a larger number of TPC tracks for matching to CRT Hits.

The ICARUS data processing has two initial stages to create files which have reconstruction data products from all three subsystems present. There are the main output files which format their outputs in terms of special ICARUS/SBN data products, while a secondary product is also made called a calibration NTuple at the end of the second stage which does not contain the full information, dropping things like individual waveforms of TPC tracks and other more 'primitive' signals that are unneccessary for detector calibration, but does keep all of the basic data products from each of the subsystems. One roadblock that kept me from using calibration NTuples early on in development was that they only contained cathode-crossing tracks by default. In Summer 2023, I learned there was a way to include all TPC tracks in the outputs, as well as the individual TPC Hits/Trajectory Points which I needed for projecting the TPC track back to the CRT (see Section 5.2). This led me to organize the analysis around use of these NTuples, and for me to learn how to make my own versions of calibration NTuples on the Fermilab Computing Grid in order to be able to generate my own custom NTuples. These custom NTuples include things like the CRT by-channel PEs or the Side CRT Hit flags worked on by Anna Heggestuen which I believed could be useful in a Side CRT analysis.

Once calibration NTuples were created to my specifications, I ran ROOT macros over them to do the matching or other related analysis with the data products from the TPC and CRT subsystems. The run and event numbers were used to ensure only data products from the same event were being compared, and a separate analysis is also performed alongside the matching to keep tabs of the number of events analyzed and some basic meta-information about each event is tracked, such as the number of TPC tracks in each event and the number of CRT Hits in each region for each event. Having the events analyzed and tracked in this way allows for an easy check to be done once the matching outputs are completed, checking that no two events in a given run are present more than once in the dataset. This tool ensures that no double counting of TPC tracks or other products could cause biases in the final result.

Chapter 5

Cosmic Ray Tagger Efficiency Measurement

To characterize CRT performance, we use the TPC as a hodoscope that provides well-reconstructed cosmic ray tracks that project back to the CRT. The TPC reconstruction efficiency is not directly relevant so long as tracks are not being selected in such a way that there is a bias that will impact the CRT efficiency interpretation. An example of this kind of bias through TPC selection would be only probing certain regions due to geometry of the tracks being selected; making such a selection will impact the interpretation of the CRT efficiency measurement.

The CRT efficiency can be expressed by the number of reconstructed muon tracks from the TPC that have a CRT Hit that can be identified as a match divided by the total number of tracks that pass through the CRT. The first step is to ensure that the reconstructed track is a primary muon; not all tracks coming from the TPC reconstruction algorithm will be from primary muons, even in offbeam data.

In this chapter, the first section discusses how TPC tracks are selected as cosmic candidates. Then I discuss a measurement done with Monte Carlo simulation to determine how many tracks will be missed by the CRT due purely to geometry to set a baseline of the best possible matching efficiency possible. Next is an estimate of the expected multiple coulomb scattering of a typical muon to set a scale for the expected deflection between the Top CRT and the top of the ICARUS TPC. Finally, I present the methodology used to do CRT-TPC matching for this efficiency, followed by a report of the measured efficiencies and a study of the sensitivity of the results to the choice of parameter values.

5.1 Non-Cathode Crossing TPC Track Drift Direction

The fundamental function of TPCs are to read charge signals from drifted electrons over time in their wire planes, then process those signals into likely hit and track signals. In order to calculate a TPC track's postion in X (along the drift direction), the Pandora algorithm assigns the position the

track would have at the time of the event trigger. This is done for all tracks except cathode-crossers (which as discussed in section 4.1 are tracks with a timestamp due to being present in two separate TPC volumes), leading to cases where the initial X positions of the hits of a given track can all be outside the TPC volume. Each track must therefore have a valid time range in the trigger window, associated with the range of times for the track which have all points alongside the track inside the physical bounds of the TPC. To adjust for a track's X position at a given time, the TPC drift velocity can be used in conjunction with the timestamp to calculate where the track would be at the time of the CRT Hit; this is used to determine if a TPC track is in-time with associated CRT Hits.

5.2 MC Study: Principle Component Analysis TPC Track Projection

To project a track trajectory back to where it intersects the CRT subsystem, the Hits from near the endpoints of each track are fitted by a method known as Principal Component analysis, or PCA. To perform PCA, the positions of all TPC trajectory points are collected within 10 cm of either the track's Pandora-provided start or end points. The covariance matrix of these trajectory points is calculated, at which point the eigenvalues and eigenvectors of the covariance matrix are calculated using ROOT's TMatrixDEigen class. The eigenvector corresponding to the largest eigenvalue is taken as as a best-fit line for the trajectory points, centered at the average of the points used. Doing this for both of a track's endpoints allows flexibility when working to match with CRT Hits, allowing the analyzer to use the PCA projection for the endpoint which is closer to the edge of the TPC active volume nearest the CRT plane. Each endpoint has two PCA-related vectors in data: a normalized best fit directional vector, and another that holds the average position of all trajectory points input to the PCA. This collection of average position plus directional fit allows for easy projection back to CRT regional volumes.

In the initial analysis I used a length of 10 cm from a Pandora endpoint to select trajectory points for the PCA projection, motivated by a number determined by the ICARUS Machine Learn-

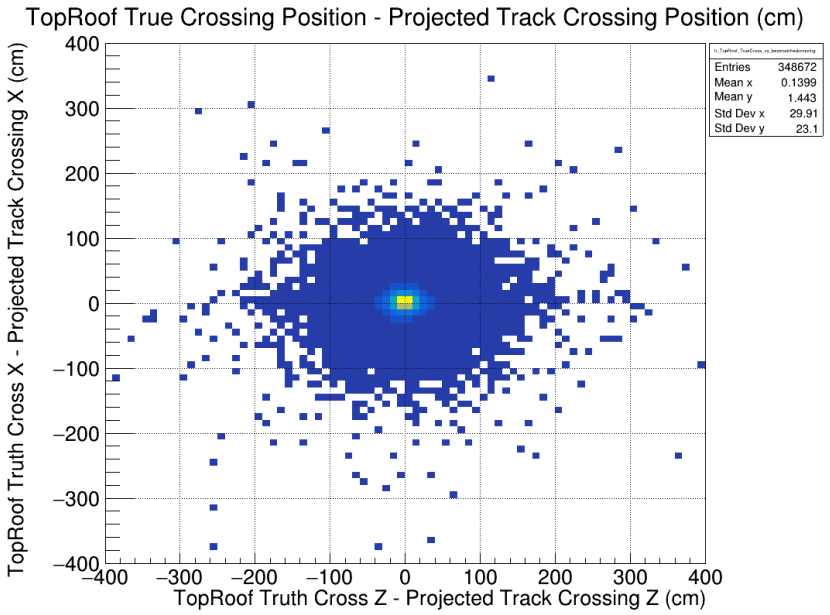

Figure 5.1: Distribution showing the difference between the true crossing point of a TPC track on the Top Roof CRT region versus where the track was projected to intercept the region for tracks that had been truth matched to the correct CRT Hit through running the CRT-TPC matching using **5 cm** of track length on each endpoint to make the PCA projection.

ing group for their own analyses. Using this as a reasonable starting point, I performed a study of the PCA approach using the ICARUS Monte Carlo to investigate the optimal setting. By taking tracks whose corresponding truth position when crossing the CRT Top Roof was within the resolution of the Top CRT of the CRT Hit being matched to, I found an easy way to identify tracks matched to true signals. For each PCA fit length [5 cm, 10 cm, 30 cm, 50 cm, 70 cm, and one using the full length of each track (variable length)], I plotted the difference in X and Z between the true track crossing position and the projected TPC track position for tracks that had been matched to the true CRT Hit. Figures 5.1 through 5.6 show this distribution. By comparing the standard deviation of the distributions, I found that increasing the distance from the endpoint for the trajectory points to be included in the PCA would slowly reduce the overall width of the distribution in both X and Z until somewhere between 30 and 50 cm. Then, likely because of scattering that occurs over the length of each track, the inclusion of more points in the PCA decreases the precision of the PCA projection. Based on these results, I use a 'PCA cut' of 50 cm as a near-optimal value.

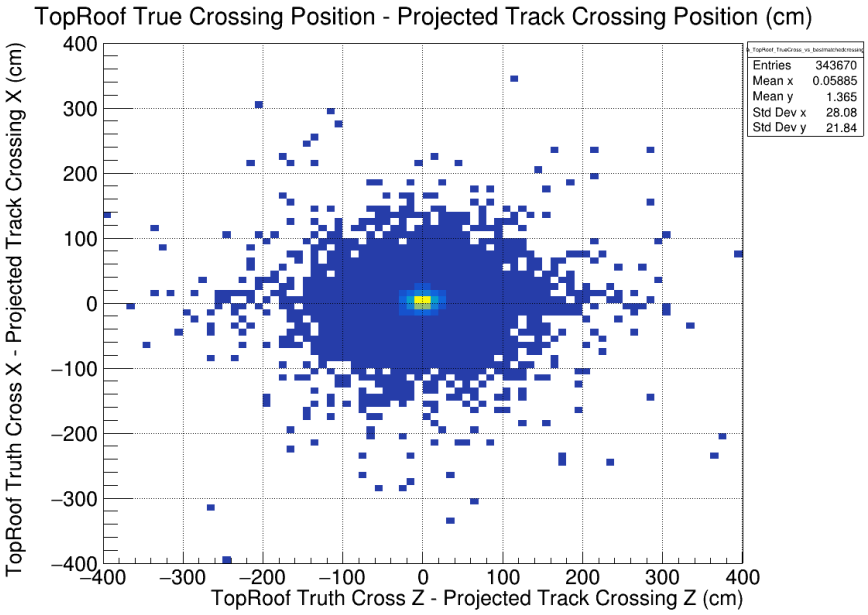

Figure 5.2: Distribution showing the difference between the true crossing point of a TPC track on the Top Roof CRT region versus where the track was projected to intercept the region for tracks that had been truth matched to the correct CRT Hit through running the CRT-TPC matching using **10** cm (standard) of track length on each endpoint to make the PCA projection.

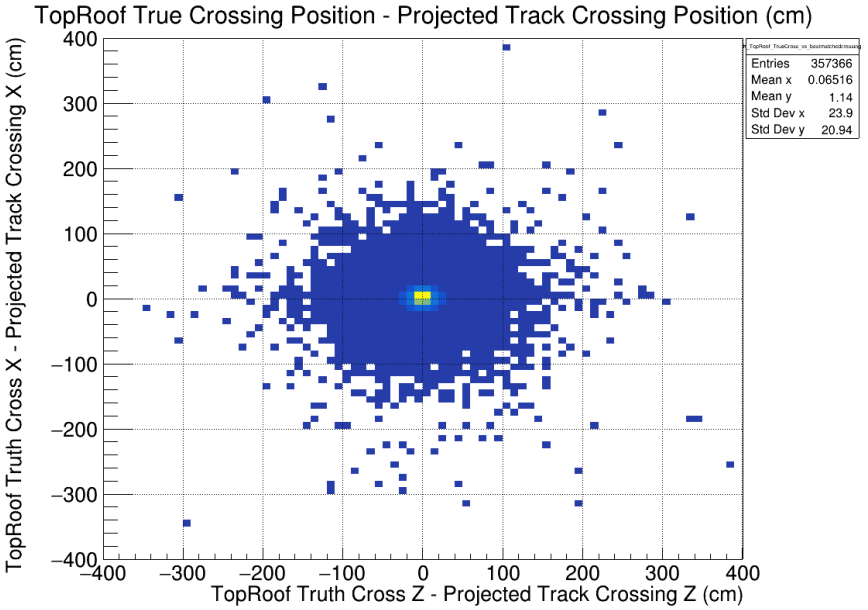

Figure 5.3: Distribution showing the difference between the true crossing point of a TPC track on the Top Roof CRT region versus where the track was projected to intercept the region for tracks that had been truth matched to the correct CRT Hit through running the CRT-TPC matching using **30** cm of track length on each endpoint to make the PCA projection.

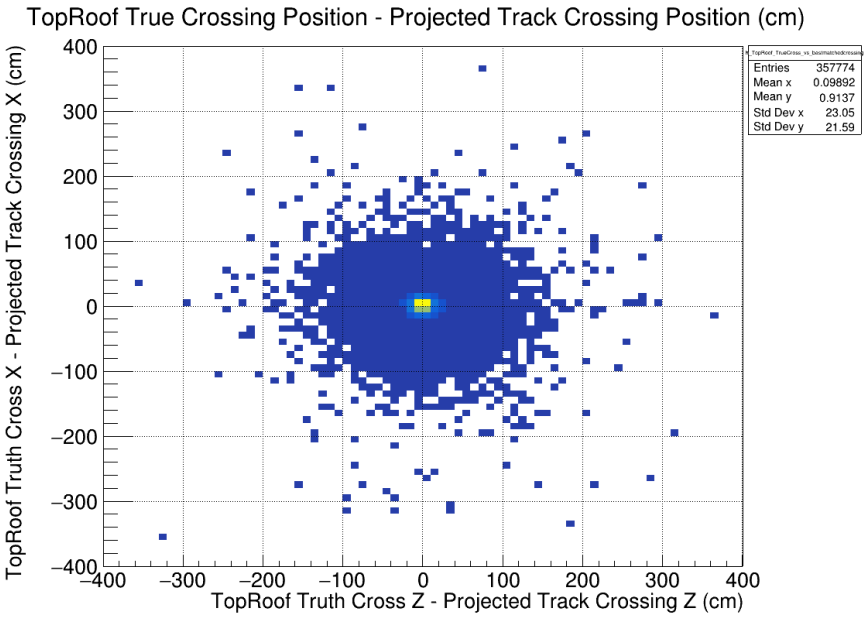

Figure 5.4: Distribution showing the difference between the true crossing point of a TPC track on the Top Roof CRT region versus where the track was projected to intercept the region for tracks that had been truth matched to the correct CRT Hit through running the CRT-TPC matching using **50 cm** of track length on each endpoint to make the PCA projection.

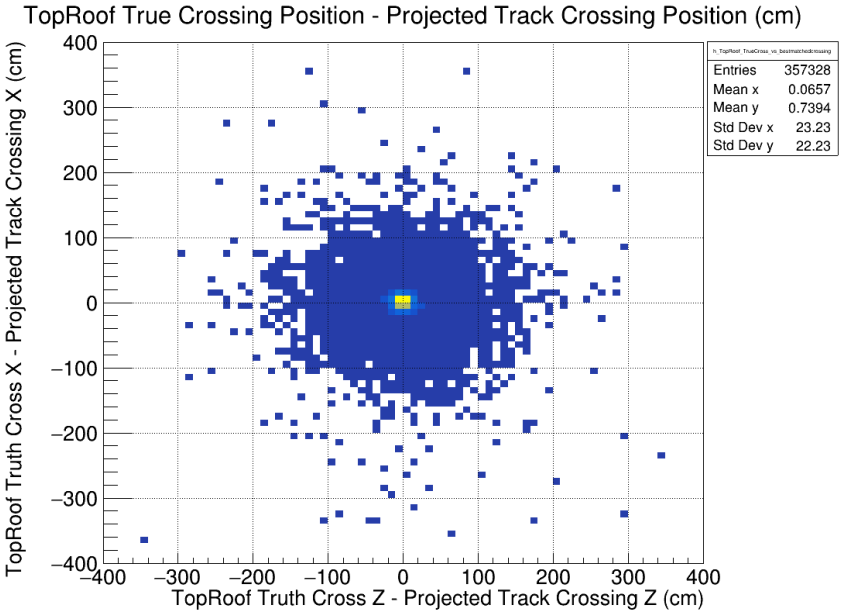

Figure 5.5: Distribution showing the difference between the true crossing point of a TPC track on the Top Roof CRT region versus where the track was projected to intercept the region for tracks that had been truth matched to the correct CRT Hit through running the CRT-TPC matching using **70 cm** of track length on each endpoint to make the PCA projection.

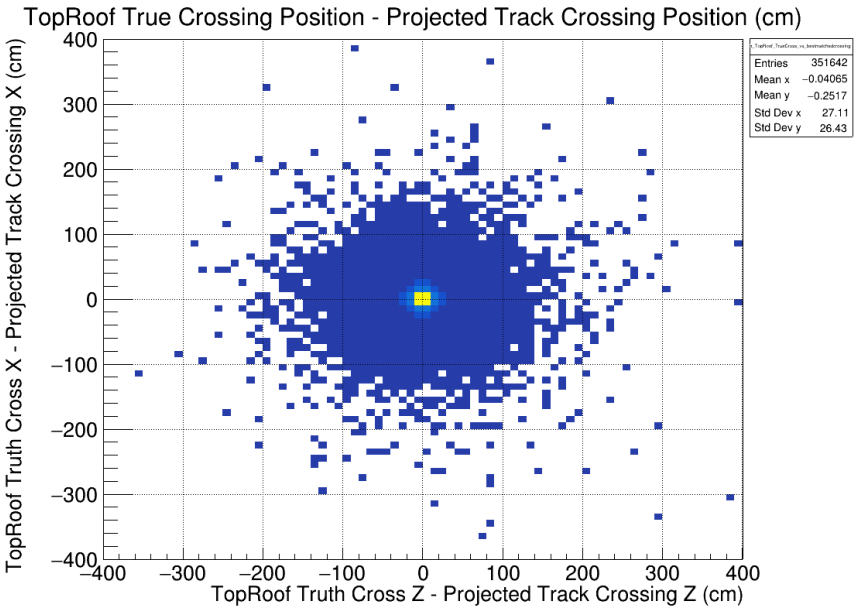

Figure 5.6: Distribution showing the difference between the true crossing point of a TPC track on the Top Roof CRT region versus where the track was projected to intercept the region for tracks that had been truth matched to the correct CRT Hit through running the CRT-TPC matching using **all track trajectory points** to make the PCA projection.

5.3 MC Study: TPC Track Selection

In total there were 1,285 Pandora [22] reconstructed tracks generated in the the 100 single-muon event sample. Most of the tracks in this sample were or other such secondary particles with very small track lengths. Figure 5.7 shows the track lengths of all TPC tracks generated. Note the two main distributions of tracks, one near 0 cm and another at around 300 cm. From the truth objects associated with these tracks, no tracks below 50 cm in reconstructed track length were the primary muon. The few tracks near 60-70 cm were split tracks, and everything above was associated with the main muon. For this analysis, I used a minimum track length of 70 cm to reduce the chance of split tracks, deltas or other such detector phenomena that do not represent the main particle.

For the purposes of efficiency measurement, I derived a method for selecting TPC track candidates on a per-CRT-region basis. I first take each TPC track and see if either the Pandora start or end points fit within the criteria laid out in Table 5.1. If the track is cathode-crossing, its X position is constrained already, so the only check for cathode-crossing tracks is to see if the PCA projec-

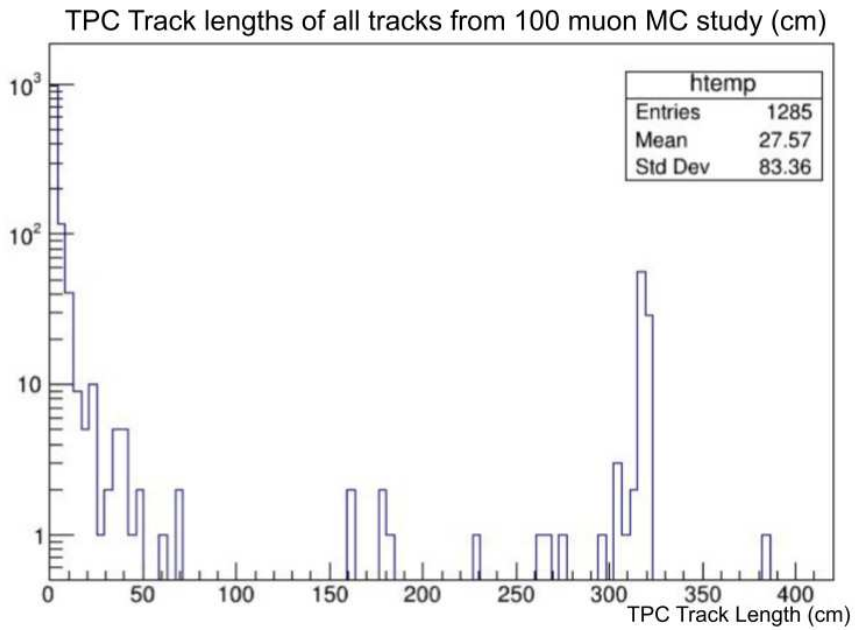

Figure 5.7: Track lengths from MC study of 100 true muons, used to determine a useful cut value to remove likely background tracks.

tion of the selected endpoint will intersect with the simulated CRT regional volumes as laid out in Section 5.2. The PCA projection central point is placed at the average position of input points as described in Section 5.2. If the projection from that average position using the PCA projection direction intersects with the CRT region volume as described in Section 2.1.5, the track then has a Boolean associated with being a candidate for the CRT region set to 'true' (default is false for each new track). This allows for quick selection of track candidates for each region in the final stage of analysis in which the results of the matching are examined.

For tracks that do not cross the cathode, the X position is not constrained, apart from knowing that it must be somewhere in the TPC active region. So, a more involved second stage check is needed. First, if the Pandora endpoints of the track pass a check for being in a valid region of the TPC (see table 5.1 for qualifications for each CRT region), then the second stage check is to ensure that the track will point to a CRT region for its full range of possible X positions. To do this, the position of the PCA projection has its X value varied between the minimum and maximum X for the TPC volume the track is in. If the PCA projection intersects the CRT region at the minimum and maximum possible X, the track is marked as a candidate with a Boolean for

Table 5.1: Requirements for TPC track endpoints to qualify as a candidate for each CRT region. The *N* cm can be varied, by default has been 10 cm from the value used by analyzers for neutrino analyses.

Region #	Name	Track endpoint must be within...
30	Top Roof	N cm of top of TPC Y maximum
31	Top Rim West	N cm of top of TPC Y maximum OR in WW TPC
32	Top Rim East	N cm of top of TPC Y maximum OR in EE TPC
33	Top Rim South	N cm of top of TPC Y maximum OR N cm of TPC Z minimum
34	Top Rim North	N cm of top of TPC Y maximum OR N cm of TPC Z maximum
40	Side West-South	WW TPC and is most West of start+end
41	Side West-Center	WW TPC and is most West of start+end
42	Side West-North	WW TPC and is most West of start+end
43	Side East-South	EE TPC and is most East of start+end
44	Side East-Center	EE TPC and is most East of start+end
45	Side East-North	EE TPC and is most East of start+end
46	Side South	N cm of TPC Z minimum
47	Side North	N cm of TPC Z maximum

that CRT region. This should remove any ambiguity about whether a track should be expected to have passed through a given region, only relying on the fixed CRT geometry to confirm if a track is a regional candidate for non-cathode crossing tracks. These select for track candidates that are counted in the denominator of the efficiency calculation (along with a minimum reconstructed track length cut).

5.4 MC Study: Geometrical Efficiency

In this measurement, I use the established CRT geometry for the Top and Side subsystems in a Monte Carlo study in which I generated a cosmic background similar to what is expected at the ICARUS detector hall. Using the Monte Carlo truth information I calculated how many of the true particles that generated tracks in the TPCs would also enter the CRT volumes. For this study, I generated 59,000 Monte Carlo events using the CORSIKA generator [11].

By selecting TPC tracks with a Pandora reconstructed length over 70 cm made in the reconstruction stage of the Monte Carlo (to exclude signals that in reconstruction would be discarded as stub tracks), I identified all of the unique 'MCParticles' that represent the truth objects used in the simulation stage, as well as filter those with a Particle Data Group (PDG) code that corresponds to

Table 5.2: Results from Monte Carlo geometrical efficiency study calculating the percentage of MCParticles that produced candidate TPC tracks would intercept CRT regions.

MCParticle category	# particles	% of total MCParticles
# MCParticles with no true crossing	18,413	3.2
# MCParticles with only Top crossing	245,590	43.2
# MCParticles with only Side crossing	98,442	17.3
# MCParticles with both Side and Top crossings	206,094	36.2
Total # MCParticles	568,539	100

the muon or antimuon ($\pm$13). I filtered out duplicate tracks made by the same MCParticle using the truth IDs and event numbers of each to ensure no double-counting. These unique MCParticles were iterated through, using their positions as a function of time to trace out their true paths in the detector hall to determine which CRT regions that the truth object likely crossed. This was determined by finding positions closest to the opposing sides of each CRT region volume (using the geometry outlined in section 2.1.5), checking that the line connecting those positions closest to the opposite sides of the CRT volume would pass through the active area of the CRT region. This was done for all regions for every unique MCParticle, probing which regions were intercepting true particles more often than others.

The results are summarized in Table 5.2. I find that 3.2% of MCParticles which would be observed as track candidates in the ICARUS TPCs would miss the CRT entirely due to geometrical effects. This sets the best possible efficiency for the CRT system by this method as 96.8%.

5.5 Multiple Coulomb Scattering Calculation: Top CRT

When a charged particle moves through a material, it will undergo multiple scatters due to Coulomb interactions with atomic nuclei in the material. This will lead to an average angular deflection for a particle incident due to its passage through the material. To estimate this value for muons entering the Top CRT that will then pass into the TPC, I use the formula by Lynch and Dahl [23]:

$$\theta_{MCS} = \frac{13.6\ MeV}{\beta cp} z \sqrt{\frac{x}{X_0}} \left(1 + 0.038\ ln(\frac{xz^2}{X_0\beta^2})\right) \tag{5.1}$$

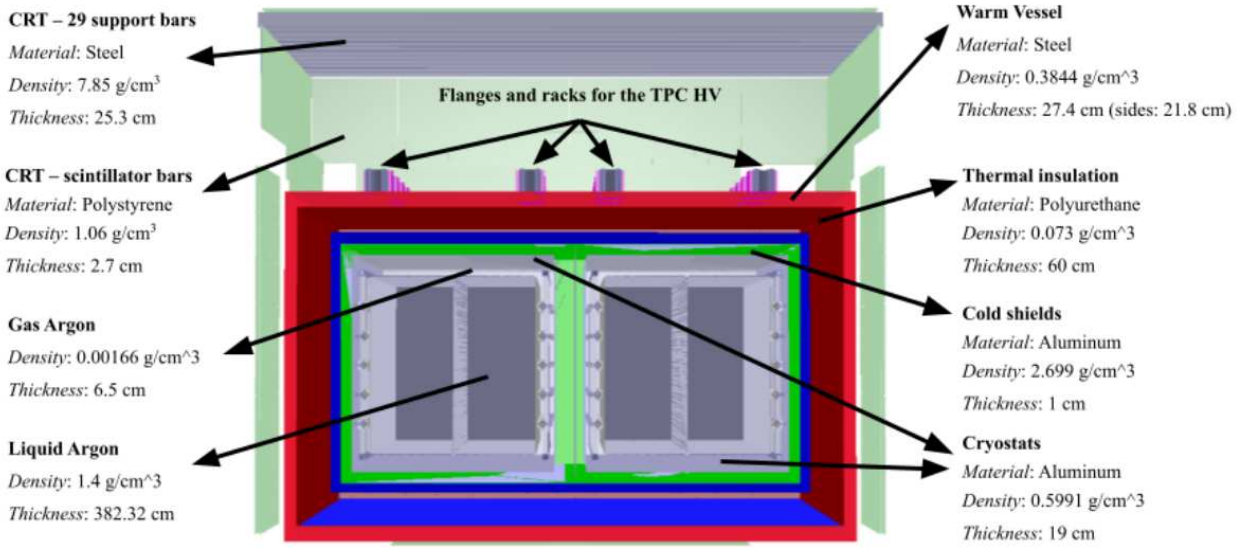

Figure 5.8: Diagram of detector components used to calculated expected MCS.

Momentum p is the particle momentum in MeV, velocity β is the particle velocity over the speed of light, and charge number z traveling through x lengths of a medium with radiation length X_0. For the thickness in radiation lengths, I used an accounting of the material in and around the ICARUS TPCs and CRT modules catalogued by Biswaranjan Behera for his study of the impact of the ICARUS overburden [24]. Figure 5.9 shows this geometry in detail, including the materials used and the thickness of each.

To calculate thickness in radiation lengths for each material, I approximated the materials quoted in Figure 5.9 as the closest monoatomic materials I could find for them. Figure 5.9 shows how I abstracted the layers into corresponding monoatomic materials, and also provides the path lengths for each material taken from Figure 5.9.

Table 5.3 has the calculations for a 4000 MeV muon (the average expected energy at the Top CRT), including the X_0 lengths calculated from an equation in the Particle Data Group's chapter on passage of particles through matter [25]. Adding up all deflections gives 0.03 radians, or about 1.7° over the full path length. Over the distance between the Top CRT and the top of the TPC active volume, this should lead to an average deflection of 14.3 cm for a vertical muon. This approximately half of a Top CRT strip, but is not a very large deflection on the scale of the full

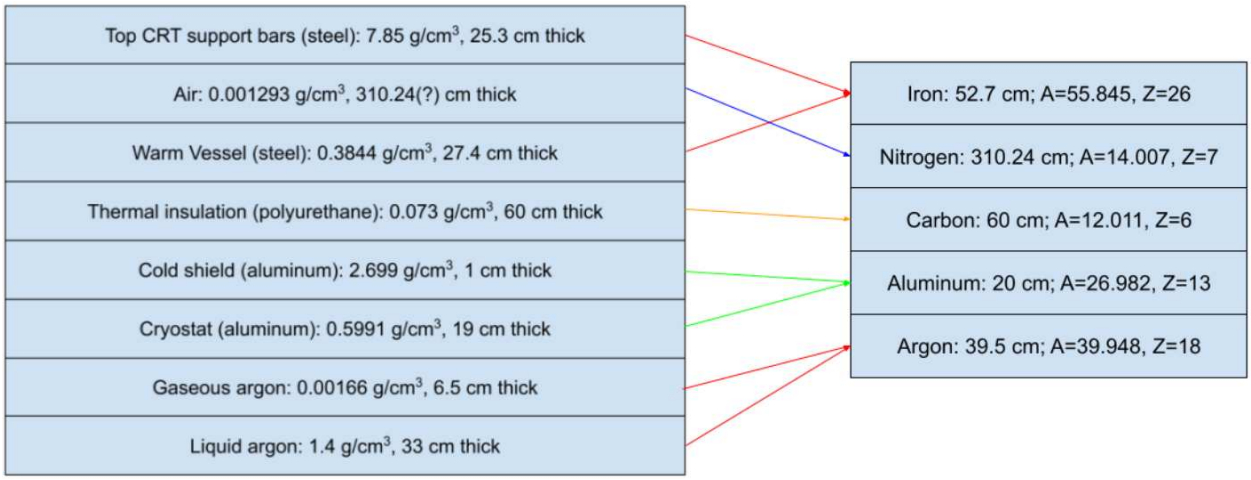

Figure 5.9: Diagram of how layers were abstracted as monoatomic substances.

Table 5.3: Angular deflections from various materials between the Top CRT and TPC active area.

Approximate material	X_0 (cm)	Path length through material (cm)	x/X_0	θ deflection (radians)
Iron	13.8	52.7	3.82	0.0070
Nitrogen	38	310.24	8.2	0.0105
Carbon	42.7	60	1.4	0.0041
Aluminum	24	20	0.83	0.0031
Argon	19.5	39.5	2.0	0.0050

detector. Lowering the expected energy to 1000 MeV makes the expected deflection about 6.8°, which leads to an average expected deflection of 57.7 cm between the Top CRT and the top of the TPC active volume. This means the average deflection will be less than about three strips in the Top CRT.

5.6 CRT-TPC Matching Procedure

Associating CRT Hits with TPC tracks requires first projecting tracks back to the CRT, then evaluating the likelihood that the two are correlated signals. All detector data from a given event is loaded into memory, then TPC tracks from the event are iterated over one at a time, looking for potentially related signals in the CRT. A Principal Component Analysis is run on both endpoints of every track, so the matching process can switch between endpoint projections depending on where a CRT Hit is located when matching to the track.

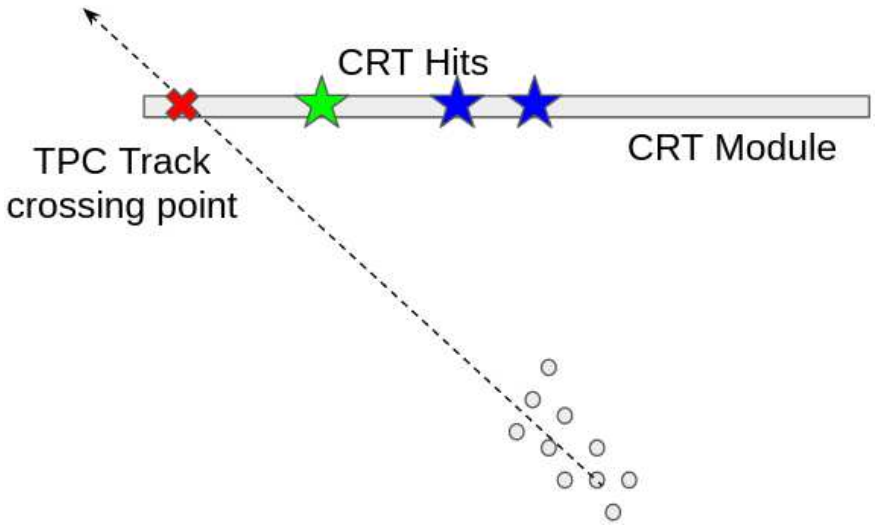

Figure 5.10: Illustration of the basic concept of DCA used in CRT-TPC matching.

Next, all CRT Hits in the event are looped through, first shifting the track in X to where it should be at the time of the CRT Hit. The matching algorithm checks that both of the track endpoints are still inside the TPC volume; if either is not, the CRT Hit is rejected as a potential match, as it is not in time with the TPC track. After this X offset correction is applied, the projection vector for the track is selected to be the endpoint which is closest to the plane of the region of the CRT Hit being matched to. For example, if the CRT Hit is in a West Side region, the endpoint selected will be the one with greater X value; if the CRT Hit is in the Top Roof, the endpoint with largest Y is selected. Whichever endpoint is chosen based on this criteria is used for projecting back to the CRT Hit, using the PCA projection from that endpoint to find the Distance of Closest Approach (DCA) in the plane of the CRT Hit between the CRT Hit and the projected crossing point of the TPC Track using the PCA fit. This is repeated for all CRT Hits, and the hit with the smallest DCA is saved as the best matched hit, the hit with second lowest DCA saved as the second best, and the hit with the third lowest DCA saved as third best. Besides these top three matches based on DCA, the best matched hit based on DCA for each CRT region to the track is also saved as a fallback for circumstances such as a shower hit the CRT in a region, causing other potential matches in other regions to not be seen in the top 3 matches based on DCA.

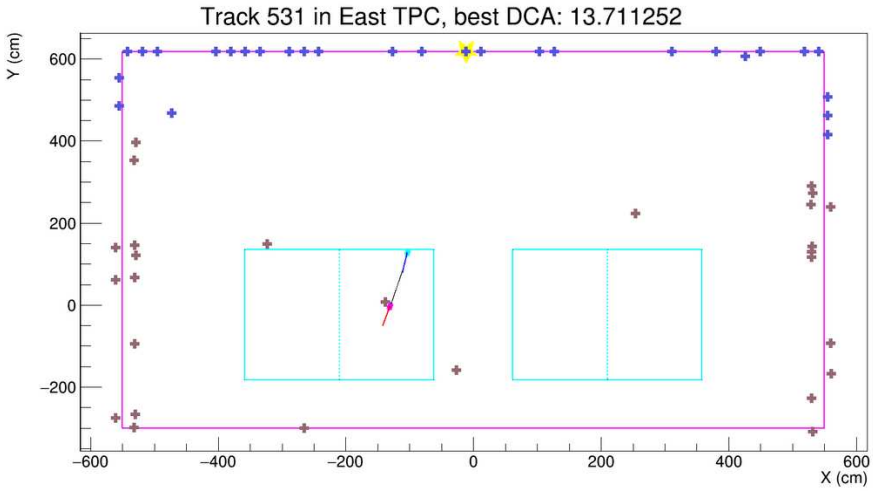

Figure 5.11: XY view of a well-matched TPC track.

Figures 5.11 and 5.12 show example simple 'event displays' which I use to inspect the matching on a track-by-track level. The large pink box is an outline of the approximate bounds of the CRT across all regions, with the CRT Hits present as the small dark blue (Top) or red (Side) cross marks. The TPC bounds are in light blue with a dashed line to show the location of the cathode. The TPC Trajectory points are plotted as a black line, the fitted endpoints of the Pandora Start and End of the track are marked with light blue and pink asterisks and the PCA from those endpoints extend from them in blue/red lines. These can be zoomed in on with the original ROOT graph to inspect the PCA projection from the collected endpoints, allowing for a check that the PCA is not somehow failing. The best matched CRT Hit is marked with a big yellow star, and the TPC track is placed where it would be at the time of that CRT Hit. All other CRT Hits on the graph are those that were candidates for matching to the TPC track, meaning they were, at minimum, in time with the track.

Once all CRT Hits in the event are scanned through, the matching saves relevant data about the TPC track and the best matched CRT hits to a ROOT TTree in an output file. This allows inspection of the results of the matching with macros which iterate through the TTrees, examining each track candidate and plotting relevant metrics about how the matching is working on a large scale.

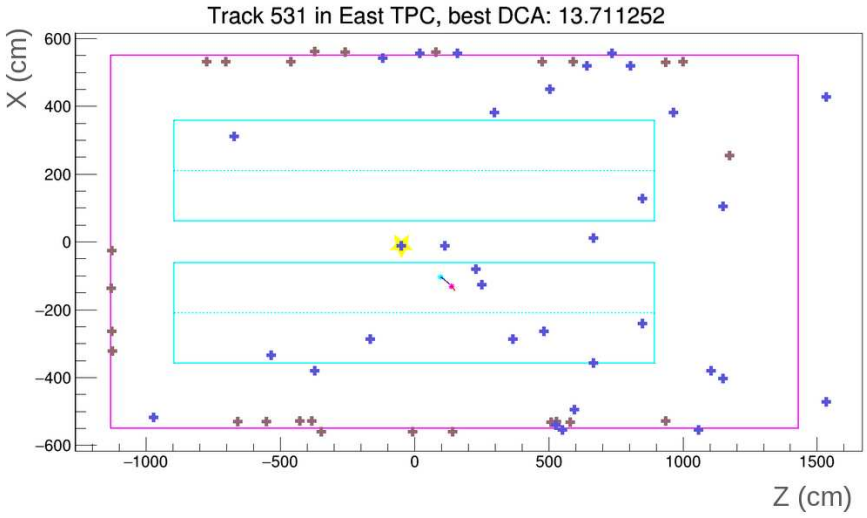

Figure 5.12: XZ view of a well-matched TPC track.

As an example of the power of this matching procedure, see Figure 5.13. These are tracks whose crossing point on the CRT region was found to be within 30 cm of the best matched CRT Hit. Note the grid structure visible; the darker areas are the spaces between strips and modules. This is showing the lower efficiency areas in the region, showing the physical structure of the detectors!

5.6.1 Data Study: CRT-TPC Selection Purity with Cathode-Crossing TPC Tracks

In this an all future data studies, the data used came from ICARUS runs 10917, 11001, and 11002, all of which used a calibration trigger which looked for five pairs of PMTs within a group of 60 to have coincident triggers within a 160 ns window. None of these runs were exposed to beam, so all detector activity recorded can be assumed to be cosmic in origin. The data used represents 702,750 events in total and all were recorded within a few weeks of each other in late 2023.

In order to quantify the purity of the CRT-TPC selection, a study was performed using cathode-crossing TPC tracks which are assigned a timestamp by stitching the tracks together from adjacent TPCs. These tracks can be used to see how well the assigned timestamp agrees with the best-

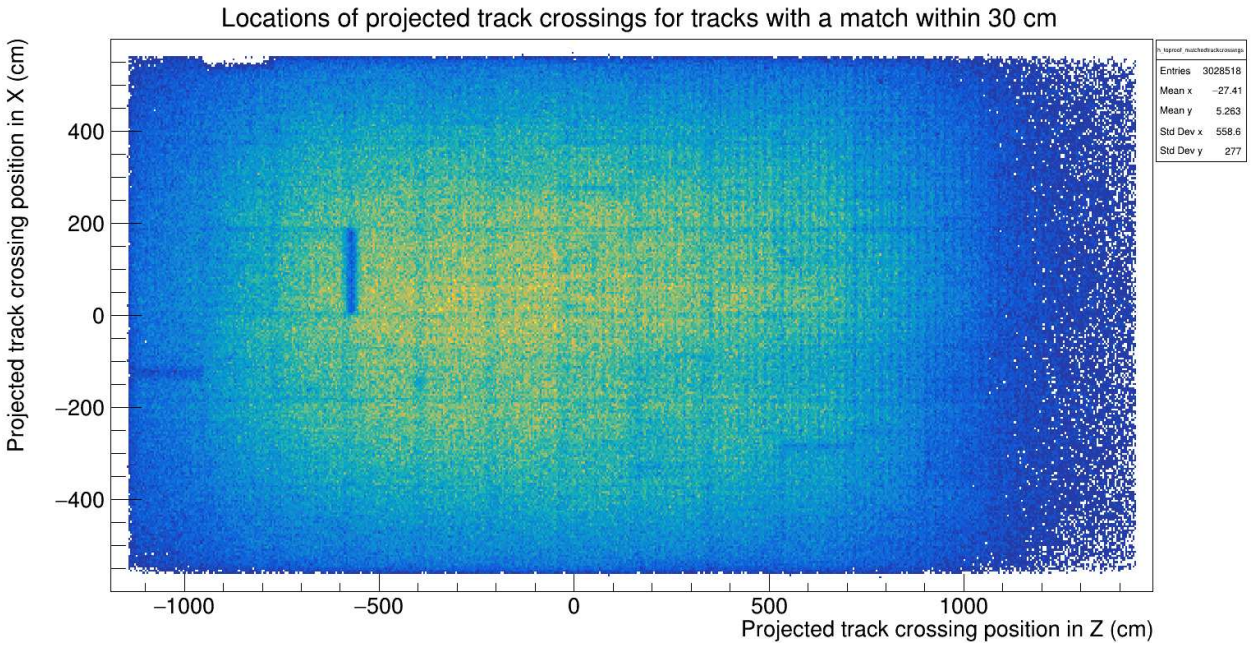

Figure 5.13: TPC tracks marked as Top Roof candidates whose track crossing position was found to be within 30 cm of the matched CRT Hit have the track crossing position plotted.

matched CRT Hit timestamp to better understand the purity of the selection. By defining an acceptable time difference between the cathode-crossing TPC track and the best matched CRT Hit, the sample of CRT Hits that are well matched in time can be compared to the total number of best matches of CRT Hits to cathode-crossing TPC tracks. The number of cathode-crossing TPC tracks whose time difference with their best matched CRT Hit is within a ± 10 μs of each other are declared as the correctly matched sample.

Figure 5.14 shows the distribution of this calculation: take the Top Roof track candidates that are cathode crossing, get their T0 timestamp and subtract from it the timestamp of the CRT Hit best matched to the track from having the smallest distance of closest approach (DCA). Figure 5.14 shows this distribution ranges over ± 4 μs, with a clear peak close to the center. If we examine the peak by looking at a tighter range around 0 ns, say ± 10 μs and fit a double Gaussian function as described in Equation 5.2, we can measure what our signal is compared to the full sample of 1,159,963 tracks for the Top Roof candidate pool. The fit parameters are: *p0*, the first Gaussian constant; *p1*, the mean of both Gaussian fits, made to be the same for both as there should not be a double peak; *p2*, the sigma or width of the first Gaussian; *p3* is the constant for the second

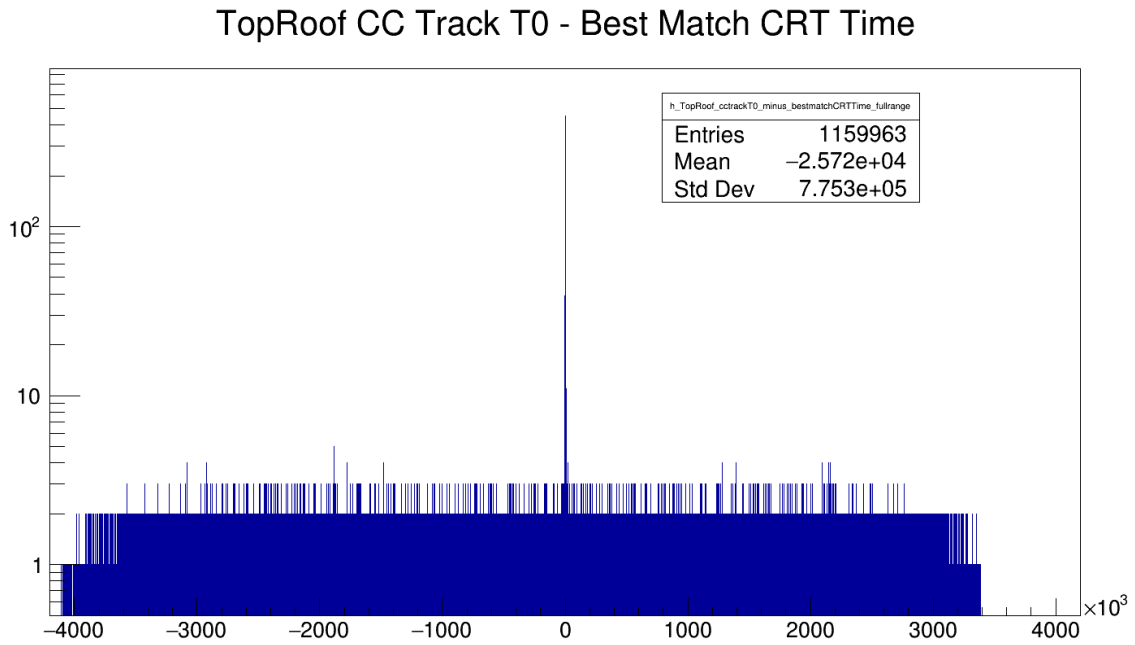

Figure 5.14: Distribution of the difference in T0 timestamps from Top Roof track candidates that were cathode crossing, and the timestamps of the CRT Hit best matched to that track by having the smallest distance of closest approach (DCA). Binning is 1 ns/bin.

Gaussian; *p4* is the sigma of the second Gaussian; and *p5* is a constant added to assist with the fit; it also represents a background that must be subtracted to get the final purity.

Figure 5.15 shows a fitting of the main signal peak on a (-10,10) μs range, along with the best fit parameters for *p0-p5*. *p1* shows that there is an offset of 2.65 μs between the TPC and CRT system, and that the time resolution between the two is approximately 722 ns, the width of the first Gaussian. After adjusting the initial fit parameters to minimize the reduced chi square (the fit chi square divided by the number of degrees of freedom), this set of fit parameters was found to be the best fit with a reduced chi square of 1.01. The integral of this function over the 20 μs period minus the fit constant gives a value of 927,135. This value divided by the total number of tracks gives a purity of 80.3%.

$$f(x) = \mathbf{p0} * exp\left[\frac{-1}{2}\left(\frac{x-\mathbf{p1}}{\mathbf{p2}}\right)^2\right] + \mathbf{p3} * exp\left[\frac{-1}{2}\left(\frac{x-\mathbf{p1}}{\mathbf{p4}}\right)^2\right] + \mathbf{p5} \tag{5.2}$$

The Top Roof region of the CRT is also the largest in cross-sectional area for the expected cosmic flux, which means it will also have a higher number of potential matches in each event (a

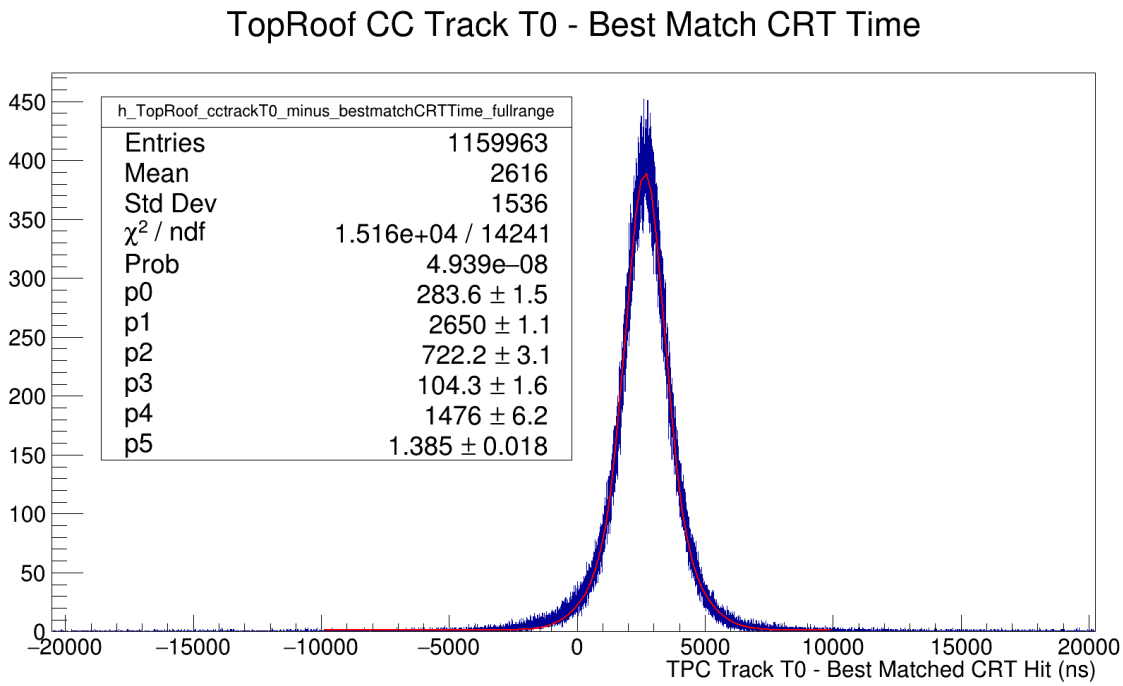

Figure 5.15: Using a fit function as described in Equation 5.2, this shows how the function fits on a range of (-10,10) μs.

mean of 146 CRT Hits per event in the Top Roof across the three ICARUS detector runs analyzed). This higher number of hits to choose from combined with the track being compared to them all will lead to a higher probability of false positive matches based purely on DCA in this sample compared to TPC tracks that only occupy a single TPC. Figures 5.16 and 5.17 show the difference in available CRT Hits for tracks that are cathode crossing versus not for Top Roof track candidates; this is a likely component of the lowered purity. Finally, cathode-crossing tracks only represent a portion of the available ICARUS geometry, so there is a bias to the areas of both the TPC and CRT being explored here compared to the full sample.

5.7 Matching Efficiency measurement

The matching efficiency for a CRT region is defined to be:

$$\epsilon_{Regional-TPC-Correlation} = \frac{\#\_TPC\_tracks\_with\_matched\_CRT\_Hit\_to\_region}{\#\_of\_TPC\_tracks\_pointed\_at\_CRT\_region} \tag{5.3}$$

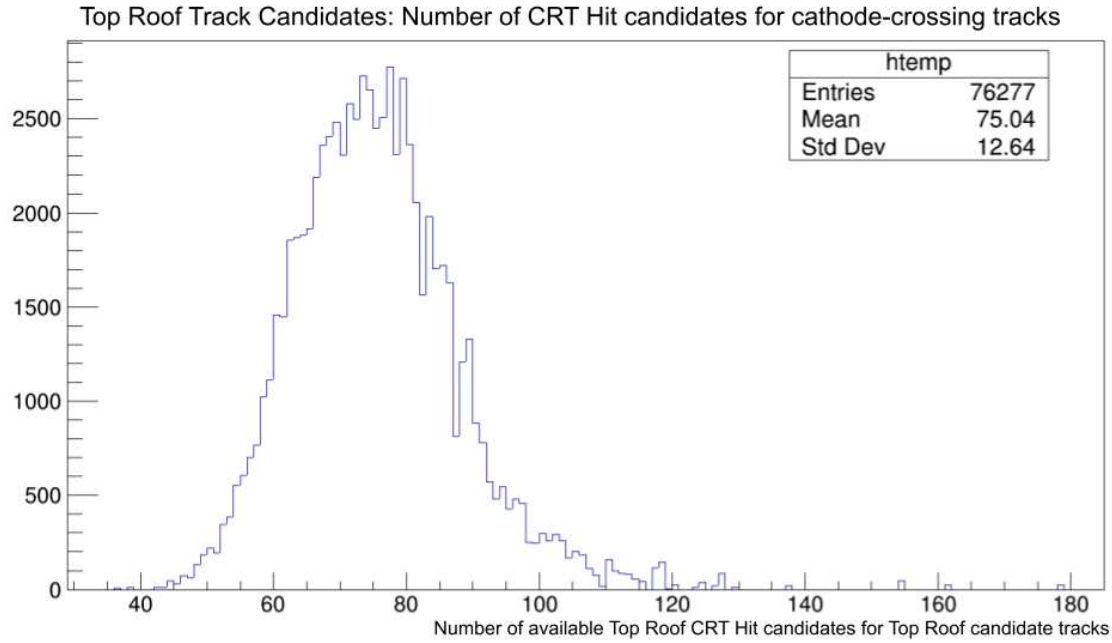

Figure 5.16: Number of CRT Hit candidates available to each Top Roof track candidate for tracks that are cathode-crossers.

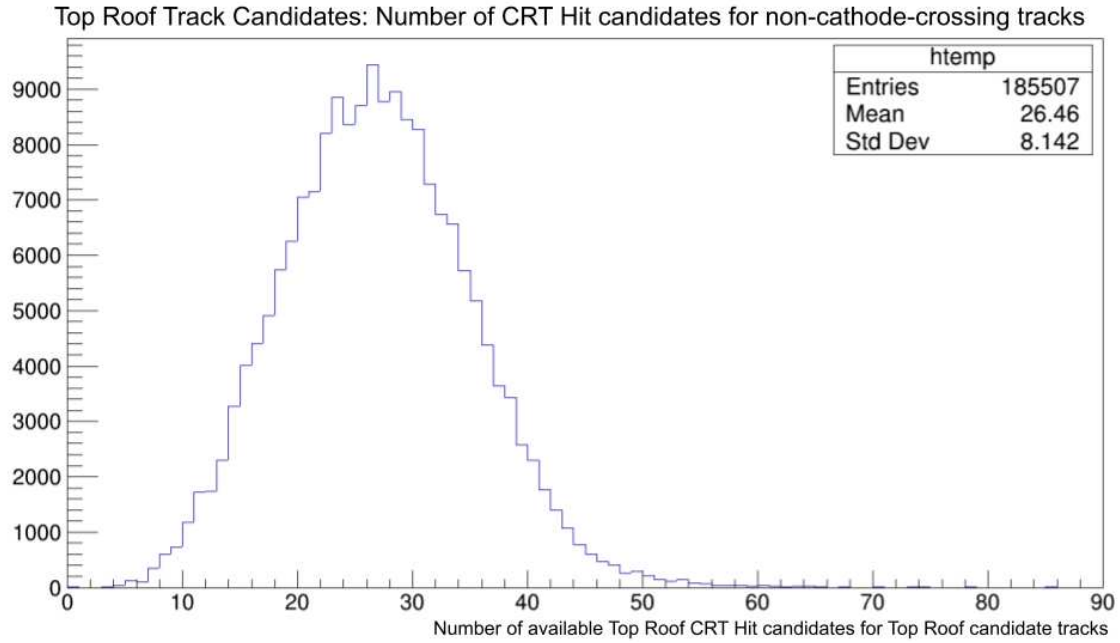

Figure 5.17: Number of CRT Hit candidates available to each Top Roof track candidate for tracks that are not cathode-crossers.

It should be noted that this will produce the efficiency of the CRT to match *a* CRT Hit to a TPC track, not necessarily the correct match. The studies I perform in MC will set a baseline quality cut to declare a match, however there will be the possibility of some tracks to be matched to a CRT Hit unrelated to it.

To calculate this efficiency, a macro reads in the output TTrees of the matching procedure and counts the number of tracks which count as a candidate for each CRT region. For any track that is identified as candidate for a given CRT region, a histogram of the DCA for the best matched hit which is in that CRT region of the top 3 possible matches saved to the track. Candidate tracks for a region with no match to CRT Hits in the region for which they are a candidate are given a DCA of -1 to flag that it is unmatched.

The number of counts in the histogram whose DCA is less than the maximum allowed DCA (and greater than -1 for candidate tracks with 0 matched hits in the region) for that CRT region is counted as the number of 'well matched' TPC tracks. The maximum allowed DCA cut will be determined below with studies on the ICARUS Monte Carlo to determine what the maximum allowable DCA should be for truth matched TPC tracks and CRT Hits. By understanding the DCA distribution for tracks that are well-matched in Monte-Carlo, we can find a cut on DCA that will

5.7.1 MC study: Maximum DCA Cut

To obtain a cut on DCA for data studies that would allow for the calculation of a matching efficiency, this study of Monte-Carlo events was performed. As discussed in section 5.4, having access to the MCParticle (a truth object used by the simulation to simulate elementary particles interacting in the detector) associated with a TPC track allows for a comparison of the position at which the MCParticle crossed a CRT volume to the matched CRT Hit position. To do such a comparison, I've used Monte Carlo files that I generated which use the CORSIKA [11] cosmic event generator to simulate cosmic activity at ICARUS.

Using CORSIKA in the ICARUS software framework, I generated 32,235 events in order to understand what cuts to make on the Distance of Closest Approach (DCA) to determine if a track

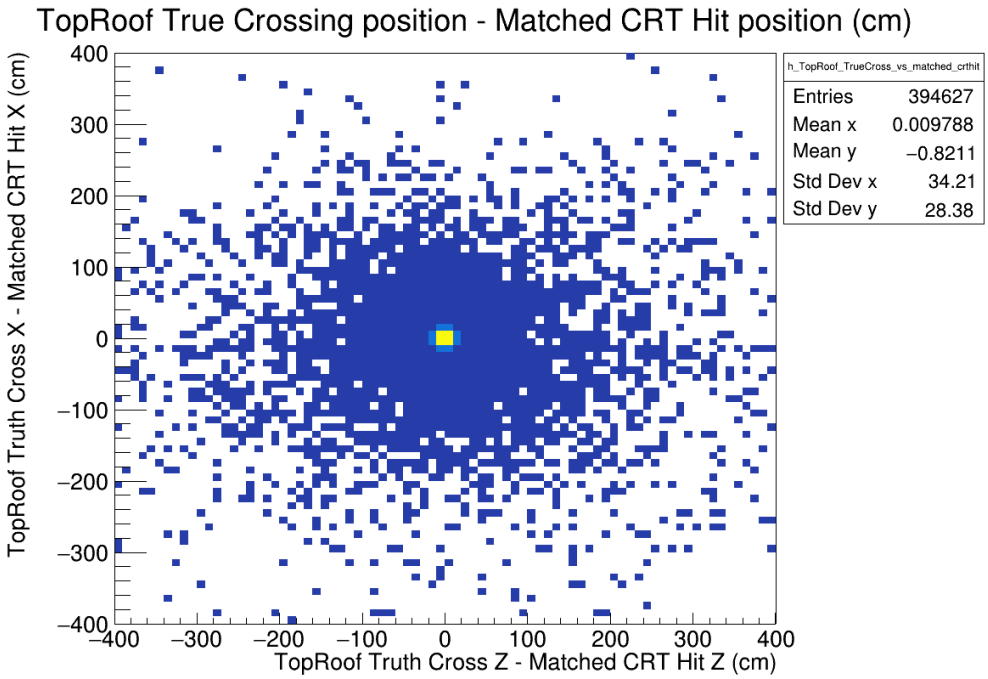

Figure 5.18: Comparison of the (X,Z) positions of the true crossing position of a TPC track to its best matched CRT Hit (X,Z) (cm).

has been 'well matched' or not. These allowed me to simulate the truth particles, determine where in truth they cross the CRT volumes, then use the reconstructed TPC tracks to see how well the matching to truth works with the simulated data products. By comparing the true crossing position to the best matched CRT Hit position, the best matches can be selected and have their DCA between the projected crossing point using the PCA and the matched CRT Hit plotted in a histogram. This will obtain a distribution of DCA for tracks that were well-matched in truth, and set a standard for what the expected DCA should be for truth matched tracks. Whatever cut on DCA is chosen can then be applied in data studies to get the matching efficiency that is the goal of this thesis.

Figure 5.18 shows the subtraction of the matched CRT Hit position from the track's true crossing position in X and Z for Top Roof TPC track candidates. Figure 5.19 adjusts the range of the axes to better show that the central distribution of hits is approximately centered on the ± 20 cm range in both X and Z. Refining the binning shows that the square is actually between ± 11.5 cm in both X and Z.

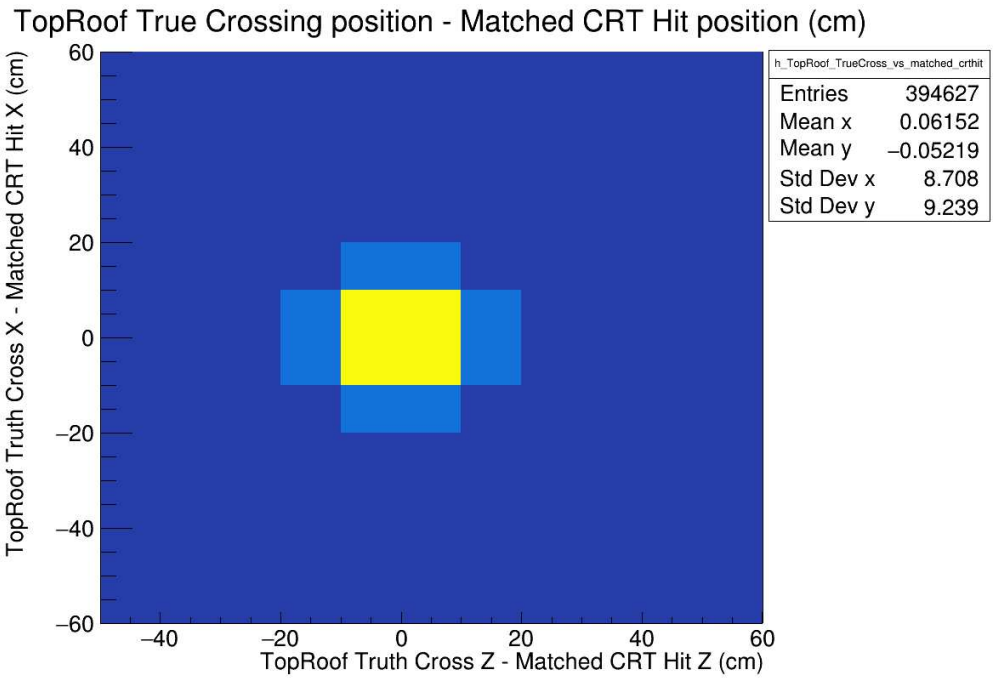

Figure 5.19: Comparison of the (X,Z) positions of the true crossing position of a TPC track to its best matched CRT Hit (X,Z) (cm), adjusted to show distribution at smaller range of (X,Z).

This makes the width 23 cm, which is the width of the Top CRT strips. As discussed in section 3.3.1, the Top CRT takes the largest signals from each layer in a module and assigns the hit position to the center of the region that is covered by both modules, which would be a 23 cm square. Therefore, all tracks with matches inside this $\pm$11.5 cm square are matched in truth to the CRT Hit which they created. This sample is shown in Figure 5.20.

Using the tracks that populate figure 5.20, a histogram is made of the DCA for those tracks in figure 5.21. Figure 5.21 shows the DCA distribution for tracks whose CRT Hits and TPC tracks were created by the same muon. The larger DCA tracks likely had a larger scattering when traveling between the CRT and TPC, leading to an overall broadening of the DCA measurement. With 100 cm as a cut on DCA, then 97.6% of truth-matched tracks would remain in the selected sample.

Repeating this process for the Top CRT regions with the same $\pm$11.5 cm selection on the distance between the true crossing point and the matched CRT Hit, we get similar results as with the Top Roof. Table 5.4 outlines the statistics generated for each Top CRT region in the MC sample

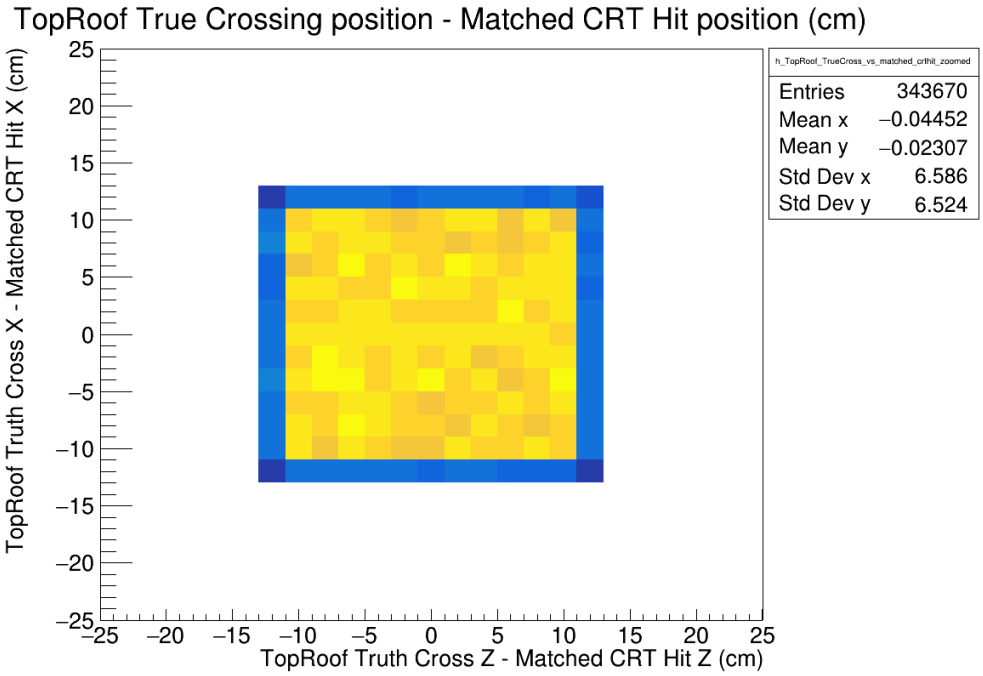

Figure 5.20: Comparison of the (X,Z) positions of the true crossing position of a TPC track to its best matched CRT Hit (X,Z) (cm), looking at tracks whose true crossing positions are within the resolution of the Top CRT detector panels.

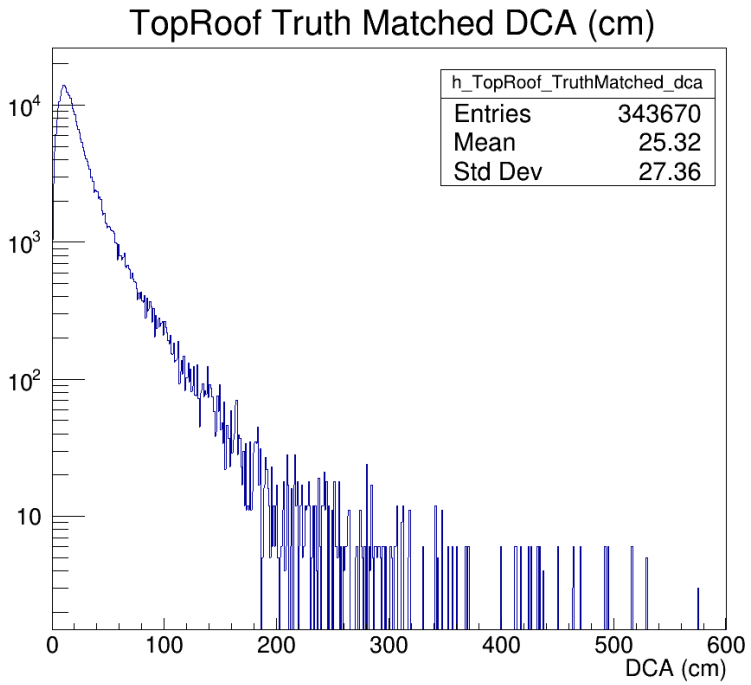

Figure 5.21: DCA distribution of tracks whose truth crossing position were within the resolution of the CRT detector to the best matched CRT Hit (cm).

Table 5.4: Top CRT MC study of how a DCA cut of 100 cm will affect a selection of truth-matched tracks.

CRT Region	# tracks found to cross region in truth	% of tracks crossing region with any match	% matched tracks with a truth match	% truth matched tracks with DCA < 100 cm
Top Roof	394,627	100.0	87.1	97.6
Top Rim West	38,889	99.8	86.1	95.3
Top Rim East	37,456	99.9	86.9	94.8
Top Rim North	3,290	100.0	89.8	90.5
Top Rim South	7,985	99.4	86.8	92.9

using this selection as truth-matched tracks, as well as looking at the overall statistics for matching in the region. This example shows that all Top CRT regions have roughly the same performance in terms of finding matches and matching to truth, though there is some variability in the percentage that will fall below 100 cm DCA. This is likely due to the different orientation of the modules, but could also be due to the regional track selection criteria as well as the available statistics in the MC sample. The North and South Rims have the lowest statistics due to their small size; the North Rim is also much farther away than any other vertically oriented CRT region, so it has less candidates that are directly correlated with TPC activity due to geometry alone, further reducing the available statistics.

The Side CRT has different hardware and thus does not have this same ± 11.5 cm window when plotting the true crossing versus best matched CRT Hit position. For all non-cut modules (all but the North and South), the module strips are 8 meters long in Z and 8 cm wide in Y, so the Y cut is close to the constraint of the physical module bounds, while the Z cut is based on the distributions seen in plots like figure 5.23. As discussed in section 3.3.1, the North and South Side regions each have their own reconstruction algorithms which are entirely different from the East and West walls. Figure 5.22 shows an example with the West-South wall in which the full set of matches is displayed. When looking closer as in figure 5.23, we see there's also a tightly constrained distribution in the Y direction, though less so along Z. This is expected due to the XX configuration of the modules (for the wide Z distribution) as well as the scale of the strip widths

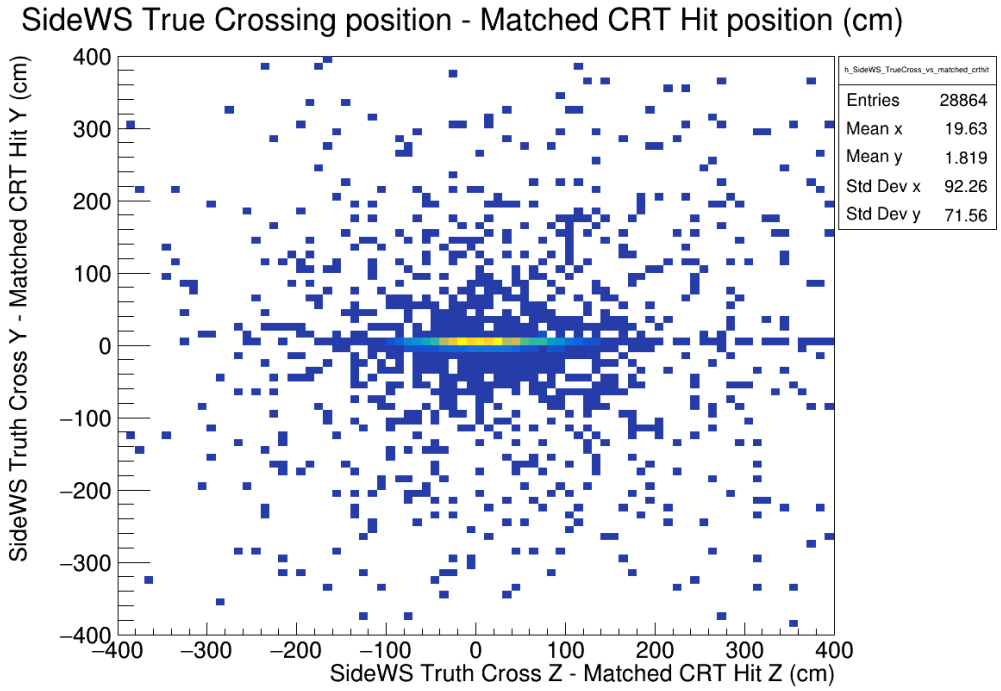

Figure 5.22: Comparison of the true crossing point of the truth particle in (Y,Z) to the (Y,Z) position of the best matched CRT Hit for the West-South Side region.

(the tight distribution in Y). As a consequence of the distribution in Z, tracks within ± 1 meter in Z and within ± 10 cm in Y are selected.

The North Side region has similar strip orientation to the Side East and Side West(though some are much shorter than 8 meters as discussed in section 2.1.5). Figure 5.24 shows the range of potential matches for the North Wall. ± 200 cm is used as a cut in X (the dimension that for the East and West modules is Z), but the same cut in Y is used since the region has the same physical constraints on the widths of the detector strips in that direction.

The South Side wall is unique as can be seen in figure 5.25. This is a narrower distribution compared to the other Side regions in both directions, since the XY coincidence provides a tighter constraint on where the hits are made compared to the other walls. Figure 5.26 shows that there is a similar core of tracks in the ± 25 cm range, so I chose this cut to select for well-matched tracks for the DCA measurement done for all regions.

Table 5.5 shows the results of using the truth selection cuts for each Side region in order to examine what the expected DCA should be for those tracks, along with the same metrics as those

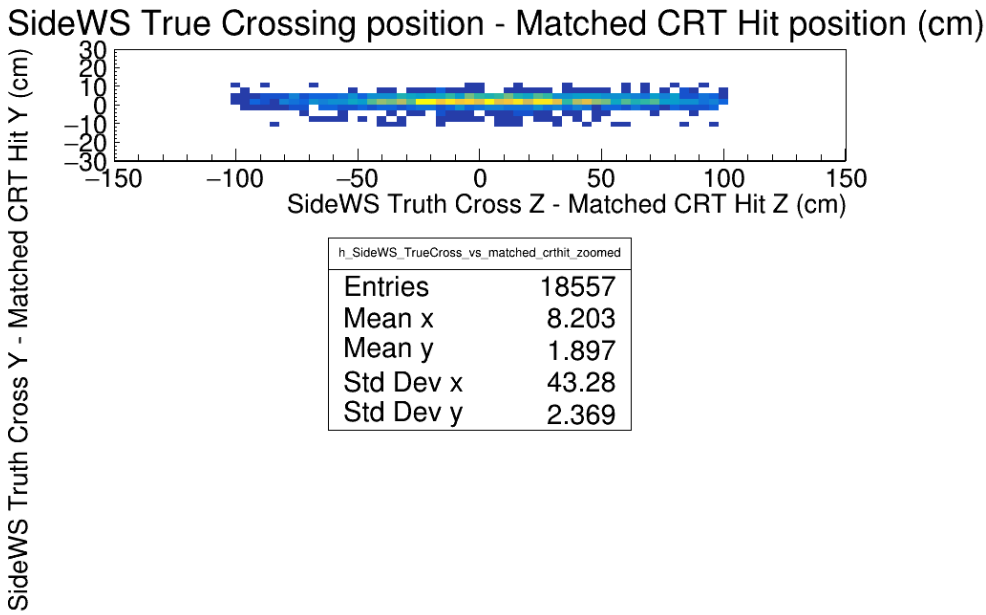

Figure 5.23: Comparing the true crossing point of the truth particle in (Y,Z) to the (Y,Z) position of the best matched CRT Hit for the West-South Side region for only tracks believed to be truth-matched.

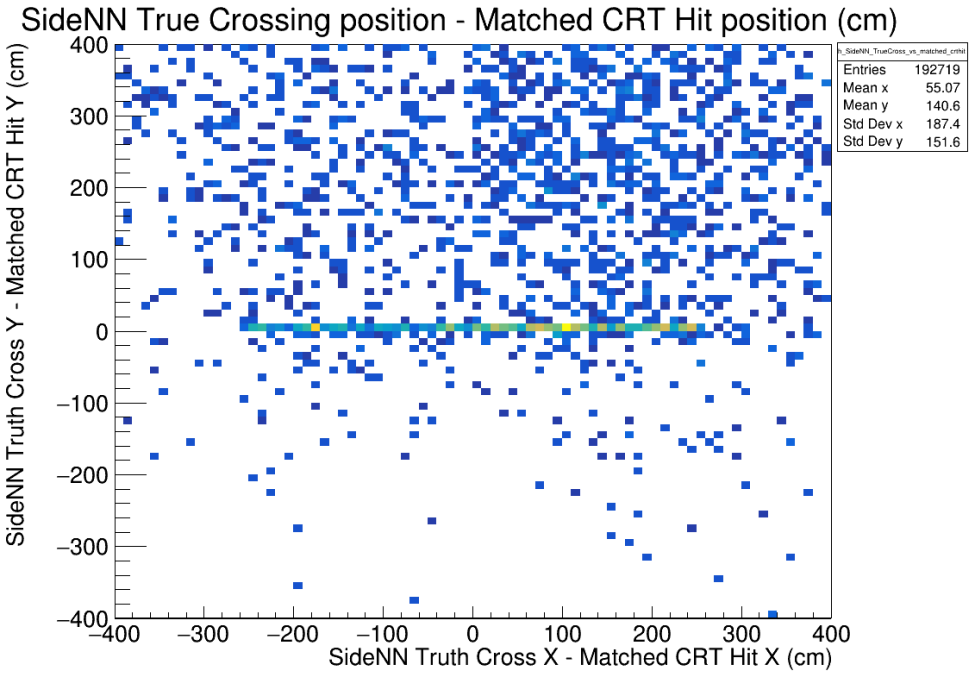

Figure 5.24: Comparison of the true crossing point of the truth particle in (X,Z) to the (X,Z) position of the best matched CRT Hit for the Side North region.

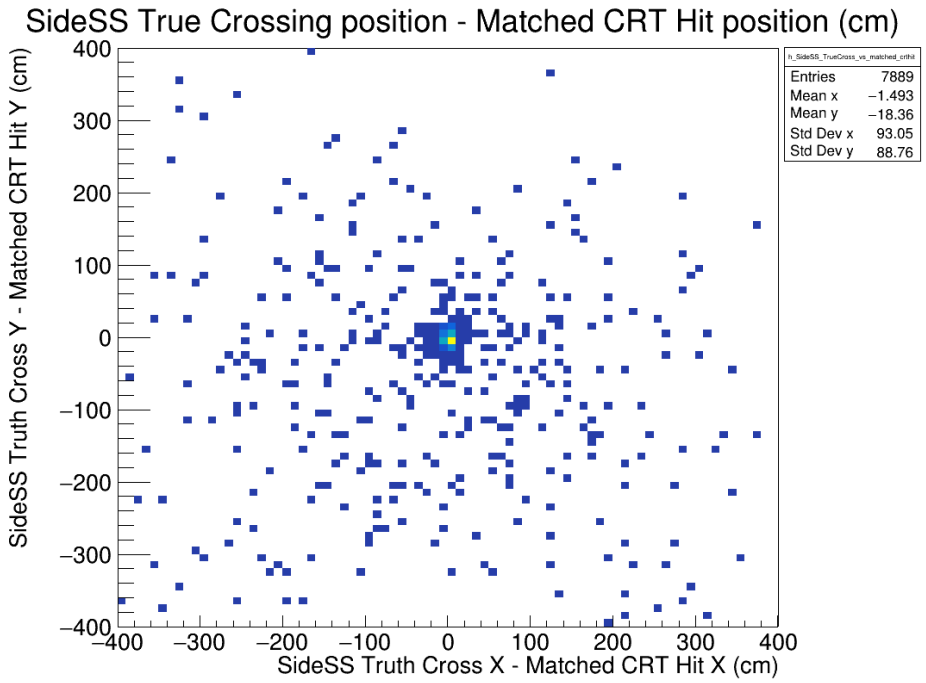

Figure 5.25: Comparison of the true crossing point of the truth particle in (X,Z) to the (X,Z) position of the best matched CRT Hit for the Side South region.

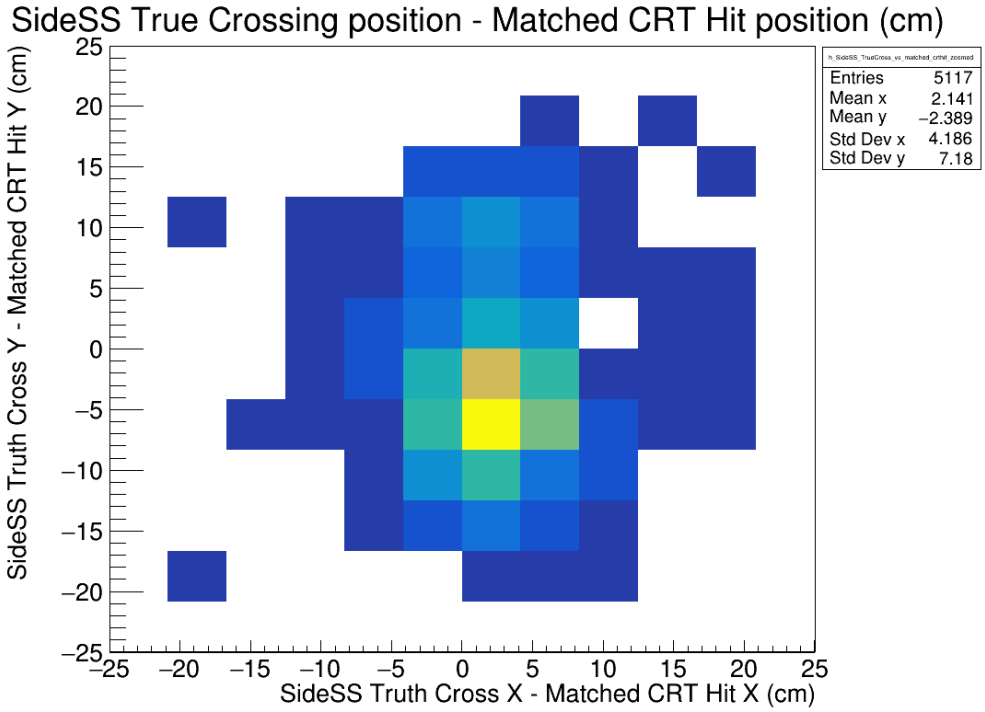

Figure 5.26: Comparing the true crossing point of the truth particle in (X,Z) to the (X,Z) position of the best matched CRT Hit for the Side South region for tracks believed to be truth-matched.

Table 5.5: Top CRT MC study of how a DCA cut of 100 cm will affect a selection of truth-matched tracks.

Side CRT Region	# tracks found to cross region in truth	% of tracks crossing region with any match	% matched tracks with a truth match	% truth matched tracks with DCA < 100 cm
West-South	30,004	96.2	64.3	96.6
West-Center	32,695	95.3	67.1	96.5
West-North	29,158	95.7	67.5	97.1
East-South	28,023	95.0	61.7	96.8
East-Center	33,148	94.9	66.5	96.8
East-North	28,797	97.1	66.9	96.7
South	8,239	95.8	64.9	97.7
North	26,877	85.9	9.0	84.6

found for the Top CRT. Like for the Top CRT, the values in the rightmost column of table 5.5 will be later used in the analysis section to adjust the final measured efficiencies to account for the estimated percentage of tracks that are left out by a 100 cm DCA cut. The North Wall is having difficulty with the tracks being marked as candidates finding the true match on the wall; this could be due to a large number of North Wall candidates being better matched to CRT Hits in other regions, suppressing potential matches in the North Wall. The Side East and West walls all have similar results, and all have a high rate of well matched tracks in truth whose DCA is lower than 100 cm, similar to the Top CRT sections.

5.7.2 Data study: Tagging Efficiency Results

All data used in this A count is made of the total number of candidate tracks using the cuts described in section 5.7.1, as well as the number of those candidates whose DCA falls below the cut for that CRT region. For the Top Roof there were a total of 1,298,951 track candidates, with 1,177,242 tracks having a valid CRT Hit in the Top Roof within 100 cm of the projected track crossing position, leading to a calculated efficiency of 90.6% with a statistical precision of 0.1%. Figure 5.27 shows the full DCA distribution for the Top Roof. From the ratio of the number of tracks under 100 cm DCA and the total number of track candidates for the Top Roof, we can get the efficiency for that region. Table 5.6 summarizes the results for all 13 regions. The 100 cm DCA cut was shown to leave some percent of TPC tracks behind in the studies done in section 5.7.1. To

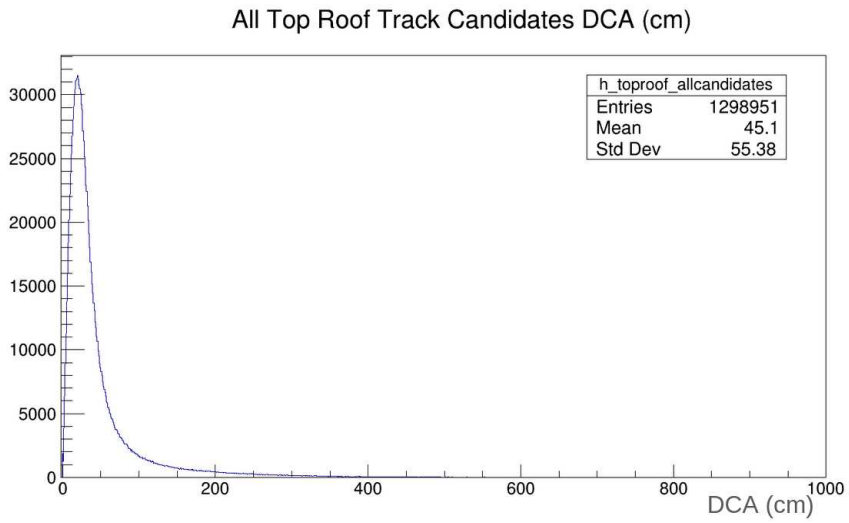

Figure 5.27: DCA distribution for Top Roof track candidates in the 'all regions' efficiency study.

adjust for the tracks left out, we can apply a factor on the measured efficiencies for each region that is proportional to the inverse of the Monte-Carlo efficiency found with the 100 cm DCA cut for that region. By doing this, we adjust the efficiency to more accurately represent what percentage of true tracks are being tagged by the CRT modules in truth. These adjusted MC efficiencies are presented in the final column of table 5.6.

There are significant differences by region. The Top Rim North and the Side North both appear to be much worse than the other regions in their subsystems; this is likely due in part to the noise identified in section 3.1. The Top North Rim is a small area very far from the detector; this means there is more material for muons incident on the CRT to pass through before they enter the TPCs, which means a much larger expected scattering angle for those muons, which in turn will affect how often the PCA works well for that region. The Side West-North has a few Front-End Boards being held at a higher threshold due to the high noise rate in that area, which could explain the lowered efficiency there. The higher noise in the north area of the building could also explain the Side East-North. Finally the Side East-South is a bit of an anomaly compared to the West-South; initially I believed this to be due to potential reconstruction-level problems hinted at by CRT-PMT measurements made earlier this year which implied the timing for the region was not

Table 5.6: Efficiency results for application of the standard CRT-TPC matching procedure.

Region Name	# of tracks meeting match criteria	# of track candidates for region	Efficiency (%)	Efficiency Adjusted to MC (%)
Top Roof	5,718,780	6,423,160	89.0	91.2
Top Rim West	159,524	189,055	84.4	88.6
Top Rim East	174,404	198,237	88.0	92.8
Top Rim South	93,897	132,940	70.6	78.0
Top Rim North	54,676	139,141	39.3	42.3
Side West-South	110,422	175,273	63.0	65.2
Side West-Center	129,346	206,336	62.7	65.0
Side West-North	72,253	185,336	39.0	40.1
Side East-South	42,218	182,391	23.1	23.9
Side East-Center	135,639	212,820	63.7	65.9
Side East-North	91,663	186,986	49.0	50.7
Side South	199,231	254,486	78.3	80.1
Side North	37,536	212,166	17.7	21.8

being properly distributed, however this is not the case. This region should be further studied to understand why this analysis is finding it underperforming compared to similar regions.

5.7.3 Data study: Selection Cut Optimization

Three variables have been identified to vary between different values to check for how the efficiency results might change due to the variation. These variables are: the reconstructed Pandora track length, the amount of the TPC track that is used for the PCA projection, and finally the length from a TPC face that allows a track to be marked as a candidate for a given region (note this will not show any change in the Side East/West regions as they have no distance-based endpoint cuts). I will refer to these as the length cut, PCA cut, and endpoint cut in this section as shorthand. When varying one parameter, the others are held at their default values; the default length cut is 70 cm, the default PCA cut is 10 cm, and the default endpoint cut is also 10 cm.

The minimum Pandora reconstructed track length cut was chosen after studies performed early in the development of this analysis with a small MC sample of high energy muons, finding that the smallest true TPC track was still above 70 cm if the track went almost vertically through the TPC volume. Using a lower value risks including stubs and tracks made from secondary activity

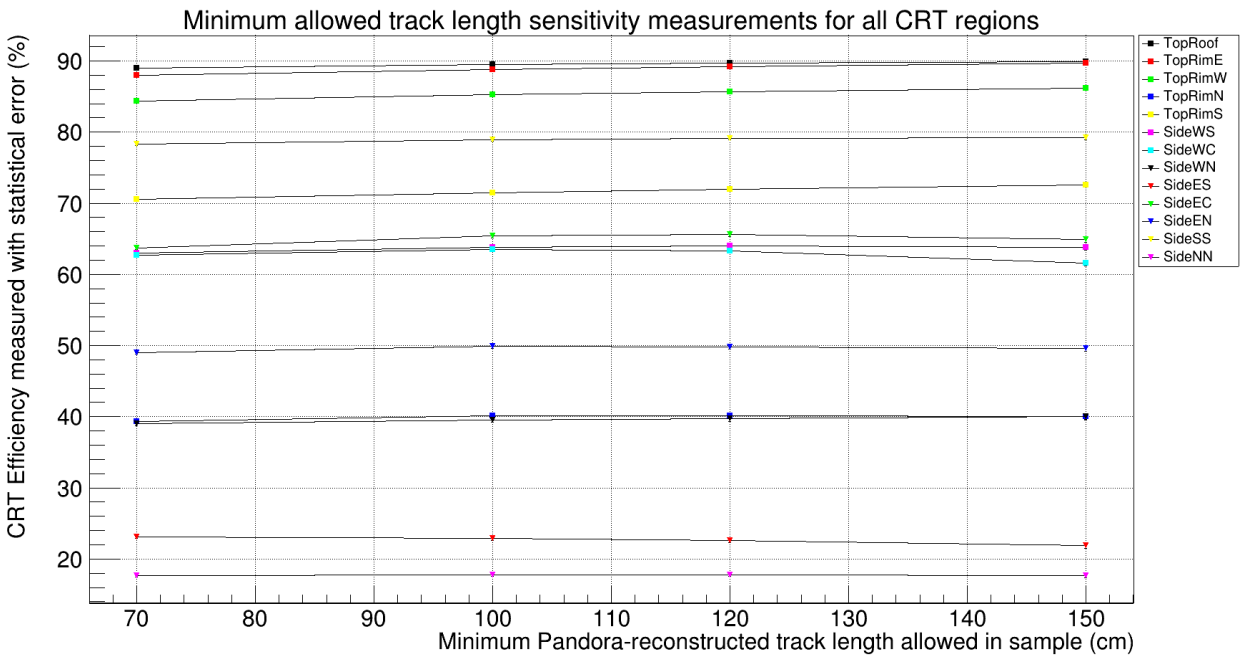

Figure 5.28: Track length sensitivity measurements for all CRT regions.

in the detector alongside the desired muons, so 70 cm is the lowest in this study. Figure 5.28 shows the effect of using longer tracks. Statistical error bars are not visible as they are smaller than the markers used to mark each point. The efficiency is quite insensitive to this parameter; there is a small increase in all regions.

The endpoint cuts only will have an effect on the Side South, Side North, and Top regions due to how the endpoint cuts are made in my analysis scheme. The standard was 10 cm, chosen because analyzers on ICARUS had been using this value for some time to wholly reject any tracks that came within that distance of an active TPC boundary, as it presents a high likelihood of being cosmic in origin. I decided to decrease this to see if we would see any increase in efficiency due to having higher confidence in a track originating from something outside the detector, and not something inside the detector that came close to the edge of the active area as it moved. Figure 5.29 shows that while we do see some shift in this direction, on the whole it is a small effect, similarly to the track length measurements.

The final sensitivity check is the amount of track from the Pandora endpoint (start or end) that is used in the PCA fit of that endpoint. By default this was 10 cm following a study by the

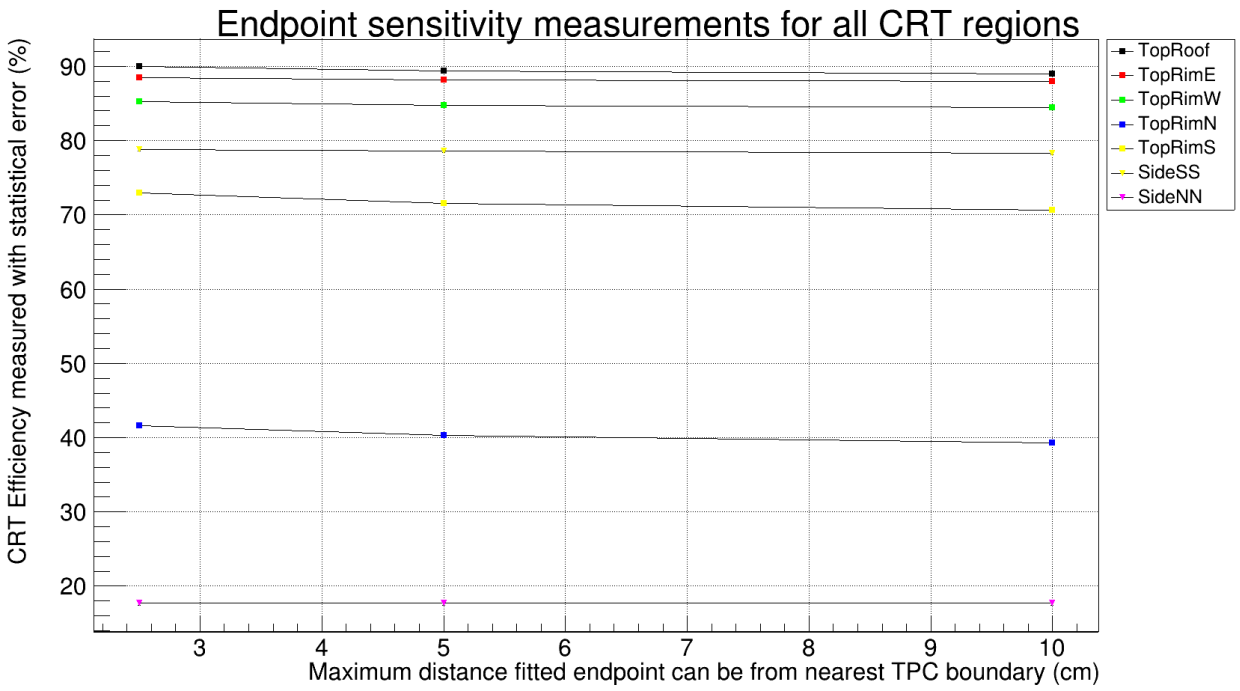

Figure 5.29: Endpoint sensitivity measurement for all regions affected by the shift.

ICARUS machine learning group.Figure 5.30 shows the CRT efficiency for 30 cm, 50 cm, 60 cm, 70 cm, and the full track length. Note that these are largely insensitive to variation, with the local maximum appearing to be somewhere between 40 and 60 cm for the Top regions as well as the Side South wall. The remaining regions appear to hit a plateau at 70 cm; this could partially due to the full-track PCA run having a minimum PCA of 70 cm, meaning for a lot of tracks there was likely not a big difference in the final PCA projection.

We have seen that the sensitivity measurements show some very small variation as the applied cuts are varied. While small, a difference of 1-2% is enough to warrant a final analysis with variables that maximize the measured efficiency from each sensitivity measurement. This leads to a PCA cut of 50 cm, an endpoint cut of 2.5 cm, and a track length cut of 150 cm. The efficiencies measured are in table 5.7. While the selection cuts lead to lower overall statistics in each region, the overall measured efficiencies have increased for all regions except the East-South.

The final DCA-cut adjusted efficiency for the Top Roof was found to be 94.9%, matching the goal set in the SBN proposal and consistent with the average per-module efficiency measured dur-

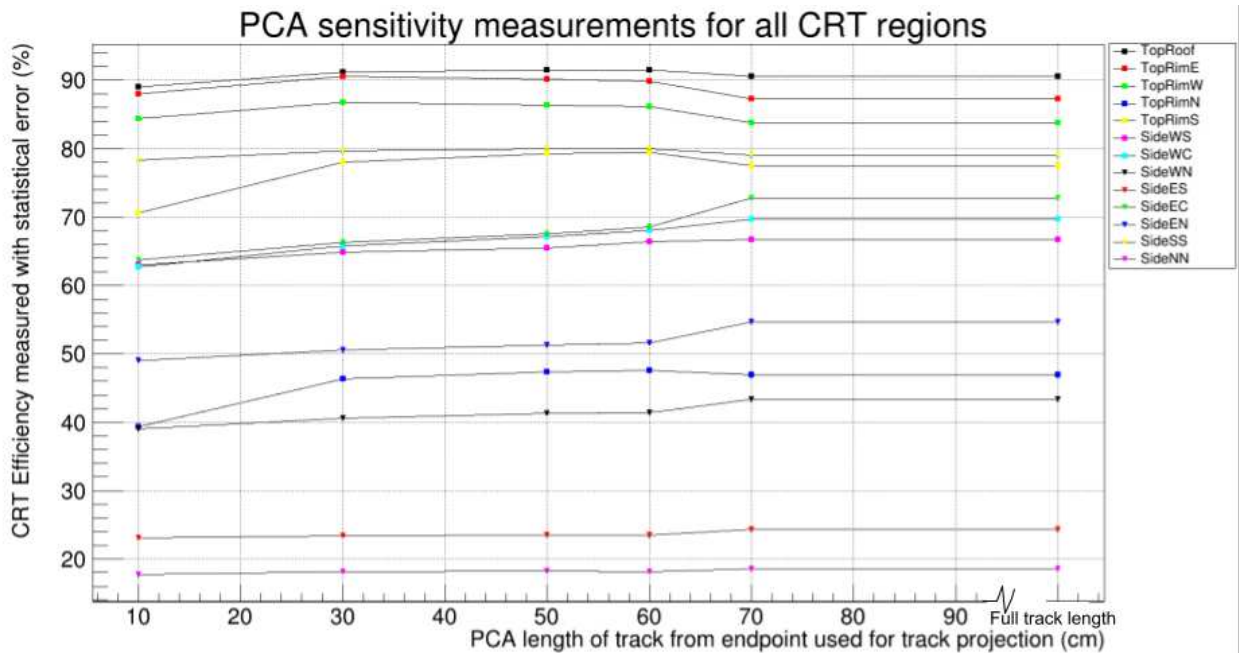

Figure 5.30: PCA sensitivity measurements for all regions.

Table 5.7: Efficiency results for application of the standard CRT-TPC matching procedure using 'best' settings for selection cuts.

Region Name	# of tracks meeting match criteria	# of track candidates for region	Efficiency (%)	Efficiency Adjusted to MC (%)
Top Roof	3,866,770	4,171,930	92.7	94.9
Top Rim West	125,206	142,905	87.6	92.0
Top Rim East	135,853	149,152	91.1	96.1
Top Rim South	70,140	84,482	83.0	91.7
Top Rim North	46,881	89,778	52.2	56.2
Side West-South	37,474	55,968	67.0	69.3
Side West-Center	41,374	61,560	67.2	69.7
Side West-North	52,188	58,538	43.0	44.3
Side East-South	12,915	57,698	22.4	23.1
Side East-Center	44,212	63,833	69.3	71.6
Side East-North	30,785	58,876	52.3	54.1
Side South	123,882	152,913	81.0	82.9
Side North	23,710	129,308	18.3	22.6

ing the production process at the Frascati test stand for the Top CRT modules. This is not the case for other regions of the CRT. The Top CRT regions except the North Rim have an efficiency above 90%, which instills a high confidence in these regions that are expected to see $\sim$80% of muons that will create TPC tracks as found in section in 5.4. The lower apparent efficiency measured for the North Rim is likely due to the matching method being optimized for the Top Roof, a horizontal plane that intercepts the majority of the cosmic flux. The North Rim is a much smaller detector significantly further from the TPC which is being used to project back to the CRT than the other similarly oriented South Rim, and therefore is more sensitive to geometrical and multiple scattering effects when projecting TPC tracks back to the region.

The Side North region also has a very low efficiency; this has been discussed in section 3.1 as being partly due to the high noise rate observed by the subsystem, which has resulted in the threshold setting on the front-end electronics for the Side North, Side East-North and Side West-North regions to be higher than other Side CRT regions in order to not overwhelm the DAQ. The Side North also only has single ended readouts in XX coincidence, both of these factors lead to a much lower tagging ability. The Side East-South is the region that is most in need of further investigation; earlier in the CRT-PMT studies performed by Anna Heggestuen and Francesco Poppi they discovered the region had an offset between the CRT and PMT subsystems that was not consistent with the other regions, possibly pointing to a problem with the timing distribution. However, this inconsistency does not appear in the runs used for the analysis that measures the regional efficiencies, so it is unclear what else is causing the lower efficiency in that region. The Side South region has the best efficiency due to its XY coincidence.

Chapter 6

Conclusion

The ICARUS Cosmic Ray Tagger is a robust detector subsystem that has been shown in this thesis to have excellent capability to be matched spatially and temporally with activity in the ICARUS TPC. The system is very stable, with few technical problems during ICARUS data runs since beam operation began in 2021. The Top and Side subsystems have been integrated into regular data taking since first physics running, and the Bottom subsystem has been taking data for several months despite a portion being damaged in a flood. This thesis provides an overview of the cosmic tagger and tracking subsystems and how they operate, focusing on the Top and Side.

With this study, I have established a baseline understanding of the tagging efficiency of the ICARUS CRT. This will in turn be useful in future for those wanting to use the CRT for cosmic event rejection, as well as demonstrating how this kind of 'auxiliary' detector can be leveraged to its fullest potential to serve the primary detector(s). I have shown that the CRT detectors work well for correlating signals with the ICARUS TPC. With further study, the CRT group will be able to improve on this correlation.

The CRT-TPC projection is also being made available within the files used by analyzers for neutrino and other analyses, allowing future analyzers to make use of the projection to exclude CRT-matched TPC tracks and allow for triple matching in those files, and making the matching process more accessible. Colleagues on ICARUS are making use of the PCA projection method recently in efforts to perform 'triple matching', using CRT-TPC-PMT for full validation of cosmic signals.

Bibliography

[1] R. Acciarri et. al. A Proposal for a Three Detector Short-Baseline Neutrino Oscillation Program in the Fermilab Booster Neutrino Beam, 2015.

[2] Hamamatsu. MPPC® (Multi-Pixel Photon Counter) S14160/S14161 series datasheet. https://www.hamamatsu.com/content/dam/hamamatsu-photonics/sites/documents/99_SALES_LIBRARY/ssd/s14160_s14161_series_kapd1064e.pdf.

[3] CAEN. User manual um5833, a1702/dt5702, 32-channel silicon photomultipliers readout front-end board. https://www.caen.it/download/?filter=A1702.

[4] M. et al. Antonello. Operation and performance of the ICARUS T600 cryogenic plant at Gran Sasso underground Laboratory. *Journal of Instrumentation*, 10(12):P12004–P12004, December 2015.

[5] Biswaranjan Behera. Cosmogenic background suppression at the ICARUS using a concrete overburden, 2021.

[6] Cancia, Nicola. The icarus expriment at lngs underground laboratory. *EPJ Web of Conferences*, 70:00055, 2014.

[7] Fermilab website. Short-Baseline Neutrino Detector (SBND). https://sbn-nd.fnal.gov/.

[8] Pedro A.N. Machado, Ornella Palamara, and David W. Schmitz. The Short-Baseline Neutrino Program at Fermilab. *Annual Review of Nuclear and Particle Science*, 69(1):363–387, October 2019.

[9] C. Rubbia. The Liquid Argon Time Projection Chamber: A New Concept for Neutrino Detectors. 5 1977.

[10] I. Stancu et al. Technical Design Report for the 8 GeV Beam. Technical report, The BooNE Collaboration, 2001.

[11] D. Heck, J. Knapp, J. N. Capdevielle, G. Schatz, and T. Thouw. *CORSIKA: a Monte Carlo code to simulate extensive air showers.* 1998.

[12] Rubbia, C. et al. Underground operation of the ICARUS T600 LAr-TPC: first results. *Journal of Instrumentation*, 6(07):P07011–P07011, July 2011.

[13] Christopher Hilgenberg. *Cosmogenic Background Rejection for the Sterile Neutrino Search with the Short-Baseline Neutrino Program Far Detector*. PhD thesis, Department of Physics, Colorado State University, Fort Collins, CO, 2020.

[14] D.G. Michael et al. The magnetized steel and scintillator calorimeters of the MINOS experiment. *Nuclear Instruments and Methods in Physics Research Section A: Accelerators, Spectrometers, Detectors and Associated Equipment*, 596(2):190–228, November 2008.

[15] Kuraray. Plastic scintillating fibers. https://www.kuraray.com/uploads/5a717515df6f5/PR0150_psf01.pdf.

[16] Hamamatsu. MPPC® (Multi-Pixel Photon Counter) s13360 series datasheet. https://www.hamamatsu.com/content/dam/hamamatsu-photonics/sites/documents/99_SALES_LIBRARY/ssd/s13360_series_kapd1052e.pdf.

[17] *Brief Introduction to Silicon Photomultipliers*.

[18] Francesco Poppi. *The cosmic ray tagger of the ICARUS detector: construction, commissioning and performances in the first physics run*. PhD thesis, alma, Giugno 2023.

[19] M. Auger, A. Ereditato, D. Goeldi, I. Kreslo, D. Lorca, M. Luethi, C. Rudolf von Rohr, J. Sinclair, and M. S. Weber. Multi-channel front-end board for sipm readout. *Journal of Instrumentation*, 11(10):P10005–P10005, October 2016.

[20] Adamson, P. et al. The numi neutrino beam. *Nuclear Instruments and Methods in Physics Research Section A: Accelerators, Spectrometers, Detectors and Associated Equipment*, 806:279–306, January 2016.

[21] CERN. The White Rabbit Project. https://white-rabbit.web.cern.ch/.

[22] J. S. Marshall and M. A. Thomson. The Pandora software development kit for pattern recognition. *The European Physical Journal C*, 75(9), September 2015.

[23] Gerald R. Lynch and Orin I. Dahl. Approximations to multiple coulomb scattering. *Nuclear Instruments and Methods in Physics Research Section B: Beam Interactions with Materials and Atoms*, 58(1):6–10, 1991.

[24] Biswaranjan Behera. Cosmogenic background suppression at icarus. *Physical Sciences Forum*, 8(1), 2023.

[25] Particle Data Group. Review of Particle Physics. *Progress of Theoretical and Experimental Physics*, 2020(8):083C01, 08 2020.

Glossary

LArTPC Liquid Argon Time Projection Chamber. 4

PMT Photomultiplier Tube. 5, 10, 41

SiPM Silicon Photomultiplier, the kind of light detector used by the Top and Side CRT. 10